NCNR

NIST CENTER FOR NEUTRON RESEARCH

2004

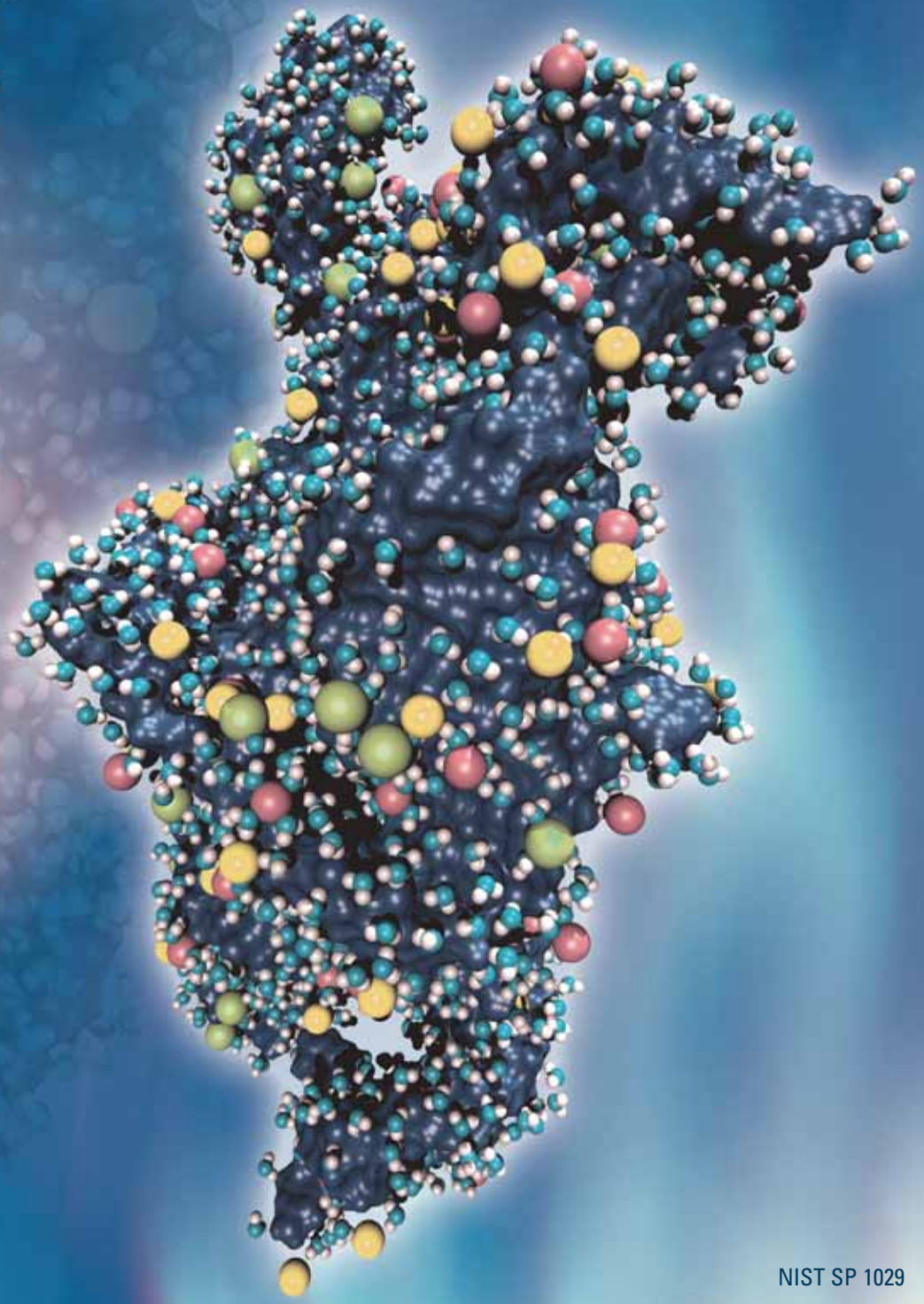

NIST SP 1029

Accomplishments and Opportunities

NIST
National Institute of Standards and Technology
Technology Administration, U.S. Department of Commerce

Structure of a folded catalytic RNA (ribozyme) of the *Azoarcus* bacterium obtained from a fully solvated atomistic molecular dynamics simulation calibrated to experimental SANS and DCS neutron data. Shown with the surface representation of the RNA molecule (dark blue) are space-filling representations of waters (light blue and white) along with sodium (green), chloride (yellow), and magnesium (orange) ions. (See highlight by J. E. Curtis ***et al***.)

NCNR 2004

NIST CENTER FOR
NEUTRON RESEARCH

Accomplishments and Opportunities

NIST Special Publication 1029

Patrick D. Gallagher, Director

Ronald L. Cappelletti, Editor

September 2004

National Institute of Standards and Technology
Arden L. Bement, Jr., Director

Technology Administration
Phillip J. Bond, Under Secretary of Commerce for Technology

U.S. Department of Commerce
Donald L. Evans, Secretary

Disclaimer

Certain commercial entities, equipment, or materials may be identified in this document in order to describe an experimental procedure or concept adequately. Such identification is not intended to imply recommendation or endorsement by the National Institute of Standards and Technology, nor is it intended to imply that the entities, materials, or equipment are necessarily the best available for the purpose.

National Institute of Standards
and Technology Special Publication 1029

Natl. Inst. Stand. Technol. Spec. Publ. 1029, 88 pages
(September 2004)

CODEN: NSPUE2

U.S. GOVERNMENT PRINTING OFFICE - WASHINGTON: 2004

For sale by the Superintendent of Documents,
U.S. Government Printing Office

Internet: bookstore.gpo.gov ■ Phone: 202.512.1800
Fax: 202.512.2250 ■ Mail: Stop SSOP, Washington, DC 20402-0001

Table of Contents

Foreword

It is my pleasure to share with you the many accomplishments of the NIST Center for Neutron Research over the past year. This has been a period of change for the NCNR. Mike Rowe, our Director since 1989, retired on March 26, 2004 after a 31 year career at NIST/National Bureau of Standards. The remarkable growth of the NCNR into the nation's leading neutron research facility is due in large part to Mike's vision and leadership over this period. For this, Mike was honored in June of this year by receiving the first Clifford G. Shull Prize, which is awarded by the Neutron Scattering Society of America for outstanding research in neutron scattering and for leadership in promoting the North American neutron scattering community. We at the NCNR owe him a direct debt of gratitude for his achievements. Those who know Mike personally are aware that his leadership style was characterized by his warmth, integrity, and wisdom—characteristics that have set the tone for doing things the "NCNR way". As a result, Mike has left a very strong organization poised for even greater achievements. For my part, I am committed to doing my best to live up to his high standard of excellence. Fortunately, Mike continues to work with us on a variety of technical issues, and we look forward to many more years of his company as a colleague and friend.

Sadly this year we also unexpectedly lost a great friend and colleague, Nick Rosov, who led the development of NCNR's Neutron Spin Echo Spectrometer and its growing user program. His presence and his great personal qualities will be sorely missed, but his contributions will continue to have an enormous impact on the NCNR and on those who come to use the facility for a very long time.

This has also been a period of challenges for the NCNR. Reductions in funding for the NCNR in the FY04 Omnibus Appropriations Bill have forced us to take several actions including reducing time on several instruments, and deferring or canceling some instrument development activities. On the other hand, the strong demonstration of support by our users has been deeply gratifying to all of us here at the NCNR.

This year, the NCNR was honored to host the second annual American Conference on Neutron Scattering, held in College Park, Maryland in early June. The Conference, sponsored by the Neutron Scattering Society of America, brings together a broad spectrum of researchers from across the United States and Canada to showcase recent work in neutron science across a wide range of scientific disciplines. The record attendance, diverse representation, and the excitement reflected in the presented work bode well for the future of neutron scattering in North America.

The operation of the reactor, cold source, and beam systems over the past twelve months has been outstanding. This year, the reactor is running a full schedule and the cold source was available 100 % of the time that the reactor was ready to run. This is a remarkable record and a tribute to the hard work of those that make it happen. We recently submitted an application to the U.S. Nuclear Regulatory Commission requesting a renewal of our operating license for an additional 20-year period. Behind the scenes, we continue to upgrade equipment and systems to prepare the facility for many more years of highly reliable operation.

Despite the budget limitations, instrument development remains a priority since improvements in capability reflect the future success of our facility. We are in the advanced stages of manufacturing and installation of two new crystal spectrometers that will bring enormous improvements in capability for inelastic neutron measurements to the NCNR and open up new research opportunities for our users. One of these projects is a partnership between NIST, the National Science Foundation and The Johns Hopkins University and provides another excellent example of how our partners are the key to our success.

In the end, all of our efforts are focused on the science made possible through neutron scattering. It is by the results of the research performed at the NCNR that we measure our success, and from which we derive our satisfaction and enjoyment. In this report we have selected a few of the many examples of exciting research results from the past year. I think you will agree that they reflect an amazing breadth and depth of research performed at the NCNR, and capture the enthusiasm of those performing the work.

I want to extend my sincere thanks to everyone who contributed to another successful year!

Pat Gallagher

Remembering Nick Rosov
1959 - 2004

Lead scientist for the
Neutron Spin Echo Spectrometer

The NIST Center for Neutron Research (NCNR)

Neutrons are powerful probes of the structure and dynamics of materials ranging from molecules inserted into membranes that mimic cell walls to protons migrating through fuel cells. The unique properties of neutrons (discussed below) can be exploited using a variety of measurement techniques to provide information not available by other means. They are particularly well suited to investigate all forms of magnetic materials such as those used in computer memory storage and retrieval. Atomic motion, especially that of hydrogen, can be measured and monitored, like that of water during the setting of cement. Residual stresses such as those inside stamped steel automobile parts can be mapped. Neutron-based research covers a broad spectrum of disciplines, including engineering, biology, materials science, polymers, chemistry, and physics.

The NCNR's neutron source provides the intense beams of neutrons required for these types of measurements. In addition to the thermal neutron beams from the heavy water or graphite moderators, the NCNR has a large area liquid hydrogen moderator, or cold source, that provides intense neutron beams for the only cold neutron facility presently operating in the U.S.

There are currently 29 experiment stations: four provide high neutron flux positions for irradiation, and 25 are beam facilities most of which are used for neutron scattering research. The following pages show a schematic layout of the beam facilities. More complete descriptions of instruments can be found at www.ncnr.nist.gov.

Instruments in the cold neutron guide hall.

The NCNR supports important NIST research needs, but is also operated as a major national user facility with merit-based access made available to the entire U.S. technological community. Each year, almost 2000 research participants from all areas of the country, from industry, academia, and government use the facility for measurements. Beam time for research to be published in the open literature is without cost to the user, but full operating costs are recovered for proprietary research. Access is gained mainly through a peer-reviewed, web-based proposal system with beam time allocated by a Program Advisory Committee twice a year. For details see www.ncnr.nist.gov/beamtime.html. The National Science Foundation and NIST co-fund the Center for High Resolution Neutron Scattering (CHRNS) that operates six of the world's most advanced instruments. Time on CHRNS instruments is made available through the proposal system. Some access to beam time for collaborative measurements with the NIST science staff can also be arranged on other instruments.

Why Neutrons?

Neutrons reveal properties not available to other probes. They can behave like microscopic magnets, they can diffract like waves, they can set particles into motion losing or gaining energy and momentum in the process and they can be absorbed.

Wavelengths—range from 0.1 Å to 100 Å, (1 Å = 0.1 nm) allowing them to form observable ripple patterns from structures as small as atoms to as large as proteins.

Energies—of millielectronvolts, of the same order as those of motions of atoms in solids or liquids, waves in magnetic materials, and vibrations in molecules. Exchanges of energy between neutrons and matter as small as nanoelectronvolts and as large as tenths of electronvolts can be detected.

Selectivity—in scattering power varies from nucleus to nucleus somewhat randomly. Specific isotopes can stand out from other isotopes of the same kind of atom. Specific light atoms, difficult to observe with x-rays, are revealed by neutrons. Hydrogen, especially, can be distinguished from chemically equivalent deuterium.

Magnetism—makes the neutron sensitive to the magnetic spins of both nuclei and electrons, allowing the behavior of ordinary and exotic magnets to be detailed precisely.

Neutrality—of the uncharged neutrons allows them to penetrate deeply without destroying samples, and pass through walls controlling a sample's environment allowing measurements under extreme conditions. Properties ranging from the residual stresses in steel girders to the unfolding motions of proteins are amenable to measurement by neutrons.

Capture—characteristic radiation emanating from specific nuclei capturing incident neutrons can be used to identify and quantify minute amounts of material in pollutants or ancient pottery shards.

NIST Center for Neutron Research Layout

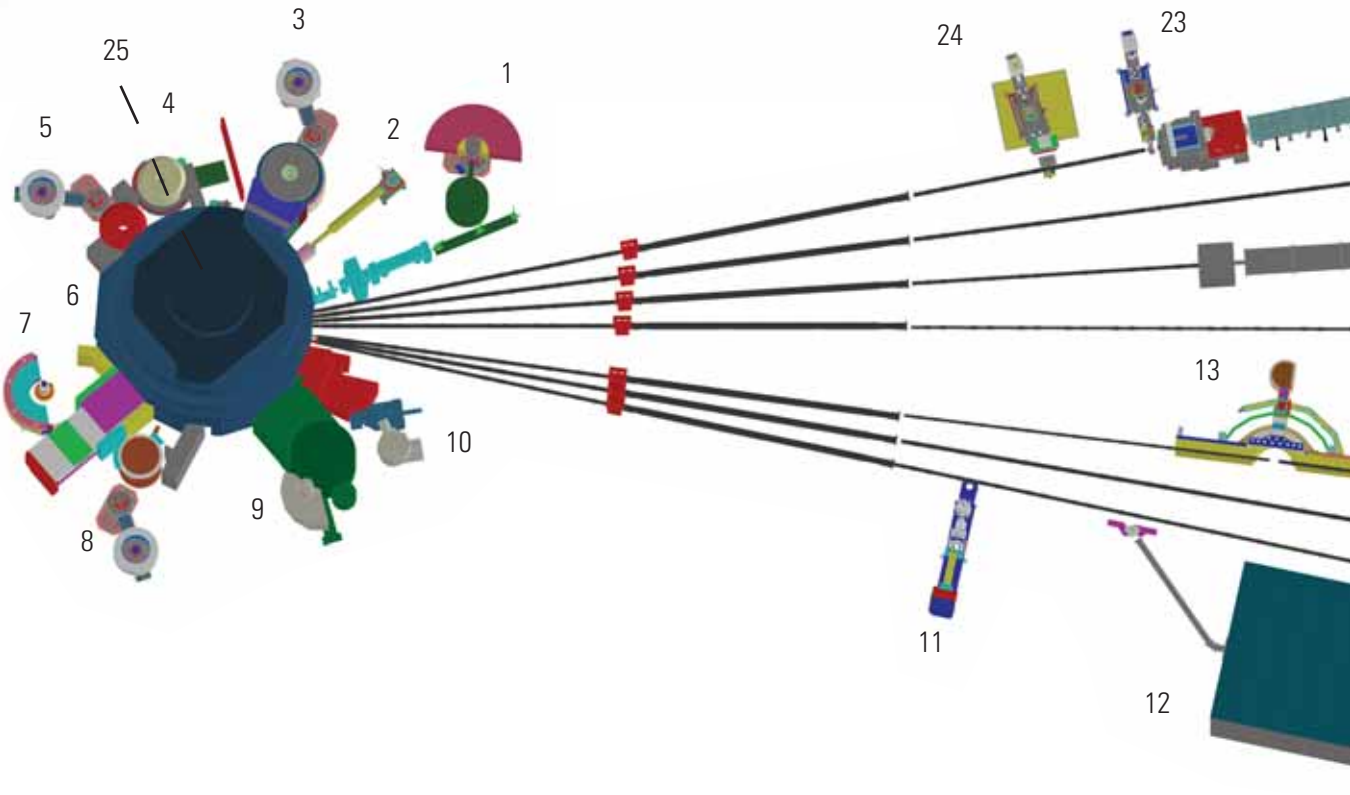

1. **A Cold Neutron Depth Profiling** instrument (not shown) for quantitative profiling of subsurface impurities currently at this site will be moved to another position. Shown is MACS, a cold neutron Triple Axis Crystal Spectrometer under construction, with double focusing monochromator and multiple crystal analyzer/detectors that can be flexibly configured for several energies simultaneously or for high throughput at one energy.
2. **BT-6 *(temporary location)* Neutron Imaging Facility** for imaging hydrogenous matter in large components such as water in fuel cells or lubricants in engines.
3. **BT-7 Thermal Triple Axis Spectrometer** with large double focusing monochromator, and interchangable analyzer/detector systems (being installed).
4. **BT-8 Residual Stress Diffractometer** optimized for depth profiling of residual stress in large components.
5. **BT-9 Triple Axis Crystal Spectrometer** for measurements of excitations and structure.
6. **Thermal Column**: a very well-thermalized beam of neutrons used for radiography, tomography, dosimetry and other experiments.
7. **BT-1 Powder Diffractometer** with 32 detectors; incident wavelengths of 0.208 nm, 0.154 nm, and 0.159 nm, with highest resolution of $\delta d/d = 8 \times 10^{-4}$.
8. **BT-2 Triple Axis Crystal Spectrometer** with polarized beam capability for measurement of magnetic dynamics and structure.
9. **BT-4 Filter Analyzer Neutron Spectrometer** with cooled Be/Graphite filter analyzer for chemical spectroscopy.
10. **BT-5 Perfect Crystal Diffractometer SANS** small angle neutron scattering instrument for microstructure up to 10^4 nm, sponsored by the National Science Foundation and NIST, part of the Center for High Resolution Neutron Scattering (CHRNS).
11. **NG-7 Horizontal Sample Reflectometer** allows reflectivity measurements of free surfaces, liquid vapor interfaces, as well as polymer coatings.
12. **Neutron Interferometry and Optics Station** with perfect silicon interferometer; vibration isolation system provides exceptional phase stability and fringe visibility.
13. **Spin Polarized Triple Axis Spectrometer (SPINS)** using cold neutrons with position sensitive detector capability for high-resolution studies—part of CHRNS.

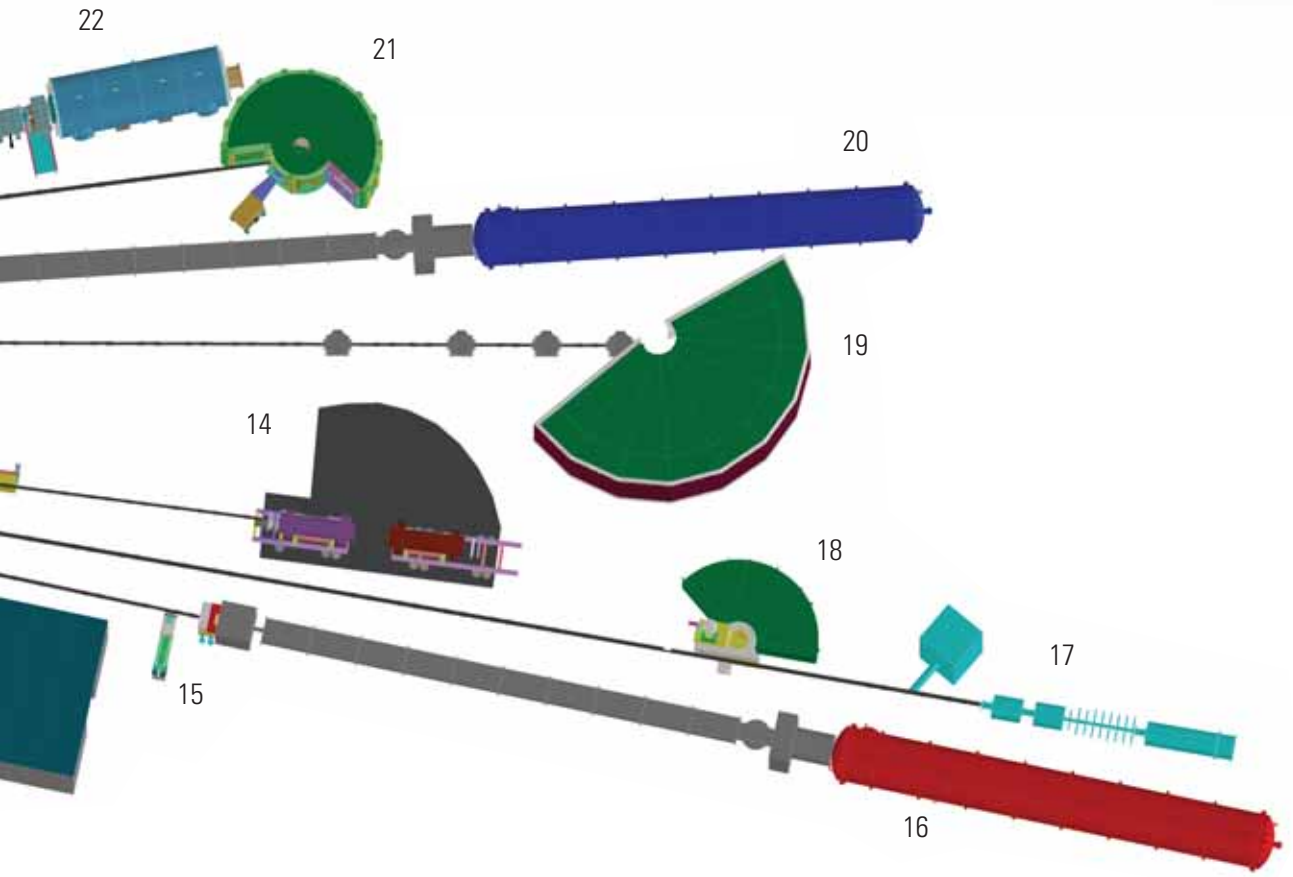

14. **Spin Echo Spectrometer** for measuring dynamics from 100 ns to 10 ps, in partnership with ExxonMobil—part of CHRNS.

15. **Prompt Gamma Activation Analysis** cold neutron fluxes allow detection limit for H of 1 μg to 10 μg. Focused beams are available for profiling.

16. **NG-7 30 m SANS** for microstructure measurements, in partnership with NIST, ExxonMobil, and the Cold Neutrons for Biology and Technology program.

17. **Neutron Physics Station** offering three cold neutron beams with wavelengths of 0.5 nm, and 0.9 nm, and a "white" beam available for fundamental neutron physics experiments.

18. **Fermi Chopper hybrid time-of-flight (TOF) Spectrometer** for inelastic scattering with selected incident wavelengths between 0.23 nm and 0.61 nm.

19. **Disk Chopper TOF Spectrometer**, for studies of diffusive motions and low energy dynamics of materials. Wavelengths from ≈ 0.18 nm to > 1.0 nm give corresponding energy resolutions from ≈ 2 meV to < 10 μeV —part of CHRNS.

20. **NG-3 30 m SANS** for microstructure measurements sponsored by the National Science Foundation and NIST—part of CHRNS.

21. **Backscattering Spectrometer** high intensity inelastic scattering instrument with energy resolution < 1 μeV, for studies of motion in molecular and biological systems—part of CHRNS.

22. **NG-1 8 m SANS** for polymer characterization being modified to 10 m and to be made available for CHRNS use along with its current use by the NIST Polymers Division.

23. **Vertical Sample Reflectometer** instrument with polarization analysis capability for measuring reflectivities down to 10^{-8} to determine subsurface structure.

24. **Advanced Neutron Diffractometer / Reflectometer (AND/R)**, a vertical sample reflectometer with polarization analysis and off-specular reflection capabilities for measuring reflectivities down to 10^{-8}. Part of the Cold Neutrons for Biology and Technology program committed to studies of biological membrane systems.

25. **Thermal Neutron Capture Prompt Gamma-ray Activation Analysis Instrument at VT-5** (above the reactor) with a neutron fluence rate of 3 x 10^8 /cm^2/s used for quantitative elemental analysis of bulk materials. Generally used for the analysis of highly hydrogenous materials (< 1 % H) such as foods, oils, and biological materials.

NCNR Images 2004

Li Liu, Gui Chuan Yu, Michael Miller, Inna Vishik, all of Stanford, loading a sample for their BT-2 experiment.

NCNR's Terry Udovic suited up at the FANS console.

NCNR's Bill Kamitakahara ready for takeoff, College Park Aviation Museum, ACNS banquet.

NCNR's Charlie Glinka and Yamali Hernandez pose for posterity during a break at the ACNS.

Pat Looney (OSTP) and Pat Gallagher (NCNR director) chatting at the ACNS.

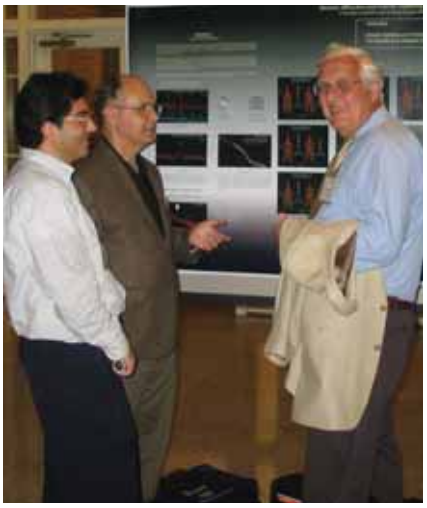

NCNR's Taner Yildirim and Ron Cappelletti talk hydrides with Brooks Harris (Penn) at an ACNS poster session.

NCNR's Dan Neumann holds forth on dynamics at the ACNS.

NCNR's John Copley (left) and Mathias Lösche (right) discuss technical matters with Mathias Gruenig (SwissNeutronics) at the ACNS banquet.

Greg Harbers (Colo. State), Duncan McGillivray (JHU/NCNR), and Divya Singh (JHU) set up a sample at the new CNBT AND/R reflectometer.

Left, Guebre Tessema (NSF) and right, Lance Haworth (NSF) hear out Ian Anderson (SNS) at the ACNS.

Bill Hamilton (ORNL), Rob McQueeney (Iowa State) cheering it up with Dan Neumann (NCNR) at the ACNS banquet.

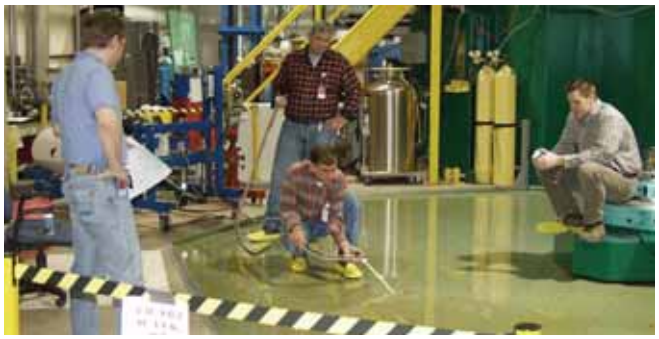

NCNR's Mike Murbach, Mike Gue, Mike Rinehart, and Colin Wrenn install the "dance floor" for the analyzer of the new BT-7 triple-axis spectrometer.

NCNR's Rob Dimeo and Larry Kneller demonstrate DAVE software at the ACNS.

Shenda Baker (Harvey Mudd), Roger Pynn (LANL), and Jeff Lynn (NCNR) share a moment with NCNR former director, Mike Rowe.

ACNS Banquet at the College Park Aviation Museum: L to R: Vladimir Luzin, Jesus Ruiz, Philippe and Suzette Mangin, Mike Rowe, Nancy Chesser, and Steve White.

Andrey Zheludev (ORNL) and Igor Zaliznyak (BNL) at the ACNS talking physics during a coffee break.

Probing the Depths of Lipid Membranes with AND/R

M. Mihailescu
University of California at Irvine
Irvine, CA 92697 and
NIST Center for Neutron Research
National Institute of Standards and Technology
Gaithersburg, MD 20899

D. Worcester
University of Missouri
Columbia, MO 65211

Lipids are the major constituent of cellular membranes. Arranged as a two-molecule-thick bilayer with a thickness of about 50 Å, they insulate the inside of cells and cell organelles from the outside. Proteins embedded in this bilayer provide the only conduits between the two sides. Intriguingly, the structures of the embedded proteins are shaped by lipid-protein interactions. In order to understand and describe these interactions quantitatively, the structures of lipid bilayers of varying lipid compositions must be determined. Neutron diffraction is a powerful tool for this purpose, as we illustrate in this brief report. We show how high instrumental resolution combined with contrast variation by hydrogen-deuterium substitution can yield a wealth of information about the structure of lipid bilayers. As an illustrative example, we present results from bilayer membranes containing cholesterol obtained during the 2004 Summer School on Neutron Scattering held at the NCNR.

The neutron diffraction data are among the first obtained using the Advanced Neutron Diffractometer/Reflectometer (AND/R), which became operational at the NIST Center for Neutron Research (NCNR) in September 2003. The AND/R was designed and optimized to meet the criteria of high resolution and efficiency that the biophysical community has long needed for studies of membrane structure. It was constructed by the Cold Neutrons for Biology and Technology (CNBT) research partnership funded principally by a grant from the NIH National Center for Research Resources awarded to the University of California at Irvine, with the additional support of NCNR, UC Irvine, and the Univ. of Pennsylvania. A highly monochromatic beam ($\Delta\lambda/\lambda$ = 1 % at a neutron wavelength λ of 5 Å), a system of computer driven slits to control the beam collimation and reduce the background caused by spurious scattering, and easy access to either a pencil detector or a 2D position-sensitive detector, are only a few of the merits of the AND/R.

Due to their dual hydrophobic-hydrophilic character, cell membrane lipids organize spontaneously into bilayers, causing the hydrophobic alkyl chains to be hidden in the bilayer center and the polar 'headgroups' to be exposed to water. The deposition of lipids from an organic solution on a solid substrate (silicon, quartz, or glass) generally results in a stack of bilayers aligned parallel to the substrate surface (Fig. 1). The samples used in our study were formed from dimyristoylphosphatidylcholine (DMPC) lipids in mixture with 0.20 mole fraction of cholesterol. Cholesterol, an essential component of mammalian membranes, participates in many physiological processes and plays an important role in organizing other lipids and membrane proteins. There is increasing evidence that it can associate preferentially with saturated lipids to form ordered domains called "rafts". These are believed to play an important role in signaling across cell membranes [1].

The usefulness of neutron diffraction for studies of DMPC-cholesterol and other membranes arises because membrane lipids and the surrounding water are rich in hydrogen atoms that can be selectively replaced with deuterium without changing the structure of the membrane. Because deuterium nuclei coherently scatter neutrons much more strongly than protons, this selective deuteration allows the deuterated atoms to be readily identified, as described below.

The structural information sought in our experiments was the scattering profile of the DMPC-cholesterol bilayers. Such profiles show how the lipid mass (scattering length density) is distributed across the thickness of the membrane. Specular diffraction on oriented lipid multilayers, (i.e. diffraction where the beam incident and emergent angles relative to the sample surface are equal), produces a diffraction peak at Bragg angles θ given by $n\lambda = 2d\sin(\theta)$, where n is the (integer) order of diffraction, and d the spacing of the layers. $Q_z = 2\pi/d$ is the scattering wavevector (Fig. 1).

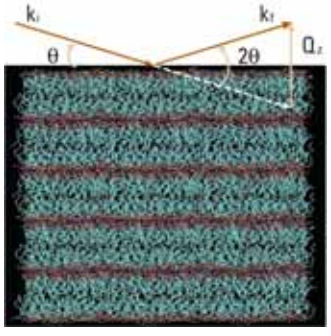

FIGURE 1:
A Molecular Dynamics simulation snapshot, performed for a stack of dioleoylphosphocholine bilayers at 66 % relative humidity, and T = 300 K. The incident (k_i) and emergent (k_f) neutron wave-vectors, and their resultant ($Q = Q_z$), are displayed, as in a specular set-up. Image courtesy of Francisco Castro-Román and Ryan Benz (University of California at Irvine).

In our experiments, the DMPC lipids were deuterium-labeled near the ends of the alkyl chains. A system of 4000 bilayers deposited on a thin glass slide was mounted vertically in the beam in a sealed sample chamber at room temperature and a controlled relative humidity of 66 %. Fig. 2 shows two sets of diffraction patterns collected in a specular set-up for two water-contrast conditions: 100 % H_2O and a mixture containing a 0.50 mole fraction of D_2O.

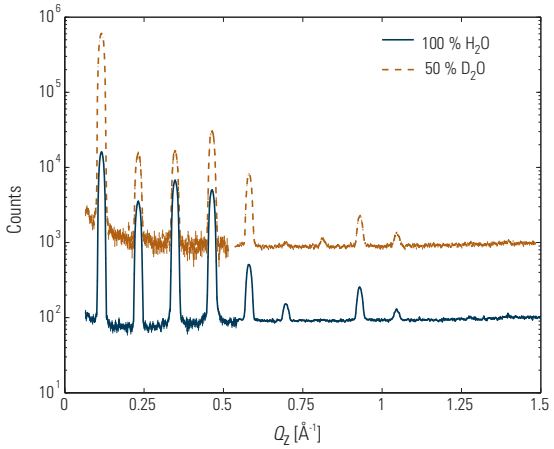

FIGURE 2:

The specular scattering intensities for oriented multilayers of DMPC + 0.20 mole fraction of cholesterol, measured at 66 % relative humidity and T = 22 °C, in two water contrast conditions. The data sets have been shifted vertically for better visibility.

The Fourier synthesis from all of the nine diffraction orders observed, in the first Born approximation [2], results in the density profile displayed in Fig. 3. The phase assignments for each diffraction order were determined from additional water contrast variation experiments [3]. A lipid bilayer is a thermally disordered system [4] (each atom will have a Gaussian distribution around its mean position in the bilayer). Nevertheless, a stack of bilayers has long-range order over experimentally accessible length scales, as is evident from the strong Bragg peaks in Fig. 2.

Previous work has shown that cholesterol increases the ordering of lipid alkyl chains within the bilayers of saturated lipids [2], but the mechanism of this ordering effect is still not very clear. The 9 orders of diffraction allow significant structural features of the bilayer to be resolved, such as the position and extension of the different submolecular groups (Fig. 3). At equilibrium, a few molecules of water are associated with the lipid polar headgroups. Therefore, replacing H_2O by D_2O in the vapor inside the sample chamber will alter the scattering-length density profile along the lipid axis (note the increase in the scattering length density close to the lipid headgroup, which peaks at position z = 27 Å, relative to the bilayer center). The bilayer thickness, as determined from the position of the diffraction maxima, is d = 54.1 Å, including the water associated with the lipid. The prominent feature appearing in the middle of the hydrocarbon region, located at 5.2 Å from the bilayer center, is due to the presence of the deuterium label near the end of the DMPC alkyl chains. Deuterium labeling at different positions along the lipids would allow determination of the positions of specifically-labeled atoms in the bilayer with a resolution of better than 1 Å.

Future experiments should reveal the exact position of cholesterol in the bilayer, the packing conformation of lipids in the presence of cholesterol, and ultimately the interplay between geometrical constraints and molecular interactions that drives the preferred association of cholesterol with certain lipids.

The Advanced Neutron Diffractometer/Reflectometer adds a powerful new instrument for structural investigations of materials at nanoscopic scales. The structural information obtained can be used in concert with molecular dynamics simulations to arrive at unprecedented dynamic structural models of lipid membranes.

We thank Prof. Stephen White for his valuable comments.

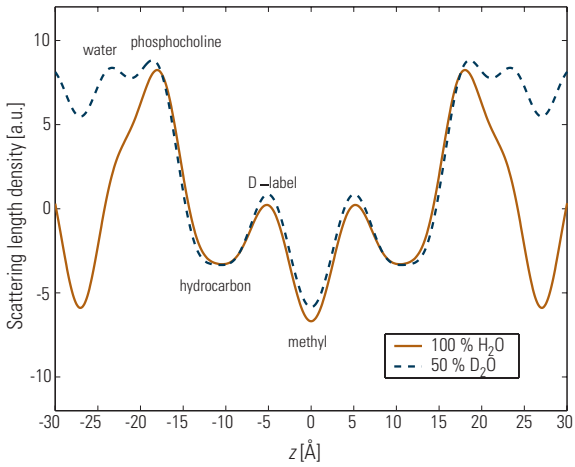

FIGURE 3:

Scattering-length-density profile for a bilayer of DMPC (deuterated near the end of the alkyl chains) in mixture with a 0.20 mole fraction of cholesterol, for two water contrast conditions: 100 % H_2O and a mixture containing 0.50 mole fraction of D_2O.

References:

[1] T. J. McIntosh, A. Vidal, S. A. Simon, Biophys. J. **85** (3), 1656, (2003).

[2] D. L. Worcester, and N. P. Franks, J. Mol. Biol., **100**, 359 (1976).

[3] D. Worcester *et al.*, *in preparation.*

[4] S. H. White and M. C. Wiener In: *Permeability and Stability of Lipid Bilayers*, edited by E. A. Disalvo and S. A. Simon, Boca Raton: CRC Press, pp. 1-19 (1995).

Protein-Solvent Coupling and Dynamics in Unary and Binary Glasses

J. E. Curtis, A. Pivovar and D.A. Neumann
NIST Center for Neutron Research
National Institute of Standards and Technology
Gaithersburg, MD 20899

M. Cicerone and C. Soles
Polymers Division
National Institute of Standards and Technology
Gaithersburg, MD 20899

D. J. Tobias
University of California at Irvine
Irvine, CA 92697

Proteins are ubiquitous high molecular weight heterogeneous polymers. Besides their obvious importance in nature, protein-based pharmaceuticals are quickly becoming a major fraction of all drugs manufactured in the world [1]. Unlike small organic molecules that are often formulated into crystalline forms, proteins are labile molecules that are typically preserved in an amorphous state to maintain the native fold and functionality over long periods of time. Attaining a vitreous state does not guarantee the stability of a protein, as specific interactions between the protein and the matrix are known to reduce the effectiveness of a given formulation [1]. Thus, understanding the molecular details and dynamics of proteins in the amorphous state is an important research challenge.

Only a few techniques exist that can even crudely probe protein structure and dynamics in the amorphous state. Fortunately, neutron scattering is proving to be a powerful method to quantitatively measure protein and glass dynamics in native and non-native environments. Molecular dynamics computer simulations, when carried out in concert with high-resolution neutron scattering experiments, can provide a detailed microscopic interpretation to macroscopic observables. This is possible since both time (fs to ns) and length (Å to nm) scales of computer simulation and neutron spectroscopy overlap, thus allowing for the validation of simulation methodologies and force field parameters.

We are applying a combined experimental and computational effort to understand the factors leading to the activation of dynamical modes in proteins. Over the last several years we have gained an understanding of proteins in native environments such as in solution, crystals, or powders [2]. The focus of this research summary is to describe results regarding the dynamics of proteins encased in unary or binary glasses. This is the first step to elucidate the factors that are necessary to allow for the intelligent design of pharmaceutical formulations based upon microscopic dynamical information.

There are many potential ingredients that can be used in the formulation of proteins including buffers, bulking agents, and stabilizers. The proper choice of a formulation is an empirical process that must be determined for each candidate protein drug. Proteins in lyophilized powders are very sensitive to moisture content, thus care must be taken in designing and carrying out experiments in order to mimic industrially relevant conditions.

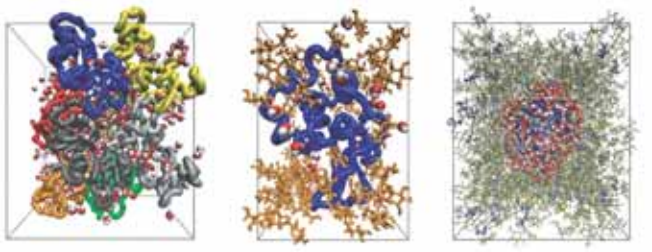

FIGURE 1.

Proteins in native hydrated powder and encased in unary and binary glasses. From left to right: Ribonuclease A (RNase) powder with eight independent protein molecules, lysozyme in a glucose glass, and RNase in a glycerol-trehalose binary glass. Proteins are represented as tubes, water as space-filling red and white solids, and polyols and sugars as stick structures.

In nearly all cases known, water is required for proteins to function by acting as a plasticizer that activates large amplitude motions that allow proteins to attain the appropriate degree of flexibility needed for biological activity. In the context of pharmaceutical applications, water can be detrimental to the long-term stability of proteins. On the other hand, a completely dehydrated protein is also not desirable as this is known to lead to conformations that are deleterious to protein stability; the conformation of the protein is altered due to a lack of satisfied hydrogen bond partners normally provided by water. Thus polyols and disacharrides, both of which contain hydroxide groups, are often used as stabilizers because they can provide the necessary hydrogen bonding to maintain protein structure while at the same time damping the amplitude of protein atom motions.

We have used neutron scattering and other spectroscopic data to validate the simulation of proteins in glycerol, trehalose and glucose unary glasses as well as trehalose-glycerol binary glasses.

Specifically, we are using the High Flux Backscattering Spectrometer (HFBS) and the Fermi-Chopper time-of-flight Spectrometer (FCS) to generate picosecond to nanosecond dynamical data on sugars and proteins in a systematic manner. Both the spatial and time-scale dynamical data are used to validate our molecular simulation methods and force field parameters. Previously, we have discovered that the relaxation of the hydrogen bond network in hydrated protein powders plays a critical role in the activation of large dynamical motions in proteins [3]. In Fig. 2 we show the intermediate scattering function of non-exchangeable protons in the protein ribonuclease A (RNase) in four separate environments as predicted by computer simulation. Proteins relax via fast (sub-picosecond) and slow (> ps) processes. The theoretical curves shown in Fig. 2 indicate that fast dynamics can be suppressed by reducing the hydration level, or by solvating the protein in glycerol or encasing into glucose or trehalose glasses. Interestingly, we find that the slow dynamics is similar for the case of low-hydration powder or encased in glasses. Also in Fig. 2, the role of hydrogen bond network relaxation is shown for RNase A in a hydrated powder or in glycerol. The fast hydrogen bond dynamics, reflected by the time constant tHB, is not affected, while the hydrogen bond network relaxation time, τ_R, clearly diverges at the dynamical transition of either solvent ($T_d(H_2O)$ = 180 K and T_d(glycerol) = 270 K).

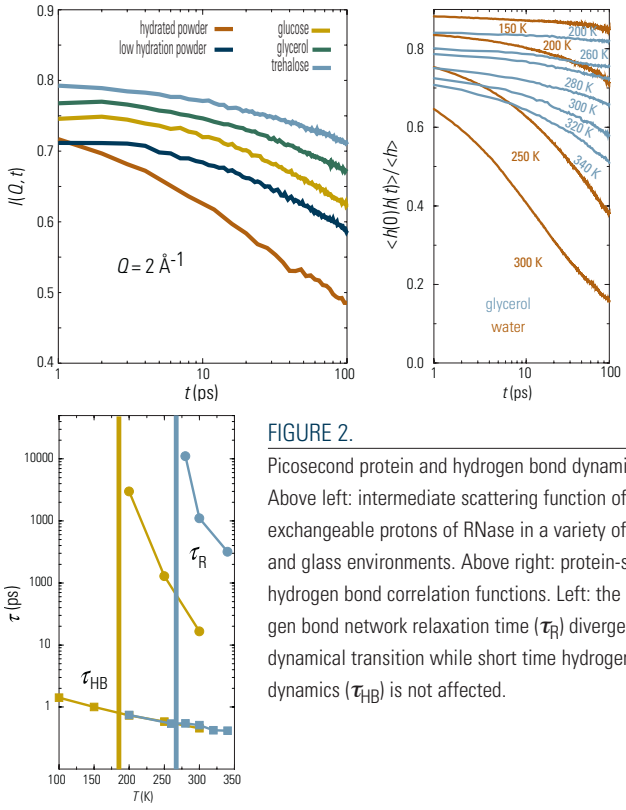

FIGURE 2.

Picosecond protein and hydrogen bond dynamics. Above left: intermediate scattering function of non-exchangeable protons of RNase in a variety of native and glass environments. Above right: protein-solvent hydrogen bond correlation functions. Left: the hydrogen bond network relaxation time (τ_R) diverges at the dynamical transition while short time hydrogen bond dynamics (τ_{HB}) is not affected.

Recently, we have found that the addition of small amounts of glycerol to trehalose to form binary trehalose-glycerol glasses can dramatically reduce the dynamics of the glass. Additionally, we have made a strong correlation between the suppression of fast dynamics and collective motions of the glass to the enhancement of protein stability [4]. We are currently dissecting the precise mechanism of protein stabilization in such glasses by molecular dynamics simulation. As shown in Fig. 3, we have found that the addition of glycerol can significantly reduce the motion of both the trehalose and protein atoms, thus providing direct microscopic connection to support the role of such binary glasses in the stabilization of protein function.

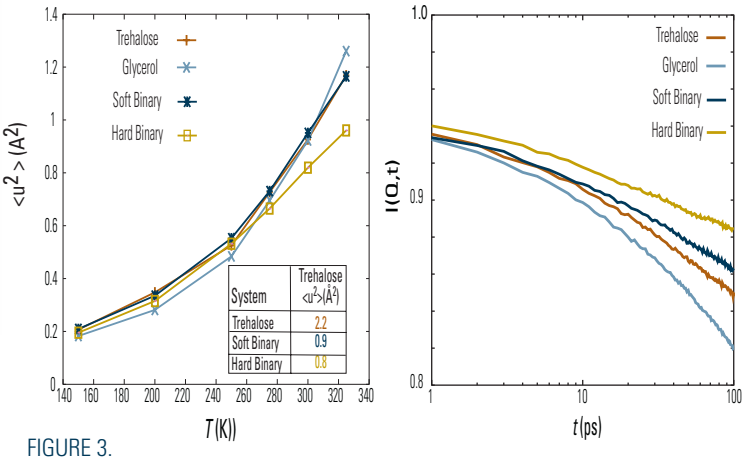

FIGURE 3.

Suppression of protein dynamics in a binary trehalose-glycerol glass. Left: Mean square displacement of non-exchangeable protons of RNase and trehalose (inset) atoms. Right: Intermediate scattering function of non-exchangeable protons of RNase shows that the short-time dynamics is dramatically reduced in the glasses and there is some suppression of picosecond dynamics.

In summary, we have used neutron scattering spectroscopy and molecular dynamics simulations to probe the role of the activation of dynamical motions that could lead to destabilization of proteins in native and non-native environments. Our preliminary results indicate that we can reproduce protein dynamics in a variety of amorphous systems by computer simulation and that a qualitative understanding of protein stabilization in a variety of environments is within reach. Further work to refine the short-time dynamics of proteins in glasses is in progress. We are continuing our joint experimental and computational approach to provide the framework for a systematic study of the microscopic spatial and time-dependent factors that influence the stabilization of proteins.

References

[1] C. J. Roberts and P. G. Debenedetti, AICHE J. **48**, 1140 (2002).

[2] M. Tarek and D. J. Tobias, Biophys. J. **79**, 3244 (2000).

[3] M. Tarek and D. J. Tobias, Phys. Rev. Lett. **88**, 138101 (2002).

[4] M. T. Cicerone and C. Soles, Biophys. J. **86**, 3836 (2004).

Anomalous Hydration Water Dynamics at a Hydrophobic Protein Interface

D. Russo, G. Hura, and T. Head-Gordon
University of California at Berkeley
Berkeley, CA 94720

D. Copley
NIST Center for Neutron Research
National Institute of Standards and Technology
Gaithersburg, MD 20899

Until a critical hydration level is reached, proteins do not function [1]. Restoration of some enzymatic activity is observed in partially hydrated protein powders, which suggests that the dynamical and structural properties of the surface water are intimately connected to protein stability and function. The molecular mechanism of the solvent motion that is required to instigate protein structural relaxation above a critical hydration level or transition temperature has yet to be determined.

Experimental limitations for studying molecular events in the dynamics of the protein water hydration arise from several factors [2]. The highly diluted protein concentrations used mean that the hydration water dynamics is overwhelmed by a bulk water signal. In other cases it is difficult to distinguish between the direct contribution of a specific water-monomer interaction as arising from a hydrophobic, hydrophilic or aromatic site and contributions arising from protein regions more generally exposed to the solvent.

In this work we use quasi-elastic neutron scattering (QENS) to investigate hydration water dynamics near a greatly simplified protein interface. We consider the hydration water dynamics at two protein concentratons (dilute: 0.5 mol/L and high: 2.0 mol/L) near the completely deuterated N-acetyl(d3)-leucine(d10)-methylamide(d3) (NALMA, MW 202.25) solute, a hydrophobic amino acid side chain attached to a polar blocked polypeptide backbone. Previous x-ray scattering experiments [3] focused on structural organization throughout the full concentration range of 0.5 mol/L to 2.0 mol/L. These studies showed that water stabilizes mono-dispersed and small clusters of amino acids, as opposed to more complete segregation of the hydrophobic monomers into a sequestered core. In particular, the 2.0 mol/L data are interesting since we know from the structural work that the solutions organize so that only one water layer separates NALMA solutes, i.e., the experiment unambiguously measures the dynamics of a single hydration layer directly. In contrast, the 0.5 mol/L solute concentration gives information on the water dynamics arising from the outer layers, i.e. only 2 to 3 hydration layers of water per solute are present at the "diluted" concentration.

The QENS experiment was performed at the NCNR using the disk chopper time of flight spectrometer (DCS) at two different incident neutron wavelengths: $\lambda = 7.5$ Å for which the elastic peak energy resolution (full width half maximum (FWHM)) is 35 μeV, and $\lambda = 5.5$ Å for which the resolution is 81 μeV. The resulting data were reduced and analyzed with NCNR's DAVE programs. Measurements were performed at –3 °C, 4 °C, 27 °C and 37 °C for the 2.0 mol/L solution, and 4 °C, 27 °C and 37 °C for the 0.5 mol/L solution [4,5]. The higher resolution experiment primarily measures the slow translational water dynamics, while the lower resolution experiment contains information about both rotational and translational water proton motion. The data from the low-resolution runs were analyzed by including the narrow translational Lorentzian functions based on the high-resolution experiment as known values.

The translational dynamics of water molecules in these biological solutions was analyzed in a first approximation with a jump diffusion model and their rotational dynamics by diffusion on a sphere. At the highest solute concentrations (2.0 mol/L) the hydration dynamics is significantly suppressed and characterized by a long rotational and residential time and a slow diffusion coefficient, similar to supercooled water. At the more dilute concentration solutions (0.5 mol/L) the translational diffusion dynamics is still suppressed, although the rotational relaxation time and residential time converge toward bulk-water values. Fig. 1 displays an Arrhenius plot of the translational diffusion coefficient of hydration water for both concentrations. The 0.5 mol/L concentration data are weakly non-Arrhenius over the temperature range from 4 °C to 37 °C, while the 2.0 mol/L data are clearly super-Arrhenius over the same temperature range. The additional QENS experiment at -3 °C confirms the super-Arrhenius character of the 2.0 mol/L water translational diffusion data. Fits to the experimental intermediate scattering function show non-exponential relations that deviate significantly from normal free diffusion [5].

The corresponding rotational relaxation time, $\tau_{rotation}$, as a function of temperature and concentration is plotted in Fig. 2. The 0.5 mol/L and the 2.0 mol/L rotational data show Arrhenius dependence, in the

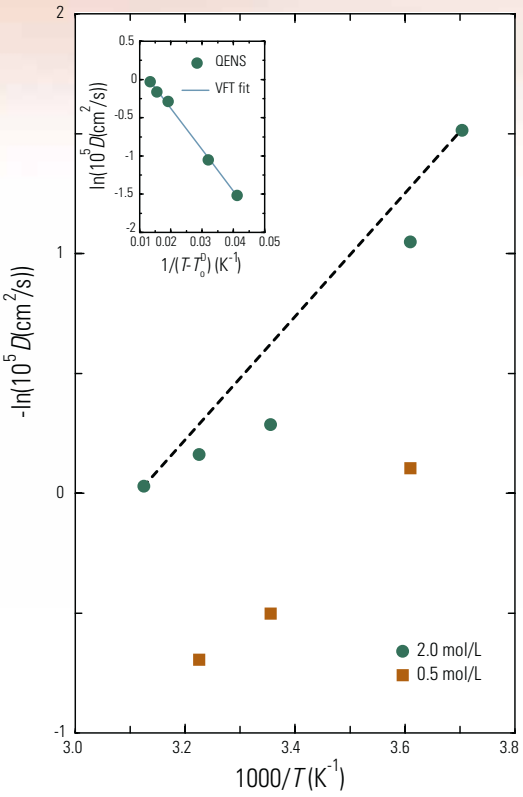

FIGURE 1.

Translational diffusion coefficients for 2.0 mol/L and 0.5mol/L NALMA concentrations. The dashed line represents a guide to the eye for the 2.0 mol/L solution in Arrhenius behavior between an "extrapolated point" at 47 °C and the experimental point at -3 °C. The inset shows the same data plotted using the Vogel-Tammann-Fulcher equation to display deviation from Arrhenius behavior.

investigated temperature range, with activation energies equal to 3 kcal/mol and 1.53 kcal/mol respectively for 0.5 mol/L and 2.0 mol/L NALMA concentrations.

While the lower concentration solution could be classified as an intermediate to strong liquid, the higher concentration is legitimately defined as a fragile liquid. The hydration dynamics of these solutions over the limited temperature range studied exhibit very good correspondence with signatures of slow diffusion, non-Arrhenius behavior and non-exponential kinetics, analogous to what is observed for supercooled water down to -25 °C to -30 °C.

We might speculate that the NALMA solute provides a template or description of different structural domains with different dynamics that might exist in bulk supercooled water. In particular, the NALMA solute provides a spatially heterogeneous environment for its interactions with water. One region permits long-lived hydrogen-bonding with the peptide backbone that nucleates and stabilizes one type of water hydrogen-bonded network. Since no hydrogen-bonding interactions exist for the hydrophobic side chain, a different and dynamically less long-lived water hydrogen bonded water network dynamics is preferred in this second region [3]. Since the water hydrogen-bonded networks in these domains are dynamically and structurally distinct, their close proximity (based on the high concentration and structural organization of these solutions) would introduce an anomaly in the water diffusion at the interface of these domains, requiring a coordination of motion of a number of water molecules to negotiate a mutually agreeable water network interface between them. More work is needed in order to confirm the usefulness of such a hypothesis.

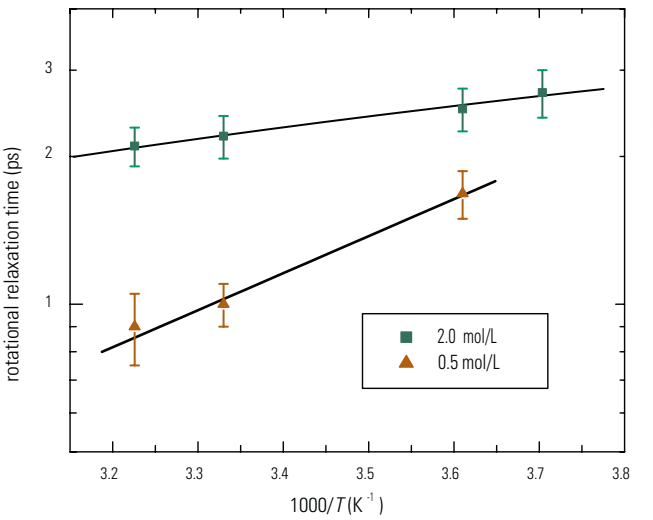

FIGURE 2.

Arrhenius representation of the rotational relaxation time for 2.0 mol/L and 0.5 mol/L NALMA solution concentrations. The straight lines are the best fits to the Arrhenius expression in the investigated temperature range, which give activation energy values of 1.5 kcal/mol and 3 kcal/mol respectively for the low and high concentrations.

References:

[1] J. A. Rupley and G. Careri, Advances in Protein Chemistry **41**, 37, (1991).

[2] D. Russo, P. Baglioni, E. Peroni, J. Teixeira, Chemical Physics **292**, 235, (2003).

[3] G. Hura, J. M. Sorenson, R. M. Glaeser, and T. Head-Gordon, Perspectives in Drug Discovery & Design **17**, 97, (1999).

[4] D. Russo, G. Hura, and T. Head-Gordon, Biophysical Journal **86**, 1852, (2003).

[5] D. Russo, R. M. Murarka, G. Hura, E. Verschell, J. R. D. Copley, and T. Head-Gordon, in preparation.

Fragile-to-Strong Liquid Transition in Deeply Supercooled Confined Water

S.-H. Chen, L. Liu, A. Faraone, C.-Y. Mou and C.-W. Yen
Massachusetts Institute of Technology
Cambridge, MA 02139

Glass is a microscopically disordered, solid form of matter that results when a fluid is cooled or compressed in such a manner that it does not crystallize. Many types of materials are capable of glass formation, such as molecular liquids, polymers, metal alloys and molten salts. Given such diversity, general principles by which different glass-forming materials can be systematically classified are invaluable. One such principle is the classification of glass-formers according to their "fragility". Fragility measures the rate with which a liquid's properties (such as structural relaxation time, viscosity or self-diffusion constant) change as the glassy state is approached from the liquid side.

By convention, the glass transition temperature T_g is where the viscosity reaches a value of 10^{12} Pa s. The approach to this large viscosity, however, differs from one liquid to another. When displayed in an Arrhenius plot of log (viscosity) versus inverse temperature $1/T$, some liquids (such as silica) show a steady, linear increase, while others display a much steeper dependence on $1/T$. The former are 'strong' liquids, and the latter are 'fragile'. Thus, the glassy liquid is called 'fragile' when its viscosity or relaxation time varies according to the so-called Vogel-Tammann-Fulcher (VTF) law: $\tau = \tau_0 \exp[DT_0/(T - T_0)]$, where T_0 is the temperature of apparent divergence of the relaxation time; and the liquid is called 'strong' when the relaxation time obeys the Arrhenius law: $\tau = \tau_0 \exp[E_A/RT]$, where E_A is the activation energy for the relaxation process and R is the gas constant [1].

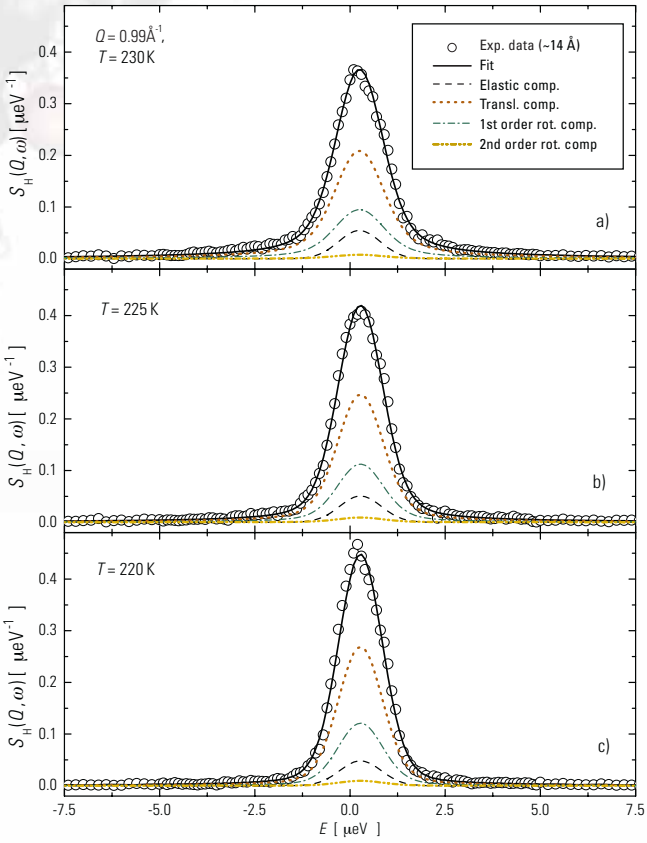

FIGURE 1:

QENS spectra taken at three temperatures, just above, at and below the strong-to-fragile transition together with fits to the data. The continuous thick line represents the result of the fit; the black dashed line is the elastic component; the tan dotted, green dash-dot, and yellow dash-dot-dot lines represent contributions to the scattering from the first three terms of the Sears [6] expansion of rotational relaxation, respectively. Note that the average translational relaxation time is extracted from the tan dotted line.

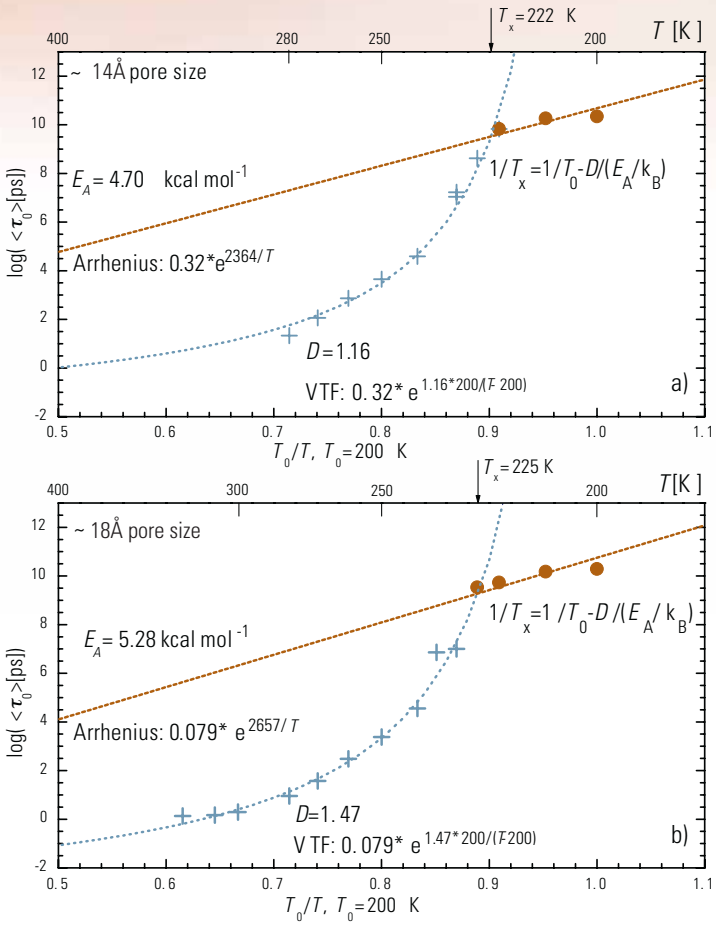

FIGURE 2:

Temperature dependence of the average translational relaxation times, $<\tau_0>$, presented in an Arrhenius plot. In panels a) and b), blue dotted lines are the fit to a VTF law for $T \geq 220$ K and to an Arrhenius law (red straight dashed lines) for $T \leq 220$ K. T_x is the cross-over temperature at which the two lines intersect, which signals the fragile-to-strong transition. Note that ordinate is the natural logarithm of $<\tau_0>$.

For water, which is a fragile liquid at room temperature and at moderate supercooled temperatures, Angell and coworkers [2] proposed that a 'fragile-to-strong' transition would occur at around 228 K, based on a thermodynamic argument. In practice, bulk water nucleates into hexagonal ice at and below $T_n = 235$ K, so the fragile-to-strong transition lies in an inaccessible region of temperatures and it has not been observed up to now [3]. By containing water in small cylindrical pores (pore size less than 20 Å) of MCM-41-S, we have been able to circumvent the homogenous nucleation process and supercool water down to 200 K.

High resolution quasielastic neutron scattering (QENS) was used to detect the fragile-to-strong transition in water by directly measuring the average translational relaxation time of water molecules from 325 K to the deeply supercooled temperature of 200 K. We used the Disk Chopper Spectrometer with 6 Å neutrons at a resolution of 30 μeV and the Backscattering Spectrometer at a resolution of 1 μeV to cover the relaxation time range from 1 ps at high temperatures to 10 ns at the lowest temperature. The QENS spectra were analyzed on an absolute scale using the Relaxing Cage Model (RCM), previously developed by our group [4,5].

Fig. 1 displays the measured spectra just above, at and below the transition together with fits to the data. It is seen that the RCM fits the spectra on an absolute scale. Fig. 2 shows the average relaxation times in an Arrhenius plot. The experimental data show clear cusps at T_x, signaling the fragile-to-strong transition. This is the most direct observation of this amorphous-to-amorphous structural transition reported to date.

We are deeply indebted to Drs. Z. Chowdhuri, I. Peral, and J. Copley for their technical assistance in taking these data.

References:

[1] C. A. Angell, J. Non-Cryst. Solids **131-133**, 13 (1991).

[2] K. Ito, C. T. Moynihan, and C. A. Angell, Nature **398**, 492 (1999).

[3] R. Bergman, and J. Swenson, Nature **403**, 283-286 (2000).

[4] S. H. Chen, C. Liao, F. Sciortino, P. Gallo, P. Tartaglia, Phys. Rev. E **59**, 6708 (1999).

[5] L. Liu, A. Faraone, S. H. Chen, Phys. Rev. E **65**, 041506 (2002).

[6] V. F. Sears, Can J. Phys. **45**, 237 (1967).

Calculations Suggest New Routes Towards High Capacity Hydrogen Storage Materials

J. Íñiguez[1,2], T. Yildirim[1], T. J. Udovic[1], M. Sulic[3]
C. M. Jensen[3]

[1] NIST Center for Neutron Research
National Institute of Standards and Technology
Gaithersburg, MD 20899

[2] University of Maryland
College Park, MD 20742

[3] University of Hawaii
Honolulu, HI 96822

Developing safe, cost-effective, and practical means of storing hydrogen is crucial for the advancement of hydrogen and fuel-cell technologies. The discovery of enhanced reversible hydrogen sorption by Ti-doped alanates [1] opened up an entirely new prospect for lightweight hydrogen storage. However, in spite of the extensive investigations of alanates, little is known about the mechanism by which Ti enhances the cycling kinetics of hydrogen. In fact, even the location of the Ti atoms remains unclear. To shed some lights on these issues, we have studied structure and dynamics of pure and Ti-doped alanates using first-principles quantum calculations and inelastic neutron scattering (INS) techniques [2].

Figure 1 shows the measured vibrational spectrum of sodium alanate, $NaAlH_4$, which exhibits several sharp phonon bands up to 250 meV. In the same figure we also show the calculated one-phonon spectrum, which clearly fails to explain many features in the data. However, including two-phonon scattering processes yields a result that is in excellent agreement with the data. Such strong and sharp multi-phonon contributions are unusual, and could have been easily mistaken as single phonons if we had not had the theoretical results. The calculations also indicate the nature of the different phonon bands in Fig.1. The low energy modes are AlH_4 translations, while those around 50 meV are rotations. The modes above 200 meV are stretching modes of the AlH_4 tetradedron. The modes between 75 meV and 125 meV are mixtures of rotations and stretches.

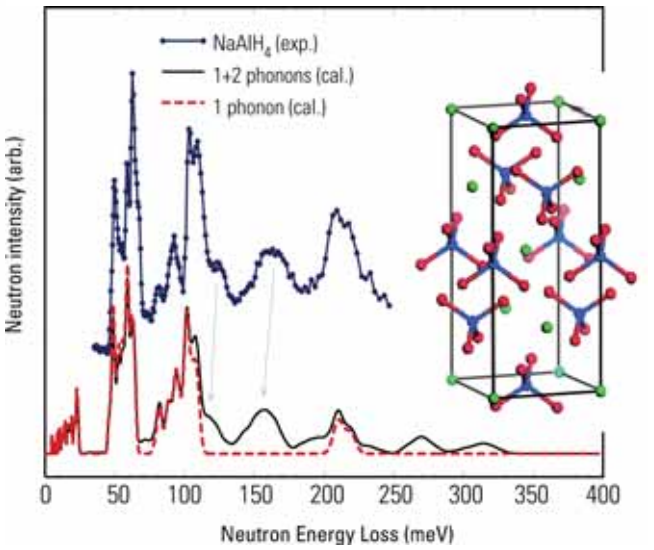

FIGURE 1.

Measured (top) and calculated (bottom) INS spectra of $NaAlH_4$. The calculated 1 and 1+2 phonon contributions are shown. The structure of $NaAlH_4$ is as shown in the inset; blue/red tetrahedra represent AlH_4 units.

The excellent agreement between the neutron data and our calculations suggest that first-principles methods describe the alanate systems accurately and therefore can be used to make predictions. We have extended our calculations to investigate the possibility of substitutional Ti doping of alanates, as well as the effect of the dopant on the surrounding hydrogen dynamics and bonding.

Systems	Ti→Al	Ti→Na	Ti→Na(H)	Ti→Na+H
E_{coh} (eV)	0.075	0.911	1.316	1.317

TABLE 1.

Calculated atomic cohesive energies per 96-atom unit cell for different doped systems. The result for pure $AlNaH_4$ (231.922 eV) is taken as the zero of energy.

From the many substitutional and interstitial doping models that could be tried, we chose two that are experimentally motivated, i.e., the substitution of Al and Na by Ti. In the following we denote these doping models by ``**Ti→Al**'' and ``**Ti→Na**'', respectively. We consider supercells containing 16 $NaAlH_4$ formula units, and substitute only one of the Al or Na atoms by Ti. The cohesive energies are obtained as the sum of the individual atom energies minus the energy of the system (see Table 1). We find both **Ti→Na** and **Ti→Al** are energetically more stable than pure alanate; i.e., the system gains energy by accepting a Ti dopant into the bulk and releasing a Na or Al atom. In addition, **Ti→Na** is found to be the most favorable substitution.

It may seem surprising that Ti→Na has a higher cohesive energy than Ti→Al. The typical valences of these atoms certainly suggest otherwise. However, Ti seems to be relatively large for the Al site. This size mismatch is the most likely cause for Ti→Al to be energetically less favorable.

The relaxed Ti→Na structure presents H atoms that come close to the Ti dopant. The shortest Ti—H distance is 2.05 Å, compared with the 2.39 Å Na—H distance in the pure system. This result suggests that Ti dopants may facilitate the breaking of the Al—H bond. We explored this possibility by moving one H atom to the immediate vicinity of the dopant and then relaxing the system. The resulting structure (see Fig. 2), which we denote by ``Ti→Na (H)'', is considerably more stable than the original Ti→Na doping model. In fact, we found that it has not one but two H atoms very close to the Ti. The shortest Ti—H distance is 1.81 Å, and the corresponding Al—H distance is 1.89 Å, i.e. 0.25 Å longer than in pure $NaAlH_4$. Thus the Ti dopant can indeed induce Al—H bond breaking, a necessary step for H_2 release.

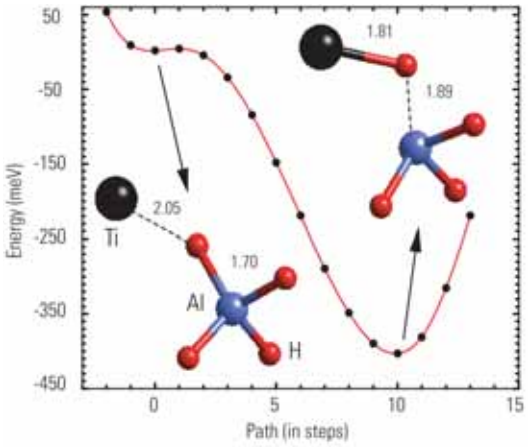

FIGURE 2.

Energy along the pathe from Ti→Na to Ti→Na (H) structures. Insets show local structure and bond distances at the two minima.

Along these lines, we also considered a less obvious possibility, namely, that Ti drags extra hydrogens into the system. We model this case by placing one extra H in the vicinity of the Ti atom. This structure, which we denote by "Ti→Na+H " in Table 1, turns out to be the most stable of the doped systems considered. We find a Ti—H bonding distance of 1.82 Å and several AlH_4 groups approaching the Ti dopant.

Finally, we study the effect of the Ti dopants on the vibrational spectrum of neighboring AlH_4 groups. We find that the Ti dopant mainly affects the high-frequency modes near 200 meV, i.e. those involving stretching of the AlH_4 tetrahedron. All the modes in that group soften differently for the Ti→Na and Ti→Al cases. This suggests that, by investigating the phonon spectrum of Ti-doped $NaAlH_4$, one might determine whether Ti dopants go into the bulk of the system and, if so, where they are located. Motivated by this possibility, we measured the phonon spectrum of a 2 % Ti-doped sample, but obtained a result essentially identical to that of the pure alanate shown in Fig.1. However, it should be noted that this does not rule out the possibility of substitutional doping in our sample since the amount of Ti is very small, and thus any dopant-induced feature in the spectrum should also be very small and hard to distinguish from the noise. In addition, the INS spectrum of pure sodium alanate presents significant two-phonon intensity in the 175 meV to 200 meV energy range (see Fig. 1), which makes it difficult to identify fine details. Higher resolution spectroscopic measurements, such as Raman scattering, might help elucidate this issue.

In conclusion, we have used *ab initio* quantum mechanics calculations and inelastic neutron scattering measurements to study pure and Ti-doped sodium alanate ($NaAlH_4$), a material that holds great promise for reversible hydrogen storage. The calculations indicate that the Ti dopant prefers to substitute for Na and attracts several hydrogen atoms, softening and breaking the corresponding Al-H bonds. Even more interestingly, we found it energetically favorable for the Ti to drag extra H atoms into the system. These results point to an interesting direction for future research, namely the possibility of producing a new material, sodium-titanium alanate that might benefit from the ability of Ti to accommodate extra hydrogens in its vicinity and thus exhibit improved H-storage capabilities.

References

[1] B. Bogdanovic and M. Schwickardi, J. Alloys Comp. **253**, 1 (1997).

[2] J. Íñiguez, T. Yildirim, T. J. Udovic, M. Sulic, and C. M. Jensen, Phys. Rev. B Rapid Com. (in press, 2004).

Annealing-Dependent Magnetic Depth Profile in $Ga_{1-x}Mn_xAs$

B. J. Kirby
University of Missouri
Columbia, MO 65211

J. A. Borchers and K. V. O'Donovan
NIST Center for Neutron Research
National Institute of Standards and Technology
Gaithersburg, MD 20899

J. J. Rhyne
Los Alamos National Laboratory
Los Alamos, NM 87545

S. G. E. te Velthuis and A. Hoffmann
Argonne National Laboratory
Argonne, IL 60439

T. Wojtowicz
University of Notre Dame
Notre Dame, IN 46556 and
Inst. of Physics of the Polish Academy of Sciences
02-688 Warsaw, Poland

X. Liu, W. L. Lim, and J. K. Furdyna
University of Notre Dame
Notre Dame, IN 46556

The continued growth in speed and density of semiconductor circuits has revolutionized data processing in recent decades. Simultaneously, enormous improvements in magnetic media have dramatically increased permanent data storage capabilities. An emerging technology called "spintronics" [1] integrates magnetic components with semiconductor devices and has the potential to dramatically increase data processing capabilities. The function of these magnetoelectronic devices, which include spin-valve transistors, spin light-emitting diodes, and non-volatile memory, requires the transfer of spin-polarized electrons across interfaces between ferromagnets and semiconductors.

Ferromagnetic semiconductors are very effective as spin injectors because of their good conductivity match with nonmagnetic semiconductors. Recent research has focused on a new magnetic semiconductor, $Ga_{1-x}Mn_xAs$ [2], which has a ferromagnetic ordering temperature (T_C) exceeding 150 K for $x \approx 0.7$ [3]. The ferromagnetic behavior in this material originates from coupling between Mn ions substituting for Ga. These substitutional Mn (Mn_{Ga}) ions act as acceptors, generating holes that mediate the ferromagnetic exchange. However, Mn_{Ga} ions are known to be partially compensated by Mn at tetrahedral interstitial sites (Mn_I). Mn_I ions are double donors, and neutralize holes needed for the ferromagnetic exchange. Additionally, calculations suggest that Mn_I align antiferromagnetically with neighboring Mn_{Ga}, effectively negating their moments. It is well established that low temperature post-growth annealing of $Ga_{1-x}Mn_xAs$ films can serve to significantly raise T_C and increase the magnetization, both phenomena being likely due to the redistribution of Mn_I [4].

To determine the actual effects of annealing, we examined the magnetic and structural depth profiles of as-grown and optimally annealed $Ga_{1-x}Mn_xAs$ thin films grown by molecular-beam epitaxy on GaAs substrates [5]. We focus here on a set of films with a $Ga_{1-x}Mn_xAs$ layer thickness of 115 nm and a nominal Mn_{Ga} concentration $x = 0.073$. One film was annealed in N_2 for 1 hour at 280 °C, while the other film was left alone. Resistivity measurements indicate that T_C increases with annealing by more than 70 K.

We probed the films with polarized neutron reflectometry (PNR) using the NG-1 Reflectometer at the NCNR. A magnetic field of $H = 0.1$ T was applied in-plane and then the sample was zero field cooled to 13 K to bring the samples near magnetic saturation. Information about the samples was then determined by fitting the measured reflectivity with a depth-dependent scattering length density (SLD) model. The SLD model can be separated into two components. The nuclear SLD, $\rho_{nuc,}$ is sensitive to changes in the chemical structure of the film, while the magnetic SLD, $\rho_{mag,}$ is proportional to the film magnetization.

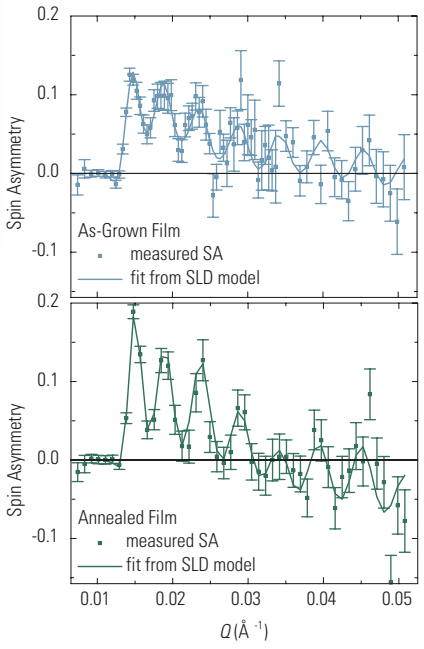

FIGURE 1.
The measured spin asymmetries for each 115 nm film, along with the fits from the corresponding SLD model.

We measured both non-spin-flip (NSF) reflectivities and spin-flip (SF) reflectivities for the 115 nm as-grown and annealed films. The SF reflectivity was determined to be near the background level. Since SF scattering is sensitive to the component of the film's magnetic moment perpendicular to ***H***, we detect no evidence of moment canting. The splitting between the NSF scattering reflectivities, $R_{++}(Q)$ and $R_{--}(Q)$, is due to the component of each film's magnetization parallel to ***H***, with the magnitude of the splitting being indicative of the magnetization at a particular length scale. The spin asymmetry, $SA(Q)=[R_{++}(Q) - R_{--}(Q)]/[R_{++}(Q) + R_{--}(Q)]$, best accentuates this splitting. The measured *SA* and fits for the 115 nm as-grown and annealed films are shown in Fig. 1. The peak amplitudes of the SA at low *Q* are determined primarily by the magnitude of the bulk magnetization of the film and show an increase upon annealing, giving the result that more of the Mn are participating in the ferromagnetic exchange after annealing. Additionally, the spin asymmetry for the annealed film displays sharper oscillations than those for the as-grown film. Since a smearing of the oscillations can be indicative of roughness, these data qualitatively suggest that the annealed film has a more uniform magnetization than the as-grown film.

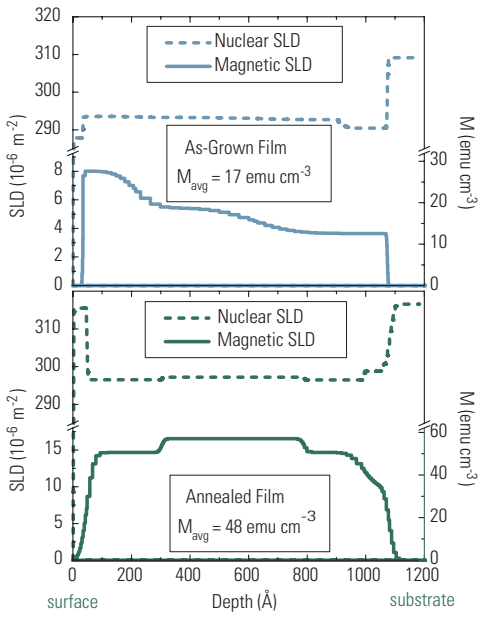

FIGURE 2.
Scattering length density models for each 115 nm film. The magnetization is proportional to the magnetic component, and is shown on the right.

The structural and magnetic depth profiles for the annealed and as-grown films obtained from the fits to the reflectivity data are shown in Fig. 2. The differences between them can be interpreted by considering the unique signature that Mn leaves on both the nuclear and magnetic SLD profiles. Since Mn has a negative scattering length, a decrease in ρ_{nuc} implies an increased concentration of Mn (and vice-versa). Since Mn_{Ga} should be the only atom in this system contributing to the ferromagnetic exchange, an increase in ρ_{mag} implies an increased concentration of Mn_{Ga} *uncompensated* by Mn_I (and vice versa). Therefore, any non-uniformity in the profiles can be attributed to variations in Mn concentration and/or site occupation.

Starting at the substrate of the as-grown film, the top panel of Fig. 2 shows that ρ_{nuc} decreases as ρ_{mag} increases, indicating an increase in Mn concentration at the substrate interface. Above that interface, ρ_{mag} climbs and shows a pronounced gradient as the surface is approached. In this same region, ρ_{nuc} shows little change, suggesting that the magnetization gradient is not due to a change in Mn concentration, but possibly to an increase in the ratio of Mn_{Ga} to Mn_I. (While the best fit is shown, models with ρ_{mag} gradients that extend over smaller regions also fit the data reasonably well.)

In comparison with the as-grown film, the annealed film's magnetic SLD profile is more uniform for most of its thickness. Starting at the substrate, the bottom panel of Fig. 2 shows a buildup of Mn, and an increase in ρ_{mag}. While this increase in ρ_{mag} is somewhat rough, these data cannot support a gradient in ρ_{mag} of the magnitude featured in the model shown for the as-grown film. At about 90 Å from the surface, ρ_{mag} drastically drops as ρ_{nuc} rises, all the way to the surface. One interpretation of this feature is that the surface layer has little to no Mn present. However, recent measurements [3] provide evidence of *increased* Mn concentration at the free surface of annealed $Ga_{1-x}Mn_xAs$ films, which is attributed to out-diffusion of Mn_I. Therefore, it is possible that MnN or a related compound may have formed at the surface during annealing in nitrogen.

PNR data and the SLD models for a thinner set of 55 nm as-grown and optimally annealed films are similar. The annealed film again exhibits a pronounced magnetization depletion, and drastic increase in ρ_{nuc} at the surface, while again only the as-grown film features a significant positive gradient of magnetization as the surface is approached.

To summarize, we have found that low temperature post-growth annealing in $Ga_{1-x}Mn_xAs$ films not only serves to increase T_C and the total magnetization, but also produces a more homogeneous distribution of magnetization as a function of depth. For the annealed films, we observe a sharp drop in the magnetization, and a drastic change in the chemical composition at the film surface, effects that are less pronounced in the as-grown films. This corroborates conclusions from other studies that the annealing process appears to liberate Mn_I and redistribute it, likely to the surface, where it can no longer disrupt the ferromagnetic exchange [3]. Our studies on these materials are ongoing and are now focused on the effects of reduced Mn concentration and of capping layers.

References:

[1] S. A. Wolf, *et al.*, Science **294**, 1488 (2001).

[2] H. Ohno, *et al.*, Appl. Phys. Lett. **69**, 363 (1996).

[3] K. W. Edmonds, *et al.*, Phys. Rev. Lett. **92**, 037201 (2004).

[4] K. M. Yu, *et al.*, Phys. Rev. B **68**, 041308(R) (2003).

[5] B. J. Kirby, J. A. Borchers, K. V. O'Donovan, J. J. Rhyne, S. G. E. te Velthuis, A. Hoffmann, T. Wojtowicz, J. K. Furdyna, and X. Liu, Phys. Rev. B **69**, 081307(R) (2004).

Residual Stresses in an Intact Railroad Rail

V. Luzin[1,2], J. Gordon[3], T. Gnäupel-Herold[1,4] and H.J. Prask[1]

[1] NIST Center for Neutron Research
National Institute of Standards and Technology
Gaithersburg, MD 20899

[2] State University of New York
Stony Brook, NY 11794

[3] Volpe National Transportation Systems Center
Cambridge, MA 02142

[4] University of Maryland
College Park, MD 20742

Residual stresses play an important role in rail integrity and the safety of rail transportation. In this report we describe neutron diffraction strain measurements carried out for the first time to obtain information about the 3D distribution of stresses in an "intact" rail. In contrast to previously reported diffraction experiments made with rail slices, which provided no information on axial stresses, we were able to measure the unperturbed 3D stress distribution. The experiment was performed using the BT-8 residual stress diffractometer at the NCNR and the results provide information critical to improving safety and durability of rails.

In the last decade significant efforts have been made, both experimentally [1-5] and by implementation of numerical methods [6,7], to characterize the residual stresses in rails, stresses that are ultimately related to rail integrity and problems of rail failures. Diffraction techniques using neutrons [1-3] and synchrotron x-rays [4,5] are two methods that have been successfully employed to map residual stress in rail slices, 4 to 10 mm in thickness. However, the axial stress component (perpendicular to the slice surface) is relaxed by the cutting so that only partial information is obtained from slices.

FIGURE 1.
The large rail piece with the position of measurements indicated.

Measurements on an intact piece of rail can only be made using neutron diffraction but have not been made previously because of the high attenuation of the radiation. In the case of a railhead with typical dimensions 75 mm by 50 mm the difference in attenuation conditions between the surface and the deepest points can result in a factor of 1000 in the loss of neutron diffraction peak intensity. Three factors made the present measurements possible: 1) A specially-designed, double-focusing silicon monochromator [8] was installed on the BT-8 instrument; 2) Primary-side collimation was opened to the maximum; and 3) Sample orientations were chosen to minimize path lengths for the three main probe directions.

The rail that was used in the investigation was commercially produced by Rocky Mountain Steel Mills with the specification 132RE. Production steps include a deep head-hardening process and roller-straightening to achieve high hardness of the rail. The samples, a long rail section and slices, were furnished by the High Tonnage Loop facility at the Federal Railroad Administration Transportation Technology Center after subjecting it to multiple 39-ton axle loads.

The length of the bulk sample (Fig. 1), approximately 530 mm, was chosen to preserve stresses intact in the middle part of the rail, as confirmed by a finite element method (FEM) calculation [9]. Because of beam attenuation the selection of the scattering geometry, gauge volume size, and sample orientation with respect to the neutron beam are critical to achieving the desired accuracy of $\Delta d/d = 5 \times 10^{-5}$. In Table 1 the choice of experimental conditions is summarized. The measurement time per point varied from 5 seconds to 8 hours depending on path length and gauge volume.

In order to get strain values from d- values, $\varepsilon = (d - d_0)/d_0$, special measurements were performed to obtain the d_0-value of the unstressed material. Five cubic coupons, 7 mm on a side, were cut by electrical discharge machining from five different locations of the same rail for the d_0 measurements (three in the rail head, one in the web and one in the foot). From the set of strains associated with each mesh point stress tensors were calculated in the usual way [1] using the appropriate diffraction elastic constants for steel. Since the measurement points were always within the material, a simple linear extrapolation was used to define stress values up to the surface for the 5x5 mm experimental mesh.

The second sample was a slice of thickness 6.3 mm saw-cut from the same rail. This piece was examined in order to make a comparison with the 3D stress measurement results. Measurements on the rail slice required only very short path lengths. The (211) reflection was

used, with a scattering angle of $2\vartheta = 90.4^{\circ}$ and a wavelength of $\lambda = 1.67$ Å. The gauge volume was reduced to 3x3x3 mm^3 with a corresponding 3x3 mm mesh. Stresses were calculated with d_0 evaluated from the requirement that the axial (normal) stress component be zero, $\sigma_{33} = 0$. Statistically more reliable results for d_0 values were obtained by averaging data from several slices of the same rail.

Results in the form of stress maps are shown in Fig. 2 for both samples. Four components of the stress tensor are plotted and minimum and maximum values are given. An error analysis based on counting statistics was performed using standard error propagation techniques resulting in typical stress value errors of ± 15 MPa for transverse and vertical components and ± 25 MPa for the axial component in the bulk sample. For the slice sample, stress errors for all components are approximately ± 20 MPa.

	*Exp. Parameters	Sample Orientation	Path Lengths (mm)
axial (*Z*)	2ϑ=60.6°/ λ=1.19Å/ 5x5x5	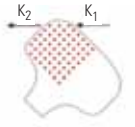	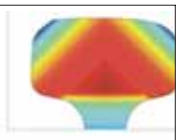
transverse (*X*)	2ϑ=102.4°/ λ=1.83Å/ 5x5x20	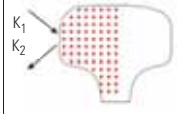	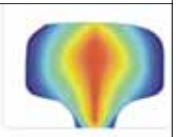
vertical (*Y*)	2ϑ=102.4°/ λ=1.83Å/ 5x5x20	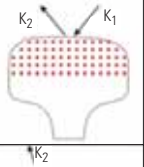	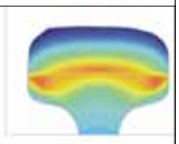
shear (*XY*)	2ϑ=102.4°/ λ=1.83Å/ 5x5x20	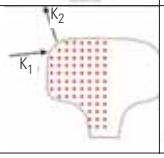	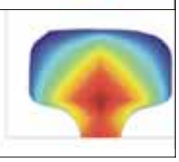

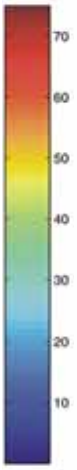

TABLE 1.

Experimental conditions for the measurements of the long rail section.

*Experimental parameters are Bragg's angle, wavelength, and gauge volume.

This is the first time a stress map of the stresses in a long piece of intact rail has been determined by any experimental technique. The 3D stresses in the bulk sample have been compared with the 2D stresses in a slice sample from the same rail. Transverse, vertical and shear stresses for the long rail piece and the slice are similar but not identical, as one would expect. No information about axial stresses comes from the measurement on a single slice. For the axial component we find that there is an area of tensile stresses in the central core of the rail surrounded by an area of moderately compressive stresses. In contrast with the highly compressive transverse stresses (at the top) and vertical stress (at the sides) there is no area of highly compressive

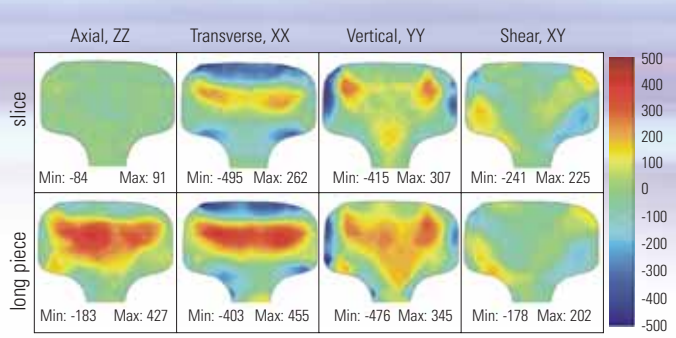

FIGURE 2.

Stress maps [MPa] for the two investigated samples.

axial stresses. Since axial stresses must balance over a plane normal to the axis, the overall tensile axial stress in the railhead must be balanced by compressive stress in the web and foot. Measurements in these regions have not yet been completed for the long rail piece. However, early measurements on longitudinal rail slices [3] and recent results using the contour method [10] indicate that regions of high compression occur in the axial direction in both the web and the foot.

In summary, the economic importance of rail integrity dictates that monitoring techniques for residual stress such as destructive sectioning/slicing methods need a clear benchmark against which their accuracy and reliability can be judged. In the present work the first nondestructive determination of the triaxial stress distribution in an intact rail piece is presented. These results provide such a benchmark.

References

[1] T. Gnaupel-Herold, P. C. Brand, H. J. Prask, "*Neutron Diffraction Investigation of Residual Stresses in Transverse/Oblique Rail Slices Subjected to Different Grinding Strategies*", NISTIR 6305, U.S. DOC, Tech. Administration, 1999.

[2] G. A. Webster *et al.* in Residual Stresses in *Rails: Effects of Rail Integrity and Railroad Economics*, Vol. I, 1992, O. Orringer *et al.* eds., Kluwer Acad. Publ., Dordrecht, Boston, London, pp. 143-152.

[3] P. J. Webster, G. Mills, X. Wang and W. P. Kang in (Rail Quality and Maintenance for Modern Railway Operation), 1993, J. J. Kalker *et al.* eds. Kluwer Acad. Publ., Dordrecht, Boston, London, pp. 307-314.

[4] D. J. Buttle *et al.*, Mater. Sci. Forum Vols. 404-407 881 (2002).

[5] P. J. Webster *et al.*, pp. 767-772 of reference 4.

[6] J. Orkisz and M. Holowinski, pp. 273-285 of reference 3.

[7] A. B. Perlman and J.E. Gordon, in Vol. 2 of ref. 2, pp. 151-177.

[8] M. Popovici *et al.*, Neutron Optics 4509, **21** (2001).

[9] B. Talamini and J.E. Gordon, to be published.

[10] J. Keleher *et al.*, Proc. of the MECA-SENS Conf., Manchester, England (2003).

Residual Stresses in Thin Sheet Metal

T. Gnäupel-Herold and H. J. Prask
NIST Center for Neutron Research
National Institute of Standards and Technology
Gaithersburg, MD 20899

L. Levine, R. Fields and T. Foecke
Metallurgy Division
National Institute of Standards and Technology
Gaithersburg, MD 20899

C. Xia
FORD Scientific Research Laboratory
Dearborn, MI 48121

E. Chu
ALCOA Technical Center
Alcoa Center, PA 75069

Due to the increasing need for weight reduction in the automotive industry there is a major shift underway to use thinner high strength steels and aluminum alloys in car body parts. One of the major problems associated with this shift is increased springback magnitudes because of the lower sheet thickness, increased residual stresses in high strength steels, and low elastic modulus in aluminum alloys. These stresses were measured on standard springback test specimens using neutron diffraction with a level of spatial resolution previously thought to be not viable for neutrons. The results provide essential data for the validation of computer modeling of springback.

Springback is the elastic shape change of sheet metal parts after a forming operation, e.g. the removal of the stamping tool. It is caused by residual stresses that are invariably produced by all forming processes. Until recently [1,2], the distribution of these stresses was largely unknown which was a serious impediment for predicting springback accurately. In order to improve the accuracy of springback modeling the automotive companies are developing a comprehensive 3D computer model to predict stress, strain and fracture in sheet metal, with the goal of a significant reduction in tool design time. The measurement of springback stresses plays an important role in this project as they provide the necessary data to evaluate the computer model.

The task of measuring stresses through a sheet thickness of ≈ 1 mm at 8 to10 locations by means of diffraction requires a spatial resolution, or, in other words, a beam size of the order of ≈ 0.1 mm with a corresponding gage volume size of ≈ 0.1 mm^3. Ordinarily, such a measurement is beyond the capabilities of neutron diffraction that typically requires a minimum gage volume of ≈ 1 mm^3 due to the low intensity scattered from such a small volume. However, sheet metal always exhibits preferred orientation, hence enabling measurements with strongly increased intensity in certain directions. The size of the gage volume can be decreased in proportion to the increase in the number of non-randomly oriented crystallites. Typical increases are from 3 to10-fold, thus allowing a spatial resolution that is normally available only with synchrotron radiation. For some coarse-grained aluminum alloys neutron diffraction is preferable to synchrotron radiation diffraction where the typical gage volume is of the order of ≈ 0.001 mm^3. Such a small gage volume severely limits the attainable grain statistics, which decreases the accuracy of the measured strains.

The prerequisite for using very small gage volumes is the knowledge of the directions within the specimen reference frame that are associated with high scattered intensity. These directions (rolling direction RD, and transverse direction TD) can be directly obtained from pole figures. This is shown in Fig.1, as an example, for the most commonly used reflections (hkl) for the bcc lattice (steel) and the fcc lattice (aluminum).

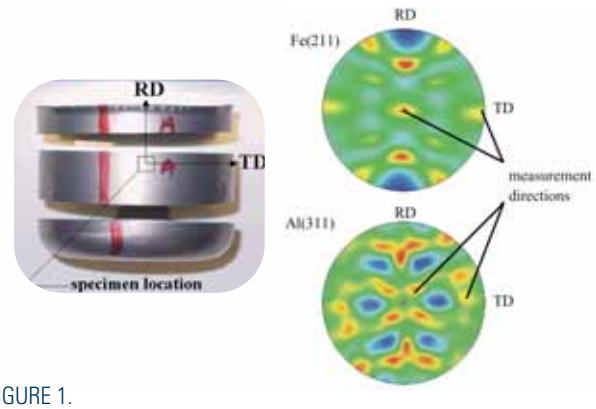

FIGURE 1.

Pole figures for the (211) reflection of steel and for the (311) reflection of aluminum. The samples were taken from the mid-section of a deep drawn cup, which is suggested as a standard specimen for springback testing. The center of the pole figures corresponds to the direction normal to the surface.

The residual stress measurements in Fig. 2 and Fig. 3 reveal the general similarity between through-thickness stresses for steel and aluminum for identical forming parameters. However, the materials have vastly different yield strengths (Al6022: $\sigma_{0.2}$ = 160 MPa; BH33: $\sigma_{0.2}$ = 330 MPa) which cause large differences in the peak stresses. ($\sigma_{0.2}$ is a yield strength at 0.2 % permanent strain.)

Early finite element methods (FEM) -models for springback prediction were based on the assumptions that the through-thickness stress profiles are independent of the axial and circumferential positions. However, the analysis of the stress data and the comparison with step-by-step refined FEM modeling showed that the accuracy of the springback prediction can be improved by incorporating data, both on the vertical dependence of springback and on local variations of plastic anisotropy, into the model as shown in Fig. 4. Plastic anisotropy is described by means of the ratio of the two plastic strains perpendicular to the RD- direction (R-values). The R-value, in turn, is closely correlated with preferred grain orientation in the sheet material.

In summary, by utilizing the texture inherent in stamped sheet metal it has been possible to achieve new levels of spatial resolution with the neutron diffraction residual stress measurement technique. As a result, residual stresses have been measured which provide a means for validation of critical details of springback model predictions.

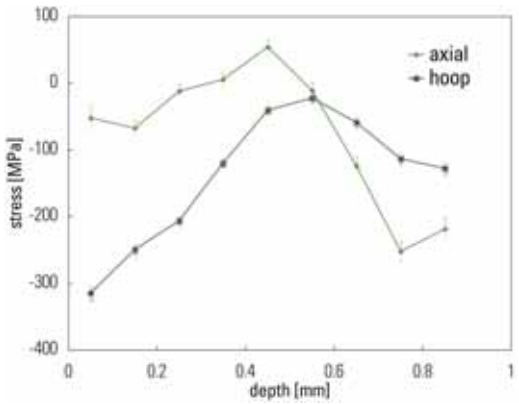

FIGURE 2.

Through-thickness stresses in the mid-section of a cup made of a BH33 bake-hardenable steel. The wall thickness is 0.95 mm.

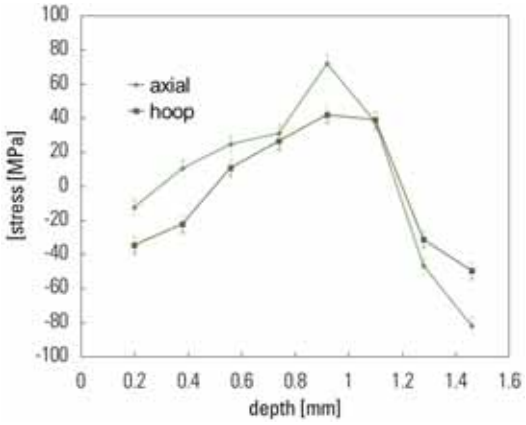

FIGURE 3.

Through-thickness stresses in the mid-section of a cup made of Al6022-T4 with a wall thickness of 1.6 mm

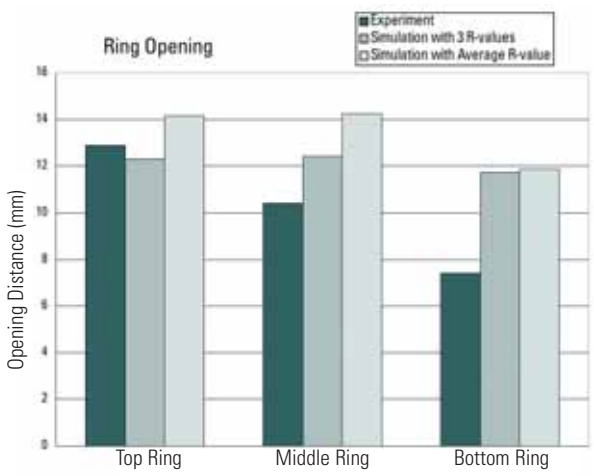

FIGURE 4.

Comparison of springback measurement and prediction for different vertical positions on a AISI1010 deep drawn cup. Predictive improvements are achieved using local values of the plastic anisotropy factor.

References

[1] T. Gnaeupel-Herold, H.J. Prask, R. J. Fields, T. J. Foecke, Z. C. Xia, U. Lienert, Mat. Sci. Eng. A**366**, 104 (2004).

[2] T. Gnaeupel-Herold, T. J. Foecke, H. J. Prask, R. J. Fields, submitted for publication in Mat. Sci. Eng. A.

Competing Magnetic Phases in the "Kagomé Staircase" Compounds $(Ni,Co)_3V_2O_8$

G. Lawes[1], M. Kenzelmann[2,3], N. Rogado[4], K. H. Kim[1], G. A. Jorge[1], R. J. Cava[4], A. Aharony[5], O. Entin-Wohlman[5], A. B. Harris[6], T. Yildirim[3], F. M. Woodward[3], Q. Z. Huang[3], S. Park[3,7], C. Broholm[2,3], A. P. Ramirez[1,8], and J. W. Lynn[3]

[1] Los Alamos National Laboratory
Los Alamos, NM 87544

[2] Johns Hopkins University
Baltimore, MD 21218

[3] NIST Center for Neutron Research
National Institute of Standards and Technology
Gaithersburg, MD 20899

[4] Princeton University
Princeton, NJ 08544

[5] Tel Aviv University
Tel Aviv 69978, Israel

[6] University of Pennsylvania
Philadelphia, PA 19104

[7] University of Maryland
College Park, MD 20742

[8] Bell Labs, Lucent Technologies
Murray Hill, NJ 07974

Geometrical magnetic frustration leads to unusual low temperature spin order and dynamics and presents new challenges for the theoretical understanding of magnetic systems. Frustrated materials are often characterized by triangle-based lattices and short-range antiferromagnetic (AF) interactions. Of particular interest has been magnetism on the two-dimensional (2D) kagomé lattice, which consists of corner-sharing triangles. Materials that approximate the kagomé AF can be expected to lie close to a quantum critical point, making their properties particularly sensitive to small perturbations of the symmetry and interactions.

Here we present our theoretical and experimental results on the magnetic phase diagrams of $Ni_3V_2O_8$ (NVO) and $Co_3V_2O_8$ (CVO), where the Ni^{+2} (Co^{+2}) S = 1 (S = 3/2) spins form the orthorhombic kagomé staircase structure shown in Fig. 1. The buckling of the quasi-kagomé planes gives rise to a high degree of anisotropy and leads to a rich variety of magnetic phases. These systems are particularly attractive because their complexities can be understood on the basis of an embellished kagomé spin Hamiltonian. Although the symmetries of the $(Ni,Co)_3V_2O_8$ compounds are identical they exhibit quite different phase diagrams, which behavior originates from small quantitative changes in the parameters that dictate the manner in which the frustration is relieved.

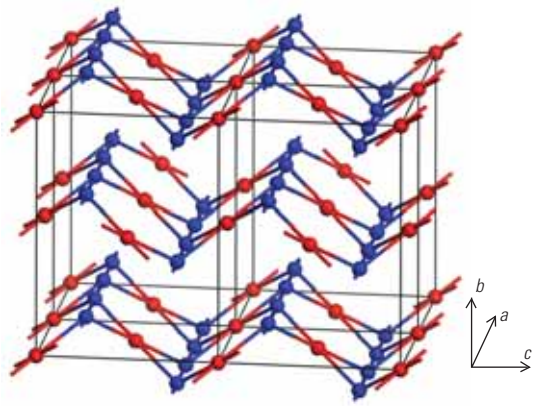

FIGURE 1.

The buckled kagomé structure of $(Ni,Co)_3V_2O_8$, showing the cross-tie (blue) and spine (red) spin sites.

Initial powder diffraction results for $Co_3V_2O_8$ indicated relatively straightforward behavior, where the system first orders at 11.2(2) K into an incommensurate spiral spin structure but then locks into a simple ferromagnetic ground state at 6.1 K. Single crystal diffraction data, on the other hand, reveal a much richer complexity of incommensurate magnetic phases interspersed with phase-locked regimes,

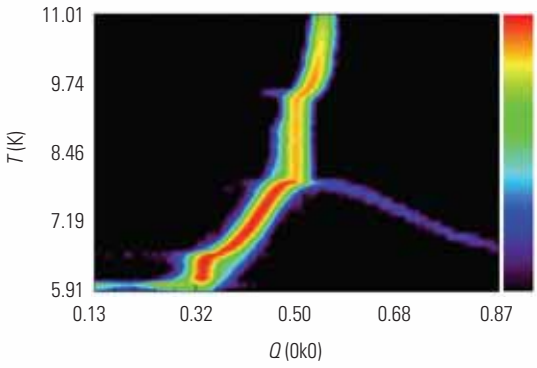

FIGURE 2.

Temperature evolution of the (0,δ,0) magnetic peak in $Co_3V_2O_8$, indicating a succession of incommensurate magnetic phase transitions intertwined with lock-in to commensurate wave vectors.

as readily visible in the data shown in Fig. 2. There are at least six separate phases; the paramagnetic phase (PM) above 11 K described by the nuclear C*mca* structure, the ferromagnetic (FM) ground state below 6 K, and four distinct states characterized by the onset of commensurate and incommensurate spiral orderings below 11.2 K.

In comparison with $Co_3V_2O_8$, $Ni_3V_2O_8$ is quite different and even more complicated as shown in Fig. 3. The system is paramagnetic above 9.4 K, then orders in a high-temperature incommensurate (HTI) phase where both the "spine" and "cross tie" spins develop long-range order (the spines along the *a*-axis and the cross ties along the *b*-axis). At 6.4 K a transition to a distinct low-temperature incommensurate (LTI) phase occurs, where the spine spins develop additional long-range order along the *c*-axis. At 3.8 K the system then enters a commensurate antiferromagnetic state that is accompanied by a weak ferromagnetic moment. The magnetic phase diagram for $Ni_3V_2O_8$ is also extremely anisotropic with applied field as indicated in Fig. 3, and the complete details of the field-dependent spin ordering transitions in $Ni_3V_2O_8$ are discussed elsewhere [1].

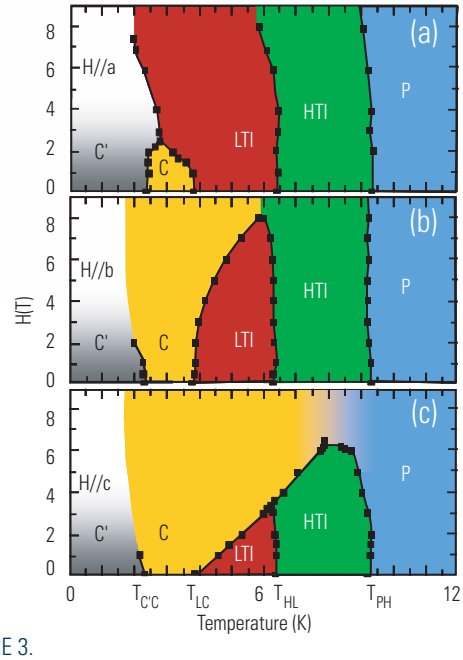

FIGURE 3.

Phase diagram for $Ni_3V_2O_8$ as a function of *T* and *H* applied along the three principal directions.

To interpret these phase diagrams theoretically it is essential to understand the ordered phases that emerge from the kagomé critical state, and symmetry plays the key role in determining these states. Considering the case of NVO, the presence of AF ordering on the spine sites and isotropic nearest-neighbor (NN) interactions produces no net interaction on cross-tie sites, so they are fully frustrated. However, the structural anisotropy of NVO induces interactions not usually considered in other frustrated systems. First, because the NiO_6 octahedra are edge-sharing, the NN Ni-O-Ni bond angle is close to 90° so the NN and next-NN (NNN) Ni-Ni interactions are both weak and similar in strength. Second, the symmetry of the crystal structure admits a Dzyaloshinskii-Moriya (DM) interaction among the NN spine spins. Structural considerations show that the DM interaction for a single spine takes the form $H_{DM} = \Sigma_n (D_c c + (-1)^n D_b b) \bullet (S(n) \times S(n+1))$, where *n* labels the spins consecutively along the spine. D_b gives rise to a linear coupling between the staggered moments of the spine along the *a*-direction and the weak ferromagnetic moment of the spine along ***c***. This weak ferromagnetic moment can induce a ferromagnetic moment along ***c*** on the cross-tie spins via an isotropic Heisenberg exchange. These interactions add to the usual isotropic NN superexchange interaction to produce the observed rich *H-T* phase diagram shown in Fig. 3.

We find for NVO that the spin-structure within the spines is controlled by competing NN and NNN isotropic Heisenberg interactions, denoted J_1 and J_2. A mean field treatment indicates that for $J_2 > |J_1|/4$ the spine Hamiltonian is minimized by a mean field spin modulation with wave vector, *q*, which satisfies $\cos(qa/2) = J_1/(4J_2)$. Putting aside the small *T*-dependence of *q*, we deduce from the experimental value ($q \sim 0.27$ a*) in the LTI and HTI phases that $J_1 \sim 2.6\ J_2$. In the presence of easy-axis anisotropy the highest-temperature ordered phase is predicted to be a longitudinally modulated phase in which the spins are confined to the easy *a*-axis, in agreement with our experiments. If the anisotropy field H_A is not too large ($H_A < H_1$), then as the temperature is lowered the longitudinally modulated phase gives way to one in which an additional transverse modulated component of spin appears, growing continuously from zero as the LTI phase is entered. This scenario is also consistent with the diffraction data, which show that the transverse direction is the *c*-direction and that the spin configuration is an elliptical spiral. At still lower *T* mean-field theory indicates that a transition to the experimentally observed commensurate AF state can occur for sufficiently large anisotropy, $H_A > H_2$. Our numerical mean field calculations show that for $J_1/J_2 = 2.6$ indeed $H_1 > H_2$, so that there is a range of anisotropy field for which mean field theory predicts the observed sequence of phase transitions versus (*H,T*).

The magnetic phase diagrams in the new kagomé staircase systems $(Ni,Co)_3V_2O_8$ turn out to be quite complicated, but can nevertheless be understood on the basis of a rather simple model that reflects the symmetry of the crystal structure. The main features of this model are the competition between nearest- and next-nearest-neighbor interactions and the importance of easy axis anisotropy and the Dzyaloshinskii-Moriya interaction. The $(Ni,Co)_3V_2O_8$ systems thus provide an elegant example of complex order from competing interactions in a highly frustrated system.

References:

[1] G. Lawes, M. Kenzelmann, N. Rogado, K. H. Kim, G. A. Jorge, R. J. Cava, A. Aharony, O. Entin-Wohlman, A. B. Harris, T. Yildirim, Q. Z. Huang, S. Park, C. Broholm, A. P. Ramirez, Phys. Rev. Lett (submitted 2004).

Spin Correlations and Magnetic Order in Nonsuperconducting $Nd_{2-x}Ce_xCuO_{4\pm\delta}$

P .K. Mang, A. Arvanitaki, and M. Greven
Stanford University
Stanford, CA 94305

O. P. Vajk and J. W. Lynn
NIST Center for Neutron Research
National Institute of Standards and Technology
Gaithersburg, MD 20899

The search for a working model to explain the complex properties of the high-temperature superconductors has generated enormous interest in the magnetism of two-dimensional (2D) systems. In particular, the spin-½ square-lattice Heisenberg antiferromagnet (SLHAF) has been found to model the magnetism of the copper-oxygen sheets in the undoped parent compounds of the high-temperature superconductors. Superconductivity can be achieved by doping the underlying copper-oxygen square lattice either with electrons or holes. Here we compare magnetic neutron scattering measurements of as-grown, non-superconducting crystals of the prototypical electron-doped superconductor $Nd_{2-x}Ce_xCuO_{4\pm\delta}$ (NCCO) ($0 \le x \le 0.18$) with numerical simulations for the randomly site-diluted SLHAF model [1]. These quantitative measurements can be expected to become benchmarks for tests of theoretical models.

Since superconductivity in the high-temperature cuprates appears in close proximity to antiferromagnetic phases, it is essential to understand the nature of nearby magnetic ground states. As-grown, the electron-doped cuprate NCCO is not superconducting, and the antiferromagnetic phase extends to the highest concentration for which samples can be produced ($x \approx 0.18$). Oxygen impurities are believed to occupy the nominally vacant apical sites, and a relatively severe oxygen reduction procedure must be applied to induce superconductivity above $x = 0.13$. Although the reduction procedure weakens the magnetism, magnetic order is still observed near optimal doping where the superconducting critical temperature T_c is 24 K. One qualitative argument often employed to explain the robustness of the antiferromagnetic phase in the electron-doped cuprates is that, whereas hole carriers are doped into the O 2*p* band and frustrate the antiferromagnetic arrangement of the neighboring Cu ions, doped electrons primarily reside on the Cu site, filling the 3d shell and removing the spin degree of freedom. New, quantitative insights have been gained recently into the role of *static* non-magnetic impurities introduced into the spin-½ SLHAF, including our detailed experimental work performed at the NCNR [2]. Here we test how well NCCO (whose doped electrons are *not* static) can be described by this model.

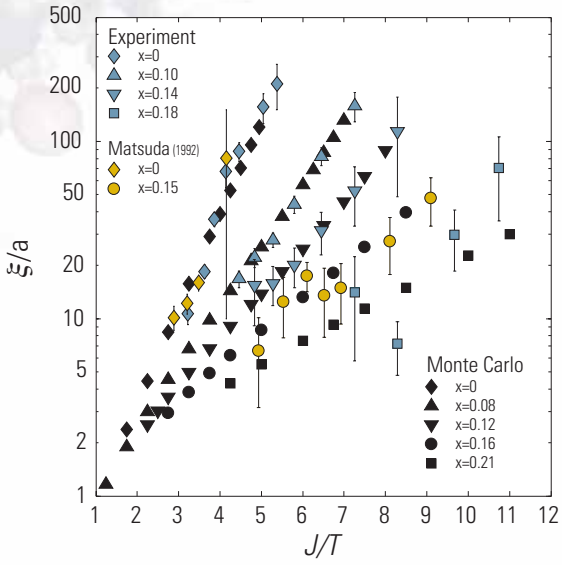

FIGURE 1.

Semi-log plot of the magnetic correlation length (in units of the lattice constant a) versus inverse temperature (in units of $J = 125$ meV) for $x = 0$, 0.10, 0.14, and 0.18. The data terminate just above the onset of Néel order at low temperature. Also displayed are previous data for $x = 0$ and $x = 0.15$ and quantum Monte Carlo results for the randomly diluted SLHAF.

Figure 1 summarizes the behavior of the instantaneous spin-spin correlation length $\xi(x,T)$, the typical distance over which spins "talk" to each other, for several Ce concentrations. Over a wide temperature range, the spin correlations exhibit an exponential dependence on inverse temperature, $\xi(x,T) \sim \exp[2\pi\rho_s(x) / T]$, where $\rho_s(x)$ is the spin stiffness, indicative of an underlying ground state with 2D antiferromagnetic order. We overlay the results of quantum Monte Carlo simulations for the randomly-diluted SLHAF. The numerical method is the same as that employed previously [2]. The data are plotted as ξ/a, the ratio of the spin-spin correlation length to the nearest-neighbor (NN) Cu-Cu distance ($a \approx 3.95$ Å), versus J/T, the ratio of the NN antiferromagnetic superexchange of Nd_2CuO_4 to the temperature. We find $J = 125(4)$ meV from comparison with our numerical results for $x = 0$, in good agreement with previous results of $J \approx 130$ meV. Assuming

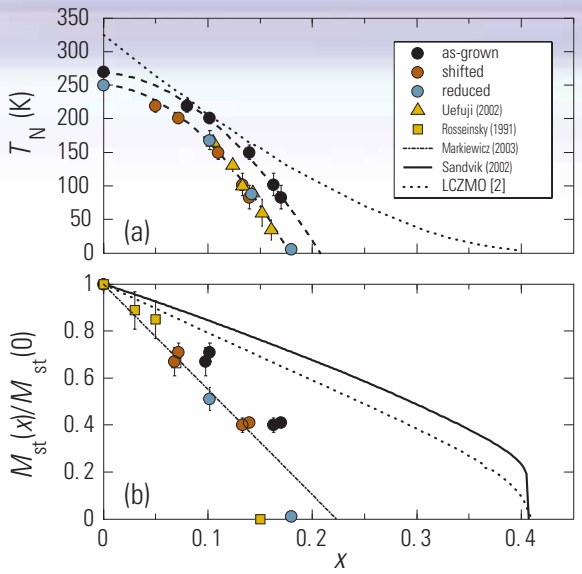

FIGURE 2.

(a) Néel temperature doping dependence. Ce-doped samples exhibit some rounding in the transition due to small oxygen and cerium inhomogeneities, which is represented by the error bars. The dashed curves are quadratic fits, and the dotted line indicates the behavior observed for LCZMO [2]. The tan circles are the as-grown data shifted by $\Delta x = -0.03$. (b) Doping dependence of the ordered copper moment per site, normalized by the value for Nd_2CuO_4. The tan circles are the as-grown data shifted by $\Delta x = -0.03$. The squares are data obtained in a previous study and the dot-dashed line is a recent theoretical prediction for the one-band Hubbard model. For comparison, Monte Carlo results for the diluted SLHAF (solid line) and the behavior observed for LCZMO (dotted line) [2] are also indicated.

J is constant for all doping levels, the only adjustable parameter in the comparison for the Ce-doped samples is the concentration of non-magnetic sites. We find good qualitative agreement between experiment and Monte Carlo if we fix this concentration to equal the nominal Ce concentration x. However, as shown in Fig. 1, the agreement becomes quantitative if we allow the effective dilution to differ slightly: $x_{eff}(x{=}0.10) = 0.08(1)$, $x_{eff}(x{=}0.14) = 0.12(1)$, and $x_{eff}(x{=}0.18) = 0.21(2)$. Also shown are previous data for as-grown samples with $x = 0$ and $x = 0.15$. The previous result for Nd_2CuO_4 agrees well with ours, and we estimate that $x_{eff}(x{=}0.15) = 0.16(2)$. The extent to which the quenched-disorder model effectively describes the spin correlations of as-grown, non-superconducting NCCO is remarkable. The observed small differences between nominal electron concentration and effective static dilution may be in part due to the uncertainty in the oxygen (and hence electron) concentration of our samples.

Figure 2(a) indicates that the Néel temperature $T_N(x)$ of our as-grown samples, as obtained from neutron diffraction, approximately follows a parabolic form, extrapolating to zero at $x \approx 0.21$. As shown in Fig. 2(a), qualitatively similar behavior has previously been found for reduced NCCO for which $T_N(x)$ is lower. The primary effect of the reduction is an approximately rigid shift of $\Delta x \approx -0.03$ due to the change in carrier density. The concave doping dependence of NCCO is contrasted by the behavior exhibited by the randomly diluted spin-½ SLHAF $La_2Cu_{1-x}(Zn,Mg)_xO_4$ (LCZMO), for which Néel order extends up to the site percolation threshold, $x_p \approx 0.41$, and the 2D spin correlations are quantitatively described by the model up to x_p [2].

In Fig. 2(b), we plot the ordered moment for several samples, as obtained from order parameter measurements at low temperature. The values are normalized to that of Nd_2CuO_4. The rate of decrease for the magnetic moment of as-grown NCCO, given by $1 - M_{st}(x)/M_{st}(0) \approx 3.5x$, is approximately twice that of the diluted SLHAF for $x < 0.20$. On the other hand, the magnetic phase extends much further than for the hole-doped cuprate $La_{2-x}Sr_xCuO_4$, for which Néel order is destroyed above $x \approx 0.02$. The moment of reduced samples is lowered further. We note that these data are again normalized by the value for as-grown Nd_2CuO_4, and that a rigid shift of $\Delta x = -0.03$ leads to good agreement of the two data sets. Our result is consistent with previous experimental work at lower concentrations.

If viewed instantaneously, so as to mitigate the effects due to the increased itinerancy upon doping, the magnetism of NCCO should indeed resemble a system with quenched random site dilution. What is surprising is that for $\xi(x,T)$ the correspondence is nearly quantitative. Since the charge carriers in as-grown NCCO are itinerant, even well below $T_N(x)$, deviations from the static model may be expected to emerge as we view the two systems on different time scales. Indeed, the ordered moment, an indicator of the strength of the magnetic order at infinitely long times, decreases much more rapidly in the case of NCCO than for the SLHAF. Recent theoretical work for the one-band Hubbard model is in semi-quantitative agreement with our results for the spin correlations and ordered moment. Although the experimentally accessible doping range is limited, our results for NCCO are consistent with the existence of a quantum critical point below x_p.

The evolution of the instantaneous spin-correlations may effectively be described by a site-dilution model, but a proper description of the magnetic degrees of freedom must necessarily include the effects of electron itinerancy. Our data should serve as a benchmark for tests of still-emerging theories for the high-temperature superconductors.

References:

[1] P. K. Mang, O. P. Vajk, A. Arvanitaki, L. Lu, J. W. Lynn and M. Greven, Phys. Rev. Lett. **93**, 027002 (2004).

[2] O. P. Vajk, P. K. Mang, M. Greven, P. M. Gehring, J. W. Lynn, Science **295**, 1691 (2002).

Disorder-induced Polaron Formation in Colossal Magnetoresistive Perovskites

T. J. Sato[1,2], J. W. Lynn[1], B. Dabrowski[3]

[1] NIST Center for Neutron Research
National Institute of Standards and Technology
Gaithersburg, MD 20899

[2] University of Tokyo
Tokai, Ibaraki 319-1106, Japan

[3] Northern Illinois University
DeKalb, IL 60115

$La_{1-x}A_xMnO_3$ (A = Ca, Sr and Ba) compounds, which exhibit enormous sensitivity of electrical resistance to magnetic fields (colossal magnetoresistance, CMR), have attracted a great deal of attention recently for their potential in technological applications, for the wide variety of physical properties these materials exhibit, and for the challenge of elucidating the fundamental origin of the CMR effect itself. In this report we examine the role of chemical disorder in these materials in promoting CMR.

These manganites have the perovskite structure (Fig.1 right), where the interplay of the spin, charge, and lattice degrees of freedom gives rise to a surprisingly rich variety of complex electronic, magnetic, and structural phases as a function of doping and temperature. In the ferromagnetic-metallic regime where CMR is observed ($x \approx 1/3$), we have found that the formation of polarons can truncate the ferromagnetic phase in a first-order ferromagnetic-metal/paramagnetic-insulator transition [1-3], making the conductivity extraordinarily sensitive to applied magnetic fields. Controlling the polaron formation is then key to tailoring the magnetoconductivity properties, and one central question to address is whether chemical disorder in these substitutional alloys affects the polarons.

Recently, $La_{0.5}Ba_{0.5}MnO_3$ has been synthesized where the *A*-sites can be ordered with LaO and BaO planes alternately stacked along the c-axis (Fig. 1 left), or the sites can be occupied randomly (Fig. 1 right). This chemical control of the A-site has allowed us to directly establish that the intrinsic inhomogeneities provided by the disordered lattice do in fact facilitate polaron formation, providing a mechanism to control the phase transition and the CMR effect [4]. Indeed, the chemical disorder drastically affects the most fundamental parameter, the ferromagnetic transition temperature; the disordered $La_{0.54}Ba_{0.46}MnO_3$ exhibits ferromagnetic order at $T_C = 300$ K, reduced from $T_C = 350$ K for the ordered sample. In this study we show that this reduction in T_C is caused by polaron formation, which truncates the ferromagnetic state in a first-order transition to the paramagnetic-polaron state.

To elucidate the nature of the phase transition, we measured the temperature dependence of the spin dynamics of *A*-site ordered and disordered $La_{0.54}Ba_{0.46}MnO_3$. Fig. 2 shows the temperature variation of the inelastic spectra observed at a momentum transfer $q = 0.07$ Å^{-1} as their respective ferromagnetic transition temperatures are approached. For the ordered sample we see spin waves in energy gain and loss, and the energies renormalize and the linewidths broaden as

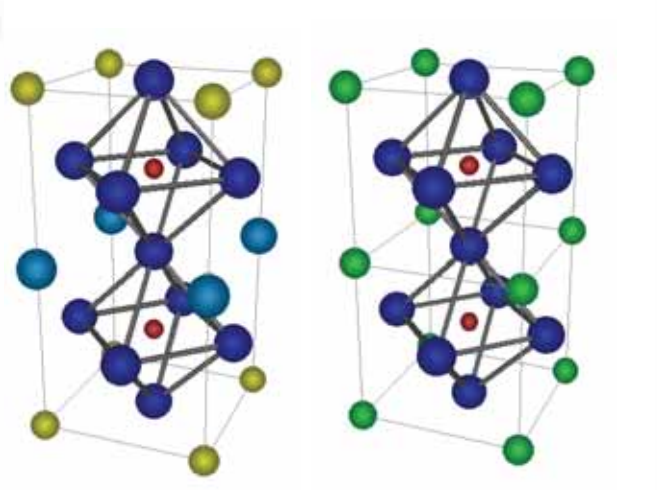

FIGURE 1.

Schematic illustrations of the crystal structures of the (left) ordered and (right) disordered (La,Ba)MnO_3 perovskites. The red, blue, yellow and light-blue spheres represent Mn, O, La and Ba sites, respectively, whereas the green spheres stand for the disordered (La, Ba) sites (A-sites). Oxygen octahedra around the Mn sites are also shown by grey bonds.

T_C is approached, as expected for a conventional second order (continuous) ferromagnetic-paramagnetic transition. The spin waves in the disordered sample are only slightly softer at low temperature, indicating that the exchange interaction is not strongly affected by the disorder. In striking contrast to the ordered sample, however, in the disordered sample we observe the development of a central quasi-elastic component to the scattering around $E \approx 0$, in addition to the renormalization of the spin waves. The intensities of the spin waves and central peak are shown in Fig. 2(e), where we see that the central component, indicative of paramagnetic spin diffusion, becomes significant ≈ 50 K below T_C, and increases as T_C is approached.

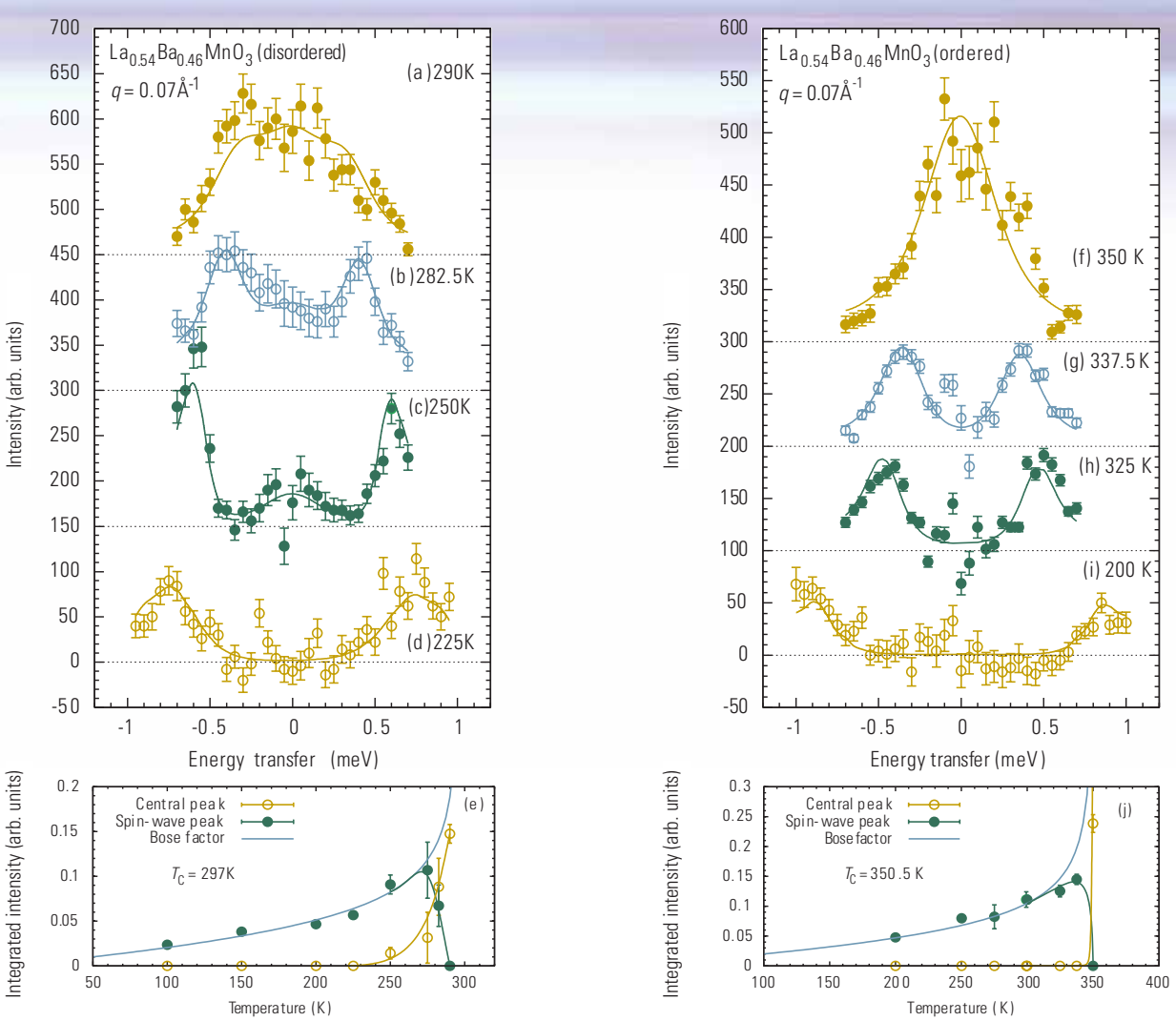

FIGURE 2.

(a-d) Inelastic excitation spectra observed in disordered $La_{0.54}Ba_{0.46}MnO_3$ at q = 0.07 Å^{-1}. Solid curves are fits to the model scattering function convoluted by the instrumental resolution. (e) Temperature dependence of the spin-wave-peak and central-peak intensity obtained from the fitting. (f-i) Inelastic excitation spectra observed in ordered $La_{0.54}Ba_{0.46}MnO_3$ at q = 0.07 Å^{-1}. (j) Temperature dependence of the spin-wave-peak and central-peak intensity.

Note in particular that when the central peak appears, the intensities of the spin waves decrease, while for the ordered sample (Fig. 2(j)) only spin wave peaks are observed below T_C, that merge to become a central spin diffusion peak at and above T_C.

The behavior of the disordered $La_{0.54}Ba_{0.46}MnO_3$ system is characteristic of a first-order transition with a two phase coexistence: ferromagnetic-metal and paramagnetic polaron insulator [1-3]. We also observe irreversibilities and long time scale relaxation behavior in the vicinity of T_C for the disordered system. This discontinuous behavior has been directly linked to the formation of polarons in perovskite manganites near optimal doping [3], and to a polaron glass state above T_C [5].

The present results demonstrate that the formation energy for lattice polarons is considerably lower in the presence of chemical disorder. If the temperature where these polarons form is in the ferromagnetic state, then the ferromagnetic state is abruptly truncated in a first-order metal/insulator: ferromagnetic/paramagnetic transition. This first-order transition is field tunable, producing the CMR effect.

References:

[1] J. W. Lynn, R. W. Erwin, J. A. Borchers, Q. Huang, A. Santoro, J.-L. Peng, and Z. Y. Li, Phys. Rev. Lett. **76**, 4046 (1996).

[2] C. P. Adams, J. W. Lynn, Y. M. Mukovskii, A. A. Arsenov, and D. A. Shulyatev, Phys. Rev. Lett. **85**, 3954 (2000).

[3] T. J. Sato, J. W. Lynn, Y.-S. Hor, and S-W. Cheong, Phys. Rev. B**68**, 214411 (2003).

[4] T. J. Sato, J. W. Lynn, and B. Dabrowski, (submitted for publication).

[5] D. N. Argyriou, J. W. Lynn, R. Osborn, B. Campbell, J. F. Mitchell, U. Ruett, H. N. Bordallo, A. Wildes, and C. D. Ling, Phys. Rev. Lett. **89**, 036401 (2002).

Crystal Structure and Lattice Dynamics of the Sodium Cobaltates

Q. Huang and J. W. Lynn
NIST Center for Neutron Research
National Institute of Standards and Technology
Gaithersburg, MD 20899

R. J. Cava
Princeton University
Princeton, NJ 08544

Y. S. Lee
Massachusetts Institute of Technology
Cambridge, MA 02139

Cobalt oxide systems are now a focus of materials researchers because of their interesting magnetic and thermoelectric properties, and because of possible analogies with colossal magnetoresistive manganite materials and/or high superconducting transition temperature cuprate oxides. For the Na_xCoO_2 system which is of particular interest in the present context, the spin entropy has been found to play an essential role in the dramatically enhanced thermopower for large sodium content ($x \approx 0.7$), while the recent discovery of superconductivity in hydrated $Na_xCoO_2 \cdot 1.4H_2O$ has been of particular interest with regard to the superconducting cuprates.

Na_xCoO_2 is a layered system where the Co^{4+} ions are in the low-spin state with S = 1/2 so that quantum effects are maximal, while the underlying lattice is triangular rather than square like the cuprates. These observations suggest that this may be the first new class of "high-T_C" superconductors since the discovery of the cuprates over 18 years ago, but of course the nature and mechanism of superconducting pairing in this new class of materials is in the early stages of being addressed. The appropriate underlying model may be a Mott insulator in two dimensions, with $S = ½$ where quantum fluctuations are optimal. The Co spins would then play a critical role in forming Cooper pairs that might have triplet symmetry as in Sr_2RuO_4 or *d*-wave symmetry as in the cuprates. On the other hand, the traditional electron-phonon interaction may establish conventional s-wave pairing, with the possibility that the anharmonic motion of the hydrogen and oxygen ions plays a role in enhancing the superconducting properties, in a manner similar to MgB_2. In this study we have investigated the crystal structure of Na_xCoO_2 as a function of doping *x*, and related the structure to the observed physical properties. We have also determined the lattice dynamics for the superconducting hydrate, and compared the behavior with the related non-superconducting compound $Na_{0.3}CoO_2$.

The phase diagram as a function of Na doping is shown in Fig. 1 [1]. Each Na ion nominally donates an electron to the CoO_2 plane, but we see that the behavior of the Na is much more complicated than this simple picture would suggest. In particular, the Na ions occupy two different sites over a wide range of *x*, as shown in Fig. 2, while the CoO_2 is structurally robust. The system is a paramagnetic metal for $x < 1/2$, with both the Na(1) and Na(2) sites being partially occupied, and the Na(2) being further split into a threefold site that is again randomly occupied. This is designated the H1 structure. At $x = 1/2$ the system exhibits a special charge and orbitally ordered structure that is insulating, with the Na ions occupying ordered positions that form one-dimensional zigzag chains [2]. For $x > 1/2$ the system returns to the H1 structure and is a Curie-Weiss metal. Around $x \approx 3/4$ the Na structure transforms to the more ordered H2 structure, where the randomness in the Na(2) site is absent. This transition can also be driven thermally as shown in Fig. 3, where we observe the quite unusual behavior of transforming from an ordered state at low *T* to a randomly

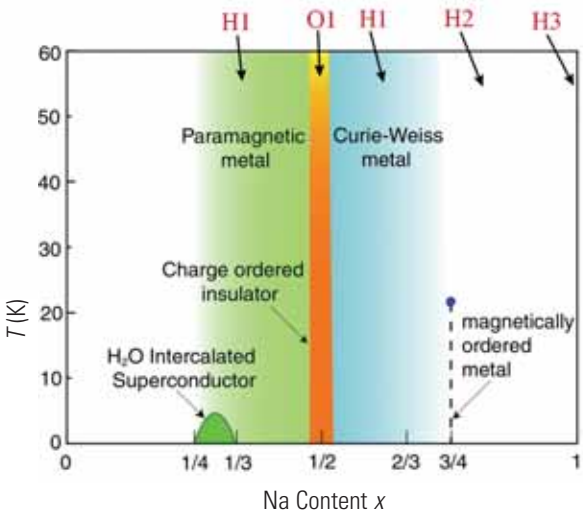

FIGURE 1.
Phase diagram for Na_xCoO_2.

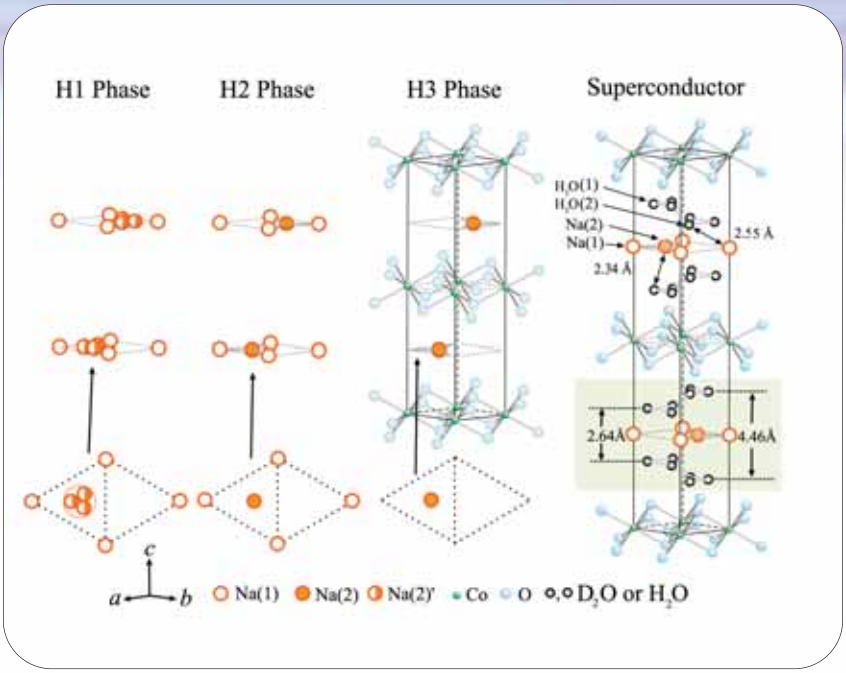

FIGURE 2.

Three different structures (designated H1, H2, and H3) for the Na ions in Na_xCoO_2. The structure on the right is for the superconductor, where we note that the Na ions shift to the other side of the unit cell to accommodate the ice-like ayer of water.

vacant [1]. The transition from the H2 to the H3 structure as a function of composition is also discontinuous in nature.

One of the amazing characteristics of this system is the discovery of superconductivity when the material is hydrated. Initially water goes into the Na layer, but then the water forms its own layer between the Na and CoO_2 layers, with the c-axis expanding from 11.2 Å to 19.5 Å and the material becoming a 5 K superconductor. Both the structure and lattice dynamics indicate that this separate water layer has the basic structure of ice as shown on the right-hand side of Fig. 2 [4]. Note in particular that the structure of the Na is different than in the parent compound, with the Na shifting to the other side of the unit cell to accommodate the water. A central question is whether the water is playing an active role in the superconducting pair formation, or is simply expanding the lattice and making the system more two-dimensional in nature. So far, however, only water has been found to render the system superconducting.

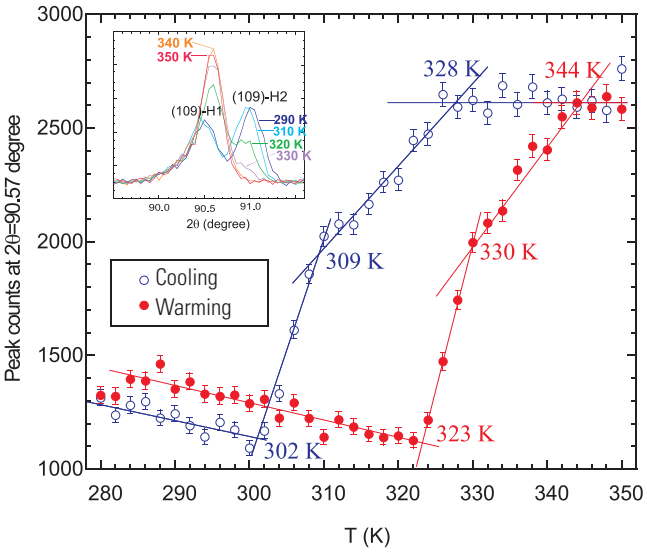

FIGURE 3.

Temperature dependence of two Bragg peaks belonging to the low temperature H1 phase and the high temperature H2 phase. These peaks are well separated, as shown in the inset. The system exhibits the very unusual behavior of transforming from an ordered structure at low *T*, to a more disordered structure at elevated *T*. The transition is first order both with temperature and doping.

occupied threefold degenerate site at elevated *T* [3]. This transition is first-order in nature in both temperature and composition. Finally, with further increase of the Na composition we realize the H3 structure, where the Na(2) site is fully occupied and the Na(1) is completely

The present work has elucidated the basic crystal structure for the Na_xCoO_2 and superconducting systems, and determined the changes in the bonding and structure as the electron count is varied. The results suggest that conducting triangular lattice systems exhibit their own type of structural and electronic phases that are distinct from square-planar systems like the cuprates, providing a rich new variety of physical phenomena to explore for both fundamental and technological purposes.

References:

[1] *Coupling of Structural and Electronic Degrees of Freedom in the Layered Triangular Lattice Conductor Na_xCoO_2*, Q. Huang, M. L. Foo, J. W. Lynn, B. H. Toby, R. A. Pascal, H. W. Zandbergen, and R. J. Cava, Phys. Rev. B (submitted).

[2] *Low Temperature Phase Transitions and Crystal Structures of $Na_{1/2}CoO_2$*, Q. Huang, M. L. Foo, J. W. Lynn, H. W. Zandbergen, G. Lawes, Y. Wang. B. Toby, A. P. Ramirez, N. P. Ong, and R. J. Cava, J. Phys.: Cond. Matter (submitted).

[3] *Structural Transition in Na_xCoO_2 with x near 0.75 due to Na Rearrangement*, Q. Huang, B. Khaykovich, F. C. Chou, J. H. Cho, J. W. Lynn, and Y. S. Lee, Phys. Rev. B (submitted).

[4] J. W. Lynn, Q. Huang, C. M. Brown, V. L. Miller, M. L. Foo, R. E. Schaak, C. Y. Jones, E. A. Mackey, and R. J. Cava, Phys. Rev. B**68**, 214516 (2003).

Neutron Spin Echo Study of a Diluted "Spin-Ice"

J. S. Gardner[1,2], G. Ehlers[3] and N. Rosov[2]

[1] Brookhaven National Laboratory
Upton, NY 11973

[2] NIST Center for Neutron Research
National Institute of Standards and Technology
Gaithersburg, MD 20899

[3] SNS Project, Oak Ridge National Laboratory
Oak Ridge, TN 37830

The demand for smaller, faster and more efficient computers has driven research into fields like spintronics, quantum algorithms and quantum magnets that show tunnelling transitions between spin states. Examples of these magnets include the dipolar magnet $LiHoF_4$ and "single molecule magnets" such as "Mn_{12}". However, elaborate cryostats that cool samples well below 1K are required to study these tunnelling events because of the intrinsically weak interactions involved. The advent of a material in which tunnelling occurs at higher temperatures would make it easier to exploit such phenomena. Here we highlight recent work that suggests that a diluted "spin-ice" material may constitute just such a system.

It is now well appreciated that the combination of antiferromagnetic interactions and certain triangular lattice symmetries leads to phenomena known broadly as geometrical frustration [1,2]. Surprisingly, ferromagnetically coupled spins on a corner sharing lattice of tetrahedra can also be highly frustrated if there is a strong tendency for the spins to point into or out of the center of the tetrahedron [2]. The magnetic correlations of geometrically frustrated magnets have been studied for some time, but in the past two years more emphasis has been placed on understanding the spin relaxation dynamics [3,4].

$Ho_2Ti_2O_7$, $Dy_2Ti_2O_7$ and $Ho_2Sn_2O_7$ are known spin-ice compounds [2] where the magnetic ground state consists of Ising spins confined along the local <111> axes by crystal field effects with a characteristic energy of over 250 K. The result is a ground-state with two spins pointing in and two spins pointing out of the individual tetrahedra. This structure is identical to the lattice formed by vector displacement arrows from the mid-points of the oxygen-oxygen bonds in water ice to the nearest hydrogen ion, hence the spin-ice label (Fig. 1). As in ice, this leads to extensive zero temperature entropy that Pauling showed results from the macroscopic ground state degeneracy [5]. In other words, the global ground state can be reached in many ways as long as each unit (tetrahedron) obeys the ice-rule. Thus there is not a unique decoration of spins on the lattice as there is on a "normal" antiferromagnet or ferromagnet, but a state that can be an enormous superposition of many configurations—an arrangement favorable to quantum computation.

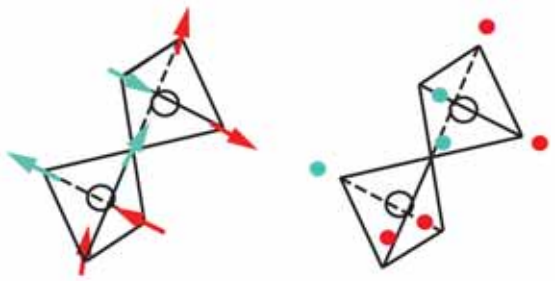

FIGURE 1.
Comparison of spin-ice to water ice, demonstrating the "ice rule": two in and two out on each tetrahedron.

In a spin-ice study [3] the authors, in collaboration with Professors S. T. Bramwell (University College, London) and A. L. Cornelius (University of Nevada Las Vegas), used NSE to conclusively show that a single ion process dominates the spin dynamics above 15 K. Complementing the NSE work with a.c. susceptibility measurements, they concluded that a "hot" spin-ice phase, where quantum mechanics dominates the relaxation processes, exists between the spin ice freezing temperature and 15 K.

Introducing non-magnetic impurities often has important effects in geometrically frustrated magnets [1]. In a diluted spin-ice study of $Dy_{2-x}Y_xTi_2O_7$ it was found that for x up to $\approx$ 0.4, the very narrow distribution of spin relaxation times becomes only slightly broadened, unlike in spin glasses where it is much wider [4]. These authors also pointed out that a 15 K peak in a.c. susceptibility does not shift but gradually disappears with doping before reappearing again at higher doping levels.

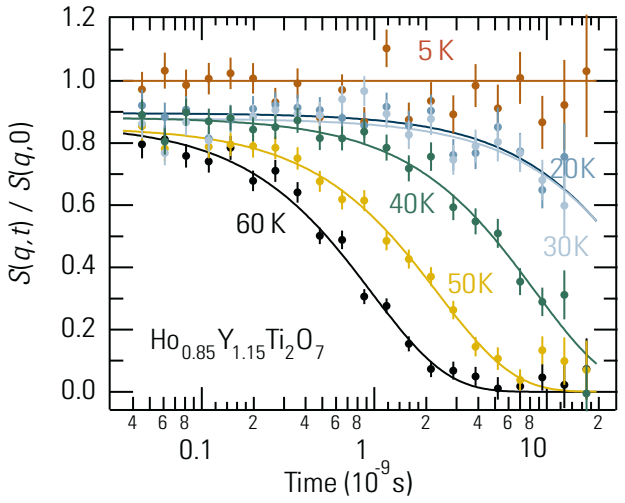

FIGURE 2.

The intermediate scattering function of the diluted spin-ice, $Ho_{0.85}Y_{1.15}Ti_2O_7$. The fact that the data at 20 K and 30 K are nearly the same points to an athermal (likely a quantum mechanical) relaxation process.

Recent improvements to the NSE spectrometer at NIST have allowed us to perform a neutron spin echo experiment on a magnetic sample for the first time in North America. This upgrade to the spectrometer includes installation of new Helmholtz coils to adiabatically change the neutron polarization at the sample into three orthogonal directions (*xyz* polarization analysis), a modified flipper correction coil, and modifications to the control software. In a magnetic NSE experiment the sample itself flips the neutron spin by π, removing the need for a π flipper at this position, but this changes the field profile of the instrument. Full *xyz* polarization analysis was performed for each individual scan in order to relate the echo amplitude to the elastic magnetic-scattering intensity. This analysis separates magnetic scattering from coherent nuclear and incoherent spin and isotope scattering contributions that make up the total signal.

We undertook a NSE study of several diluted $Ho_{2-x}Y_xTi_2O_7$ powders. A characteristic echo data set is shown in Fig. 2 with fits to a single exponential relaxation process. In all samples the single ion process, which was first revealed in the pure spin-ice compound, is dominant at high temperatures ($T > 70$ K). This is a general characteristic of a single ion effect and therefore expected. For high doping (data not shown) two exponential functions are required to describe the data fully. For low doping levels (at least 65 % holmium) the data can be described by a single exponential relaxation function in a similar manner to $Ho_2Ti_2O_7$, however there are two noticeable differences. First, unlike $Ho_2Ti_2O_7$, a small loss in initial polarization (5 % to 10 %) at $T \approx 5$ K does not occur; instead the spin system freezes. In fully frustrated $Ho_2Ti_2O_7$ this loss is associated with nuclear-electronic spin coupling as a so-called "wobble" around the Ising axis. One can imagine how this wobble is frozen out once the frustration is relieved slightly. Secondly, and more importantly, the echo in $Ho_{0.85}Y_{1.15}Ti_2O_7$ is identical at 20 and 30 K, suggesting the athermal regime has shifted to higher temperatures. The NIST NSE spectrometer permits measurements spanning the large time scale from $\approx$ 0.02 ns to $\approx$ 20 ns, which is crucial to allowing us to determine this conclusively.

To conclude, the dominant spin dynamics of $Ho_2Ti_2O_7$ does not change significantly when the magnetic sublattice is diluted with non-magnetic Y (up to 90 % Y). This result is consistent with the dominant process being the single ion effect established earlier. $Ho_{0.85}Y_{1.15}Ti_2O_7$ provides evidence that the athermal relaxation process, characteristic of a quantum process, is extended to 30 K, much higher than liquid helium temperatures. The tunnelling dynamics revealed here are an intrinsic consequence of the geometric frustration and present a very different scenario to other quantum magnets. Diluted spin-ice thus provides us with a quantum mechanical system to investigate these fundamental and technologically relevant dynamics in an accessible temperature regime.

References:

[1] *Magnetic Systems with Competing Interactions*, H. T. Diep, Ed. (World Scientific, Singapore, 1994); and Can. J. Phys., M. J. P. Gingras, Ed. **79**, (2001).

[2] S. T. Bramwell and M. J. P. Gingras, Science, **294**, 1495 (2001).

[3] G. Ehlers, *et al.*, J. Phys: Condens. Matter **15**, L9 (2003).

[4] J. Snyder, *et al.*, Phys. Rev. B **66**, 064432 (2002).

[5] L. Pauling, J. Am. Chem. Soc. **57**, 2680 (1935).

Ordering and Spin Waves in $NaNiO_2$: A Stacked Quantum Ferromagnet

B. D. Gaulin[1,2], M. J. Lewis[1], L. Filion[1]
C. Kallin[1,2], A. J. Berlinsky[1,2], H. A. Dabkowska[1]
Y. Qiu[3], and J. R. D. Copley[3]

[1] McMaster University
Hamilton, ON, L8S 4M1, Canada

[2] Canadian Institute for Advanced Research
Toronto, ON, M5G 1Z8, Canada

[3] NIST Center for Neutron Research
National Institute of Standards and Technology
Gaithersburg, MD 20899

Magnetic materials that combine quantum s = 1/2 magnetic moments and geometries that can preclude the easy formation of long range order at low temperatures have been of recent interest, as they are thought to be likely candidates for exotic quantum states of matter. For example, loosely interacting chains of quantum magnetic moments are found in some magnetic materials and it is well appreciated that these can form a disordered "spin liquid" state at low temperatures. Triangular layers of magnetic ions also constitute good venues for this type of exotica, as layered structures are themselves low dimensional and prone to strong fluctuation effects, while triangular architectures can lead to geometrical frustration when combined with antiferromagnetism. $LiNiO_2$ and $NaNiO_2$ are two of the more celebrated of such materials as both are comprised of s = 1/2 quantum magnetic moments associated with Ni^{3+}, arranged on a stacked triangular lattice. Our measurements using the Disk Chopper Spectrometer (DCS) have revealed the ground state magnetic structure and low energy spin waves in $NaNiO_2$, and in so doing we have put to rest roughly 20 years of speculation regarding the nature of this material's low temperature ground state.

$LiNiO_2$ has been widely studied for at least 20 years [1]. It is better studied than its isostructural sister compound $NaNiO_2$, as it has been of interest as a potential intercalation battery material. Both $LiNiO_2$ and $NaNiO_2$ are only available in polycrystalline form, despite many attempts to grow single crystals. Even so, their structural properties are well characterized. It is known, for example, that Li^+ and Ni^{3+} can exchange positions within $LiNiO_2$ due to the fact that their ionic radii are virtually the same [2]. This occurs at the 1 % to 3 % level even in the best prepared samples. This is not the case for Na^+ and Ni^{3+}, and $NaNiO_2$ is much better ordered structurally than is $LiNiO_2$.

There have also been numerous attempts to understand the magnetic behavior of these two materials. However their properties have remained enigmatic until just now, in large part due to the *absence* of any information from neutron scattering. Studies have been carried out in the past, but have been unsuccessful in identifying definitive magnetic scattering. The absence of identifiable magnetic neutron scattering has itself motivated conjecture that these materials have entered an exotic quantum ground state at low temperatures [3] such as the resonating valence bond proposed by P. W. Anderson [4] to describe quantum antiferromagnets on a triangular lattice. A characteristic of such a state is the absence of magnetic Bragg scattering as the ground state is a magnetic singlet.

We have used the Disk Chopper Spectrometer (DCS) to examine the magnetic structure and low energy spin dynamics of powdered $NaNiO_2$. Data taken using 5.5 Å incident neutrons is shown in Fig. 1 at three different temperatures below a phase transition near $T_N \approx 22$ K. DCS can simultaneously measure over a relevant range of wavevector transfer Q and energy transfer E in a powder, cleanly separating the elastic from the inelastic scattering. The false-color intensity scale in Fig. 1 is chosen to highlight the magnetic inelastic scattering, and we clearly observe spin wave scattering in the form of a

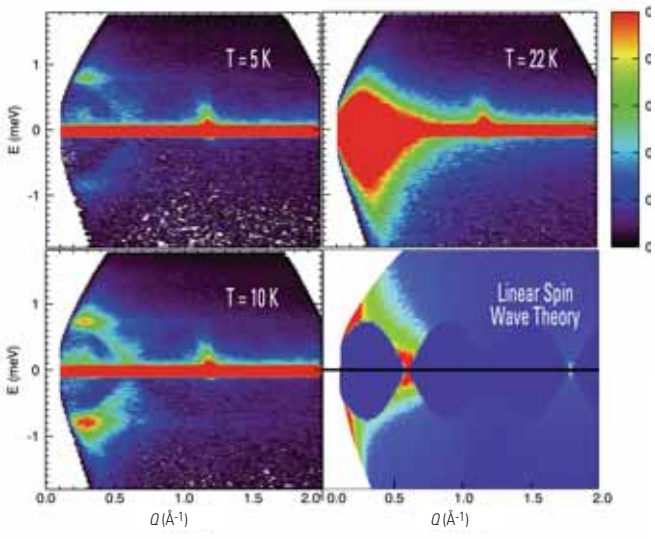

FIGURE 1.

Neutron scattering results on $NaNiO_2$ are shown at three temperatures below $T_N \approx 22$ K. The false color intensity scale has been chosen to highlight spin wave excitations going to zero energy at $Q \approx 0.6$ Å^{-1}. The bottom right panel shows a linear spin wave theory calculation that qualitatively accounts for the dispersion of the spin waves as measured in this powder sample.

rather simple sinusoidal dispersion, going to zero energy at an ordering wavevector of ≈ 0.6 Å^{-1}. Cuts of the data through the elastic scattering position are shown in Fig. 2 where we observe magnetic Bragg scattering at ≈ 0.6 Å^{-1}, and a phase transition occurring near $T_N \approx 22$ K.

These data, the first definitive determination of magnetic neutron scattering in $NaNiO_2$, lay to rest most of the speculation regarding the nature of the magnetic ground state in these materials. Both the magnetic Bragg peaks and the spin wave scattering are consistent with a simple and relatively conventional low temperature structure comprised of *ferromagnetically* aligned quantum spins within triangular planes, which are stacked antiferromagnetically on top of each other as shown in the top third of Fig. 3.

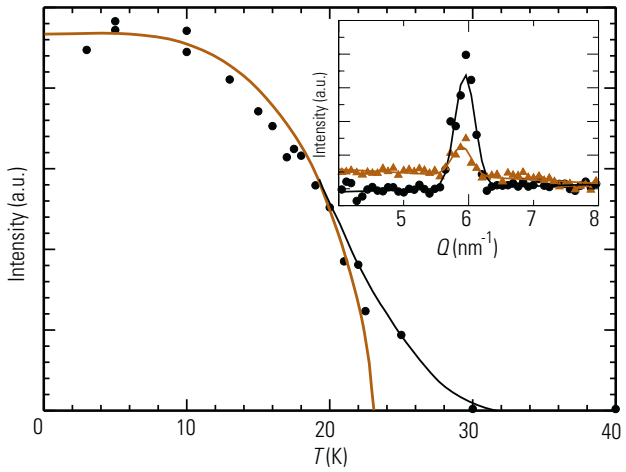

FIGURE 2.

The inset shows a cut through the elastic position as a function of Q, and magnetic Bragg peaks near $Q \approx 0.6$ Å^{-1} (6 nm^{-1}) at two temperatures below T_N. The main plot shows the integrated intensity of the magnetic Bragg scattering in $NaNiO_2$ and its fall off with temperature above T_N.

It is of great interest to note that this magnetic structure is very sensitive to mixing of the Ni and the alkali metal sublattices, as such mixing provides a strong exchange path that will frustrate the antiferromagnetic stacking sequence of the ferromagnetic triangular planes, independent of whether the impurity spins couple neighbouring planes ferromagnetically or antiferromagnetically. This explains the fact that $LiNiO_2$ displays a spin glass state at low temperatures while $NaNiO_2$ finds a conventional ordered state. Most importantly, this study demonstrates the importance of neutron scattering in understanding magnetic phenomena, and how new instrumentation enables new science.

References:

[1] K. Hirakawa, H. Kadowaki, and K. Ubukoshi, J. Phys. Soc. Jap. **54**, 3526 (1985).

[2] J. N. Reimers, J. R. Dahn, J. E. Greedan, C. V. Stager, G. Lui, I. Davidson, and U. von Sacken, J. Solid State Chem. **102**, 542 (1993).

[3] See for example: Y. Kitaoka *et al.*, J. Phys. Soc. Jap. **67**, 3703 (1998); F. Reynaud *et al.*, Phys. Rev. Lett. **86**, 3638 (2001).

[4] P. W. Anderson, Mat. Res. Bull. **8**,153 (1973).

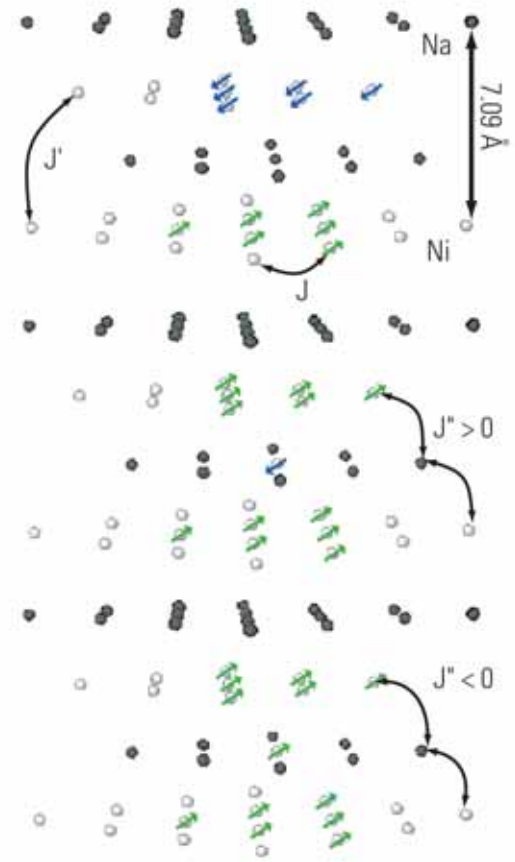

FIGURE 3.

The magnetic structure of $NaNiO_2$, as determined from the new DCS measurements, is schematically shown in the upper third of the diagram. The lower two thirds of the diagram illustrate how the antiferromagnetic stacking of ferromagnetic triangular layers is frustrated by impurity Ni ions on the Li sublattice in $LiNiO_2$, independently of whether the impurity spin couples ferromagnetically (bottom third, $J'' < 0$) or antiferromagnetically (middle third, $J'' > 0$) to moments in adjacent layers.

A Molecular Picture of Dynamics in Miscible Polymer Blends

V. García Sakai and J. K. Maranas
The Pennsylvania State University
University Park, PA 16802

Z. Chowdhuri[1,2], N. Rosov[2], I. Peral[1,2] and J. R. D. Copley[2]

[1] University of Maryland
College Park, MD 20742

[2] NIST Center for Neutron Research
National Institute of Standards and Technology
Gaithersburg, MD 20899

It is hard to imagine life without plastic bottles, car parts, computer casings, and tubing in medical and home applications. To make useful objects, polymers must be formed into the desired shape, which requires heating until they are soft enough to be manipulated. Many common objects are not composed of a single polymer but a blend of two or more polymers, occasionally leading to problems in processing. The components in polymer blends, despite thermodynamic miscibility, can retain individual dynamic behavior, often explained by an effective local concentration. Theories differ in the origin and spatial extent of this effective local concentration. Chain connectivity and concentration fluctuation models can describe some, but not all, available data. Quasielastic neutron scattering (QENS) allows spatially-resolved *observation of local motions underlying polymer softening. We use this spatial sensitivity to determine the signature of concentration fluctuations in a miscible blend, PEO/PMMA, where such fluctuations should be prominent.*

Measurements were made on three QENS instruments: DCS, HFBS, and NSE. The first two assess self-motion through incoherent scattering. Deuterium labeling is used to hide the dynamics of each component in turn: for example, a hPMMA/dPEO blend will reveal the mobility of PMMA. The spectra, measured in the energy domain, were Fourier-transformed to give intermediate scattering functions in the time domain. As PEO and PMMA have widely separated glass transition temperatures T_g, the timescales of their dynamics are well separated in the blend as illustrated in Fig. 1. All spectra with green symbols were taken at the same temperature: from this it is clear that the NSE spectra mainly probes PMMA mobility, and relative motion decays more slowly than self motion. The intermediate scattering functions were fitted with a stretched exponential function, from which the average relaxation time τ, and the stretching parameter β, were obtained. To establish the validity of the experiments, we compare fit parameters for each blend component to data available from other measurements (Fig. 2). The PEO results are consistent with NMR measurements on a PEO labeled blend. For PMMA, blend measurements are not available. Instead we compare to dielectric measurements on pure PMMA, corrected for the difference in T_g. In both cases, the QENS results are consistent with other dynamic techniques.

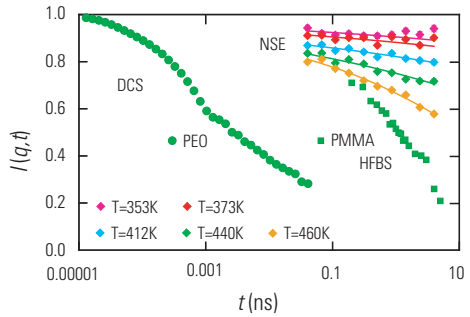

FIGURE 1.

Fig. 1. Intermediate scattering functions for the PEO/PMMA blend. PEO (T = 440 K and Q = 1.05 Å^{-1}) and PMMA (T = 440 K and Q = 0.99 Å^{-1}), are component-labeled self-motion, and the rest are relative motion obtained from NSE measurements at several temperatures.

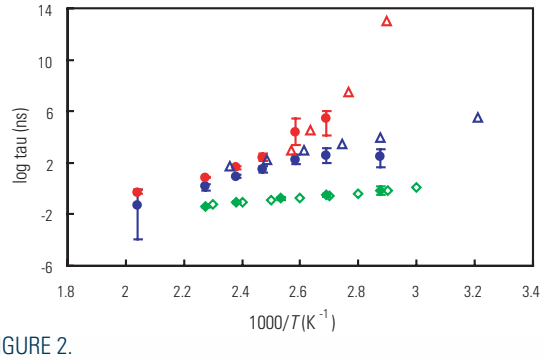

FIGURE 2.

Comparison with data from other experimental techniques for component dynamics in a 20 % blend. Filled circles: QENS data for PMMA in the blend at Q = 0.62 Å^{-1} (red) and Q = 1.51 Å^{-1} (blue); Triangles: data from dielectric spectroscopy [3] for pure PMMA shifted by T_g, for the α- (red) and β- (blue) relaxations. Green filled diamonds: QENS data for PEO in the blend at Q = 0.9 Å^{-1}; Clear green diamonds: NMR data from Lutz *et al.* [4]

Having established consistency in the measurements, we exploit the spatial resolution of QENS to identify when concentration fluctuations influence blend dynamics. Measured spectra are an average over all possible *mobile* local compositions of the specified spatial scale. If concentration fluctuations strongly influence blend dynamics, the mobility of these local compositions will vary considerably more than the pure component. This can be recognized by considering the behavior of the stretching parameter β.

A decrease in β indicates a larger variety of local environments contributing to the average response, as can be shown mathematically [1]. If all local compositions are mobile, β_{blend} will be significantly lower than β_{pure}. Restricting the range contributing to the average should lead to an increase in β_{blend} towards β_{pure}. This is easily accomplished in a QENS experiment by lowering temperature, in which case PMMA-rich regions become immobile due to the short timescale of the spectrometer, or by decreasing the spatial scale such that it is comparable to inter-chain spacing and PMMA-rich regions surrounding a PEO proton are excluded. An increase in β with decreasing temperature is opposite to what is normally observed and should give a clear indication that concentration fluctuations are important. If concentration fluctuations have little influence on dynamics, the range of local mobilities will resemble that of the pure component and β_{blend} will be similar to β_{pure} at all spatial scales, increasing with temperature from the smallest values near T_g.

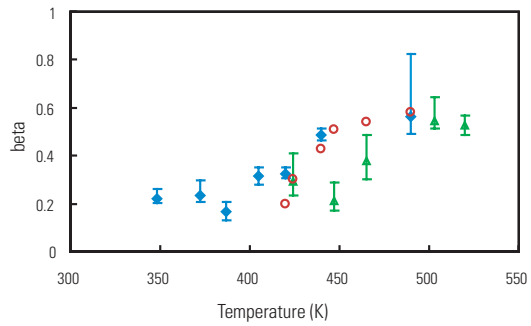

FIGURE 3.

The effect of concentration fluctuations on PMMA dynamics. Shown are stretching exponents for pure PMMA (green solid triangles) and PMMA in the blend (blue solid diamonds) at $Q = 0.62$ Å^{-1}. For comparison, results from dielectric spectroscopy [1] on pure PMMA (red open circles) are also shown.

For the high-T_g component in this blend, PMMA [2], the stretching parameters are similar in both environments (Fig. 3), suggesting that concentration fluctuations do not significantly affect PMMA dynamics. Data for PEO support the concentration fluctuation picture: results for β are shown in Fig. 4. At the larger spatial scale, β_{blend} is temperature independent and smaller than β_{pure}, consistent with the broadening effect of concentration fluctuations. When the range of mobile compositions contributing to the average is restricted (small spatial scales and low temperatures), β_{blend} increases towards β_{pure}. The length scale where this behavior begins coincides roughly with the first structure factor peak in PEO ($Q \approx 2$ Å^{-1}). This is consistent with the idea that the range of local compositions will be greatly reduced if inter-chain distances are excluded. The range of local environments reflected by β should also affect the ensemble average relaxation time. Specifically, as PMMA rich regions become improbable at small spatial scales and immobile at low temperatures, τ should be smaller than otherwise expected. This is illustrated in Fig. 5. For small spatial scales, relaxation times flatten below the T_g of PMMA. This result indicates larger than expected mobility, consistent with biased sampling of PEO rich regions.

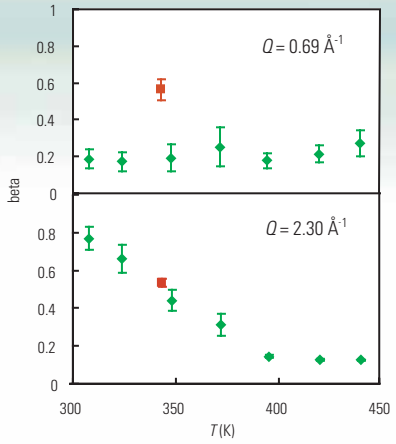

FIGURE 4.

The effect of concentration fluctuations on PEO dynamics. Stretching exponents β are shown at two spatial scales as a function of temperature. Green diamonds: 20 % hPEO/dPMMA blend. Red square: pure PEO.

We have used the spatial resolution of QENS to probe the impact of concentration fluctuations. The presence of a wide variety of local compositions decreases the stretching parameter in a stretched exponential fit significantly from pure component values. Although this may be observed with any technique, the spatial resolution of QENS allows us to restrict the range of compositions probed by the experiment, in which case effects from concentration fluctuations should disappear. By examining a blend where concentration fluctuations should be important, we identify the signature of concentration fluctuations as an increase in β with decreasing temperature, a trend opposite to what is normally observed. Identifying the origin of component dynamics in blends will allow prediction of their dynamic behavior, ultimately aiding in processing these mixtures into objects.

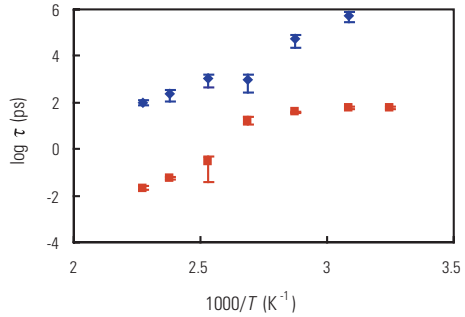

FIGURE 5.

Temperature and spatial dependence of the average relaxation time τ of PEO in a 20 % blend with PMMA: blue diamonds $Q = 0.69$ Å^{-1} and red squares $Q = 2.30$ Å^{-1}.

References:

[1] J. Colmenero, A. Arbe, A. Alegria, M. Monkenbusch, and D. Richter, Journal of Physics: Condensed Matter **11**, A363 (1999).

[2] V. García Sakai, C. Chen, J. K. Maranas and Z. Chowdhuri, Macromolecules, in review (2004).

[3] R. Bergman, F. Álvarez, A. Alegría, and J. Colmenero, J. Non-Crystalline Solids **235**, 580 (1998).

[4] T. R. Lutz, Y. He, M. D. Ediger, H. Cao, G. Lin, and A. A. Jones, Macromolecules **36**, 1724 (2003).

Counterion Associative Behavior with Flexible Polyelectrolytes

Vivek M. Prabhu and Eric J. Amis
Polymers Division
National Institute of Standards and Technology
Gaithersburg, MD 20899

Dobrin Bossev and Nicholas Rosov
NIST Center for Neutron Research
National Institute of Standards and Technology
Gaithersburg, MD 20899

Polyelectrolytes differ in chain dynamics and equilibrium structure from neutral polymers due to the presence of long-ranged electrostatic interactions. These interactions result in associative behavior and multi-mode relaxations in both synthetic and biopolymers [1]. To determine the origins of these relaxations, new experimental methods probing local structure and dynamics are required. Using neutron scattering at the NCNR, we have established the remarkable ability of counterions to conform to linear flexible polyelectrolytes. This was achieved by directly measuring the counterion partial static and dynamic structure factors, highlighting the coupled polymer and counterion associations [2]. Small-angle neutron scattering (SANS) was used to characterize the equilibrium structure while neutron spin echo (NSE) spectroscopy examined the dynamics.

The structural behavior of polyelectrolytes is usually characterized from the polymer viewpoint. Inorganic counterions such as sodium are of low contrast in SANS measurements, since the strongest contrast is achieved by hydrogen (H) and deuterium (D) isotopic substitution. To access the counterion viewpoint, the inorganic counterion (Na^+) was replaced by an organic ion tetramethylammonium ($H–TMA^+$) combined with a perdeuterated poly(styrene sulfonate) (D-PSS) in D_2O. In this case, the polymer scattering is contrast-matched with the solvent, rendering the polymer invisible, as shown schematically in Fig. 1, and allowing direct measurement of the counterion pair correlations.

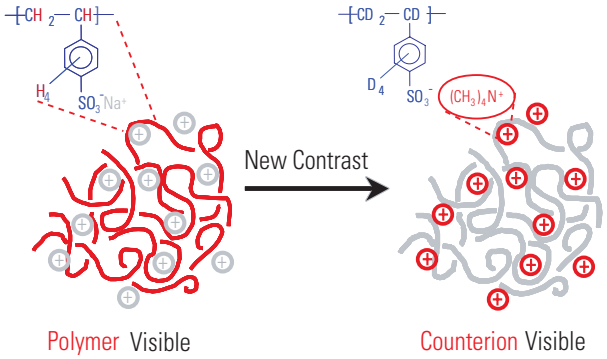

FIGURE 1.

Schematic diagram illustrating the contrast variation made possible by isotopic substitutions and the replacement of Na^+ by $H\text{-}TMA^+$, allowing direct probing of the counterions using neutron scattering.

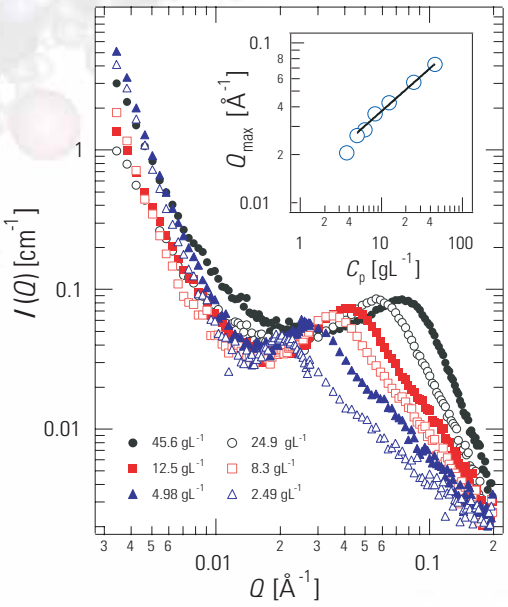

FIGURE 2.

SANS intensity from (H-TMA) D-PSS in D_2O as a function of polymer concentration under conditions that make the polymer invisible. The polymer concentration dependence of the peak value of Q is shown in the inset.

This effect was used to measure the counterion partial structure factor by SANS in low ionic strength $H\text{-}TMA^+/D_2O$ /D-PSS mixtures that render the polymer invisible. The results are shown in Fig. 2

Keeping in mind that only the counterions are visible in this experiment, two features are noted in Fig. 2: 1) the typical peak observed for a polyelectrolyte polymer is apparent, even though the polymer is invisible, and its position changes in the expected way with polymer concentration; and 2) increased intensity at low Q indicates the presence of larger scale structures in these solutions. The magnitude and scaling of the counterion correlation length ξ (from $Q_{max} = 1/\xi$) measured here agree with the result measured under the condition when only the polymer is visible [3], showing that the counterion

correlations are mediated by the highly-charged flexible polyelectrolyte. The equilibrium distribution of the counterions evidently mimics the topology of the chain, a consequence of the electrostatics.

Still under conditions where the polymer is invisible, these counterion correlations can be reduced by increasing the ionic strength of the solution with added NaCl, an "invisible" salt for SANS, as shown in Fig. 3. Without added salt, the counterion correlations emulate the typical polyelectrolyte peak, as observed in Fig 2. However, at 0.10 mol/L NaCl the peak disappears: neutral-like polymer behavior is observed. From the counterion viewpoint the influence of added salt is twofold: NaCl displaces the visible H-TMA$^+$ counterions from the chain, hence the counterion correlations are broken up (even though the polymer peak may still be present); and at 0.10 mol/L NaCl Debye-Hückel theory indicates that electrostatic interactions are screened so that the characteristic polyelectrolyte peak disappears.

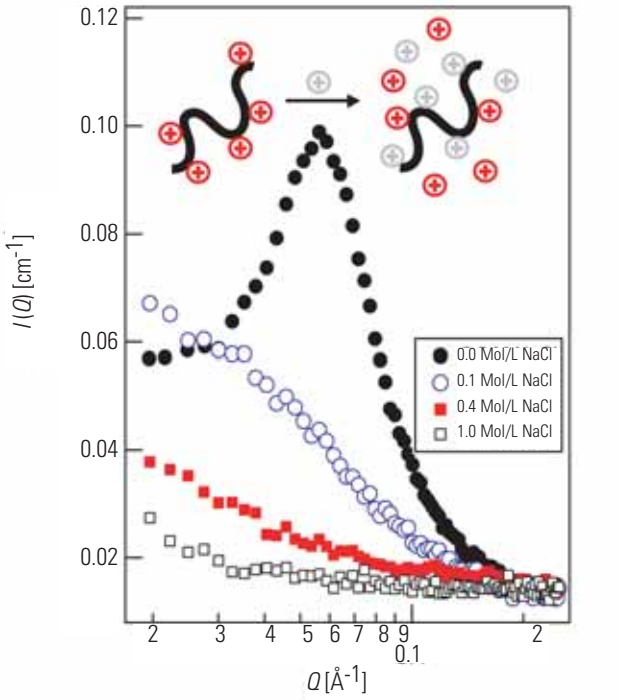

FIGURE 3.

Elimination of the polyelectrolyte peak and decrease in amplitude in the small-angle neutron scattering due to the displacement of H-TMA$^+$ counterions by added NaCl for a fixed polymer concentration C_p = 24.9 gL^{-1}.

Studying the dynamics of charged polymers presents a challenge due to the electrostatic interactions and coupled dynamics between light fast–moving counterions and heavy slow-moving polymer. Dynamic light scattering can probe dynamics at a large length scale, but local dynamics is best directly observed using neutron spin echo (NSE) spectroscopy that measures on time scales from 45 ps to 100 ns and characterizes structural information from 3 nm and 60 nm. As in the SANS experiments, we may focus on the counterion correlations, and thus observe the dynamics corresponding to the correlation length scale observed with SANS.

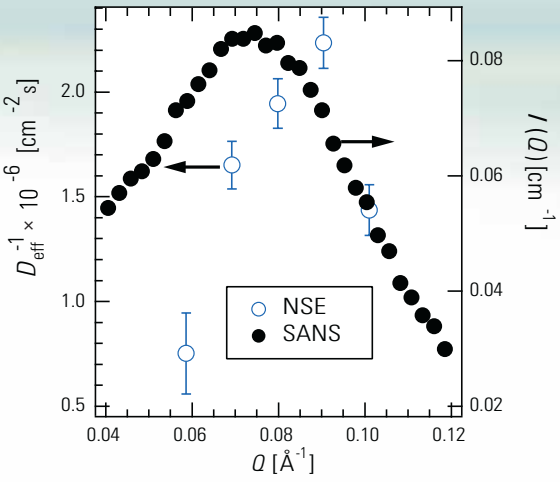

FIGURE 4.

Combined plot of SANS and NSE data illustrating the coupled dynamics slowing down near the correlation SANS peak at a polymer concentration of 45.6 gL^{-1}.

The counterion coherent dynamic structure factor, $S(Q,t)/S(Q)$, provides the direct measurement on the time scale at which pair correlations between H–TMA+ counterions decays. The nanosecond relaxation of these counterions is well resolved by NSE [2]. From the decay rate (Γ) of concentration fluctuations, the Q–dependent effective diffusion coefficient, $D_{eff} = \Gamma/Q^2$, is defined. D_{eff}^{-1} is used as a measure of the time scale of the counterion motion at a given Q. We plot the inverse effective diffusion coefficient versus Q in Fig. 4 (left axis) and the corresponding counterion SANS intensity in filled circles (right axis) for a polymer concentration of 45.6 gL^{-1}. The counterions are observed to slow down near the structural peak. Recalling that the counterion correlations mimic the polymer structure, this result suggests that we are observing coupled polyelectrolyte - counterion motions on the same length scale.

A unique contrast labeling method demonstrates the counterion viewpoint of charged polymer solution structure and dynamics. The polymer chain provides a template for the counterions under the conditions of low ionic strength leading to coupled counterion-polyelectrolyte dynamics at the nanoscale as quantified the effective diffusion coefficient.

References:

[1] Y. B. Zhang, J. Douglas, B. D. Ermi, and E. J. Amis, J. Chem. Phys. **114**, 3299 (2001).

[2] V. M. Prabhu, E. J. Amis, D. Bossev, and N. Rosov, J. Chem. Phys. **121**, 4424 (2004).

[3] V. M. Prabhu, M. Muthukumar, G. D. Wignall, Y. B. Melnichenko, J. Chem. Phys. **119**, 4085 (2003).

Improving the Shelf Life of Colloidal Suspensions

K. Chari
Eastman Kodak Company
Rochester, NY 14650

Y. -S. Seo and S. Satija
NIST Center for Neutron Research
National Institute of Standards and Technology
Gaithersburg, MD 20899

A number of commercially useful materials are formulated as aqueous colloidal suspensions. Processes such as Brownian coagulation and crystal growth that result in degradation over time influence the storage stability or shelf life of these suspensions. The degradation may be retarded using suitable surface-active additives such as surfactants or polymers. However, as illustrated in Fig.1a, the choice of proper surface-active additives is a difficult problem. Here we show a colloidal suspension of an organic compound that has been prepared by nucleation and growth using an anionic surfactant. The freshly formed suspension contains well-dispersed amorphous particles but if the suspension is left at room temperature for 49 h, one observes significant ripening and crystallization. The network of long thread-like crystals results in a loss in fluidity making the suspension unusable. If the suspension is prepared using a nonionic polymer (in addition to surfactant), the shelf life or stability is greatly enhanced (Fig. 1b). The action of surfactant and polymer is dependent on the interplay between the formation of polymer-surfactant complexes in bulk water and adsorption of the molecules at the surface of a colloidal particle in suspension. Since industrial formulations of hydrophobic colloids are relatively complex, it is useful to study adsorption at a model interface such as the air-water interface in order to better understand this part of the process.

Here we report on neutron reflectivity studies of adsorption at the air-water interface from an aqueous solution of sodium dodecyl sulfate (SDS) and Luvitec VA 64 (a random copolymer of vinyl pyrrolidone (VP) and vinyl acetate (VA) from BASF Corporation containing 60 mole % VP and 40 mole % VA and having a weight average molecular weight close to 55,000). Specifically, we consider changes at the air-water interface upon addition of this polymer to a solution of SDS that is above the critical micelle concentration (CMC). The experiments were performed at ambient temperature (21 °C) using the NG7 reflectometer.

In Fig. 2 we compare the behavior of a solution of 10^{-2} mol/L deuterated SDS (d-SDS) with that of 10^{-2} mol/L d-SDS in the presence of 2 % mass fraction Luvitec VA 64 under two different conditions based on the scattering length density (SLD) of the medium. In the first instance

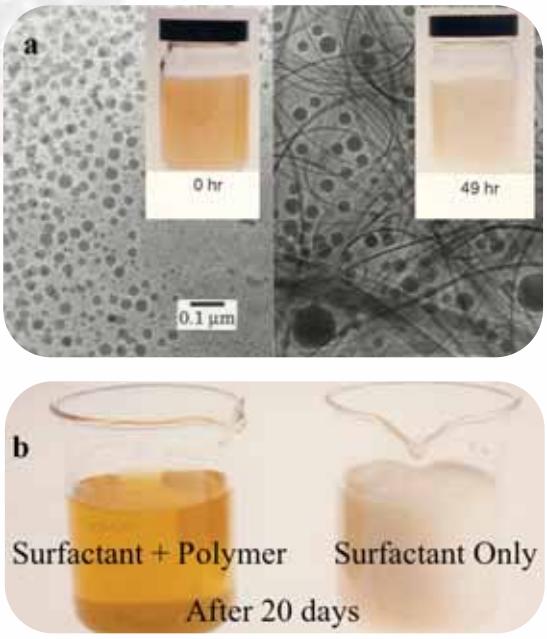

FIGURE 1.

a) Aging of a colloidal suspension of an organic compound prepared with surfactant alone at room temperature [1]. Electron micrographs show well dispersed amorphous particles in the initial (freshly formed) suspension and a network of crystals after two days under ambient conditions. b) A suspension of the same organic compound after twenty days at room temperature prepared with polymer and surfactant compared to one prepared with surfactant alone.

(Fig. 2a), we use a volume mixture of 28 % D_2O and 72 % H_2O (SLD = 1.42×10^{-6} Å^{-2}) to match the scattering length density of the medium to that of Luvitec VA 64 (making the polymer invisible.) In the second case (Fig. 2b), the scattering length density of the medium is matched to that of the surfactant; the SLD of pure D_2O (6.36×10^{-6} Å^{-2}) is very close to that of d-SDS (making the surfactant nearly invisible.) In each case reflectivity is plotted as a function of momentum transfer normal to the surface, Q_z (Å^{-1}). The solid lines represent the best fit to the experimental data and the corresponding scattering length density profiles are shown in the inset. Analysis of the data in Fig. 2a shows that the SLD of the adsorption layer decreases from $(6.5 \pm 0.3) \times 10^{-6}$ Å^{-2} for the surfactant alone to $(4.2 \pm 0.3) \times 10^{-6}$ Å^{-2} upon addition of

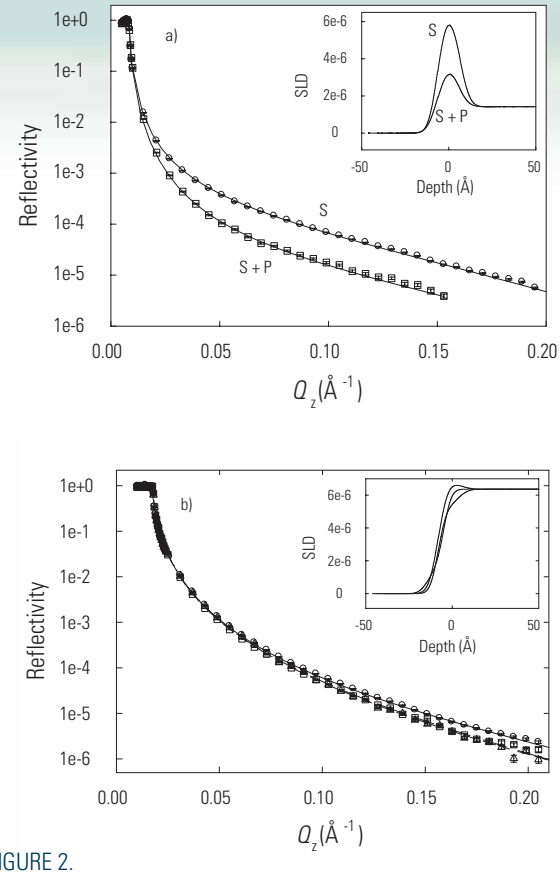

FIGURE 2.

Neutron reflectivity at the air-water interface versus Q_z for solutions in different neutron-contrast media: (a) a solution making the polymer invisible to neutrons, (b) a solution making the surfactant nearly invisible. The symbol ∘ refers to a water solution of just surfactant (S), □ refers to a solution of both surfactant and polymer (S + P), and △, refers to a solution with just polymer. The solid lines represent the best fit to the experimental data, and the corresponding SLD profiles are shown in the insets. Notice the dramatic decrease in surfactant at the interface upon adding polymer.

polymer. Furthermore, the thickness of the adsorption layer is reduced from 12.8 ± 0.5 Å to 11.0 ± 0.5 Å and the composition of the layer is changed from almost pure d-SDS to one containing only 45 % mass fraction d-SDS. The results of Fig. 2b refer to a medium of pure D_2O, the SLD of which is nearly the same as that of d-SDS. The reflectivity is reduced slightly when polymer is added to a monolayer of surfactant. It is interesting to note that the reflectivity profile upon addition of 2 % mass fraction polymer to 10^{-2} mol/L d-SDS in D_2O is almost the same as that obtained with polymer alone in D_2O. It is clear that the addition of Luvitec VA 64 to a micellar solution of d-SDS results in adsorption of the polymer at the air-water interface. Furthermore, the extent of adsorption is similar to that observed in the absence of surfactant.

The results of Fig. 2 are extremely interesting because one would not normally expect the less surface-active polymer to displace the more surface-active surfactant from the air-water interface. At the concentrations employed here the polymer can only lower surface tension at

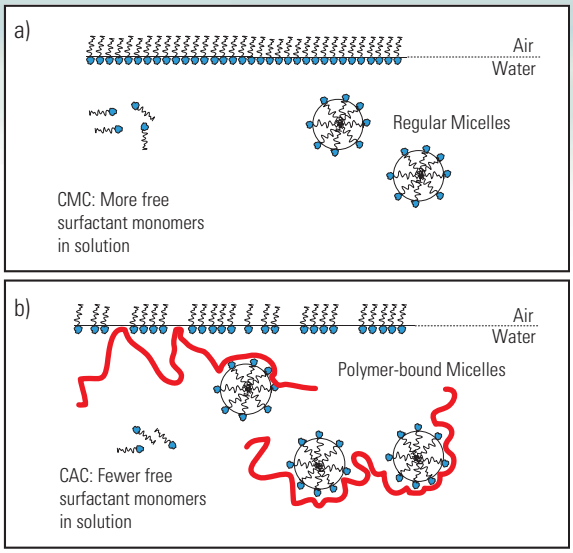

FIGURE 3.

a) Schematic representation of a 'micellar' solution of SDS. 'Regular' SDS micelles in bulk water are in equilibrium with surfactant monomer at the CMC and a fully saturated monolayer at the air-water interface. b) Upon addition of polymer to the system in Fig. 3a, the surfactant and polymer self-assemble in bulk water to form polymer-surfactant aggregates containing polymer-bound micelles. The concentration of SDS monomer in equilibrium with these aggregates is reduced from the CMC to the CAC. This results in a reduction in the amount of SDS at the air-water interface and concomitant adsorption of polymer.

the air-water interface by about 20 mN/m whereas the surfactant can lower it by more than 30 mN/m.

So why does the polymer displace the surfactant? The phenomenon is depicted in Fig. 3. In Fig. 3a we show a solution of SDS containing micelles in equilibrium with surfactant monomer at the CMC and a fully saturated monolayer at the air-water interface. If one adds to this system a polymer that can form a self-assembled complex with the micelles, then the concentration of surfactant monomer in bulk water is reduced from the CMC to the critical aggregation concentration (CAC) as the free energy of formation of polymer-bound micelles is lower. Since adsorption of surfactant at the air-water interface is governed by the concentration (or activity) of surfactant monomer in bulk water, the latter is significantly reduced (provided CAC << CMC) making room for the polymer at the interface. This clearly shows the connection between self-assembly in bulk water and adsorption at an interface, a feature having important practical consequences.

References:

[1] K. Chari, CHEMTECH **29** (6), 49 (1999).

[2] K. Chari, T. Z. Hossain, J. Phys. Chem. **95**, 3302 (1991).

[3] K. Chari, Y. S. Seo, S. K. Satija, J. Phys. Chem. B **108**, 11442 (2004).

Energetics of Membrane Fusion

L. Porcar[1,2], W. A. Hamilton[3], P. D. Butler[1,3], and G. G. Warr[4]

[1] University of Maryland
College Park, MD 20742

[2] NIST Center for Neutron Research
National Institute of Standards and Technology
Gaithersburg, MD 20899

[3] Oak Ridge National Laboratory
Oak Ridge, TN 37831

[4] University of Sydney
Sydney, NSW 2006, Australia

The fusion of membranes formed by lipid or surfactant bilayers is ubiquitous in both surfactant chemistry and cell biology. Its significance is widely recognized in living systems where membrane fusion allows controlled transport and mixing in cells. Time-slicing small angle neutron scattering is used here to study the fusion of bilayer membranes. Membranes are prepared in a stacked, parallel arrangement by steady shear, which relaxes into a multiply-connected sponge equilibrium structure on cessation of shear. The sponge is formed by the fusion of adjacent bilayers to create a network of channels in which the initial stacking direction is forgotten. By comparing this structural relaxation time to that for diffusive membrane contacts obtained from dynamic light scattering, the energy barrier to membrane fusion, which governs the relative stability of the stacked bilayer and isotropic states, is determined as a function of membrane concentration and composition.

Membrane fusion is also an important process that occurs continuously in the aptly named "sponge" surfactant phase, in which a single surfactant bilayer spans a solution in a network of randomly directed passages, shown schematically in Fig.1 [1]. The formation of a passage between two bilayer membranes proceeds in several stages as represented in Fig. 1 [2]. (i) First, the separate membranes are brought together by diffusion. (ii) On contact some initial connecting structure forms, which (iii) expands to form a solution passage. Many such events correspond to the transformation of a stack of unconnected bilayers into an isotropic sponge phase.

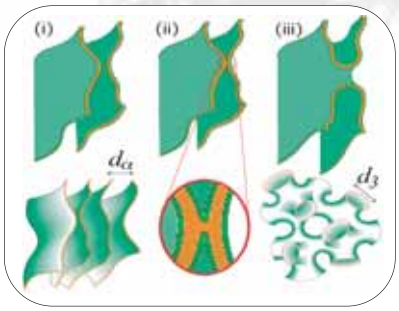

FIGURE 1.
Stages in the mechanism of membrane fusion and passage formation, and the related stacked bilayer and sponge phase geometries and characteristic sizes.

In previous work [3, 4] we showed that adding an inert thickener to the widely studied cetylpyridinium(CPCl)-hexanol mixed membrane system significantly slows membrane dynamics, making it possible to induce a sponge to transform into a stacked, passage-free, lamellar phase by application of steady shear at compositions convenient for structural and rheological characterisation. The transition depends on the shear rate, $\dot{\gamma}$, the solvent viscosity, η_s, and the membrane concentration, ϕ, with full alignment being achieved for $\dot{\gamma}\eta_s / \phi^3 \approx 2$ to 4×10^8 cPs^{-1} [5]. On cessation of shear, the lamellar phase relaxes into its equilibrium sponge phase by re-establishing the passages between membranes destroyed by the applied shear.

To track the rapidly changing structure we employed a "time slicing" technique that consists of synchronizing SANS data acquisition with

FIGURE 2.
SANS patterns for the relaxation from a stacked bilayer into a sponge. (a) Time-sliced tangential and radial SANS patterns in a Couette shear cell. Initially the bilayer membranes are aligned normal to the shear gradient direction, ∇V. After stopping the motor at $t = 0$, the isotropic sponge reforms over about 2s. (b) Normalized applied shear rate determined from the Couette motor ($\dot{\gamma}$, dashed line fit) and scattering intensity from the sponge correlation peak (I_3, dotted line fit).

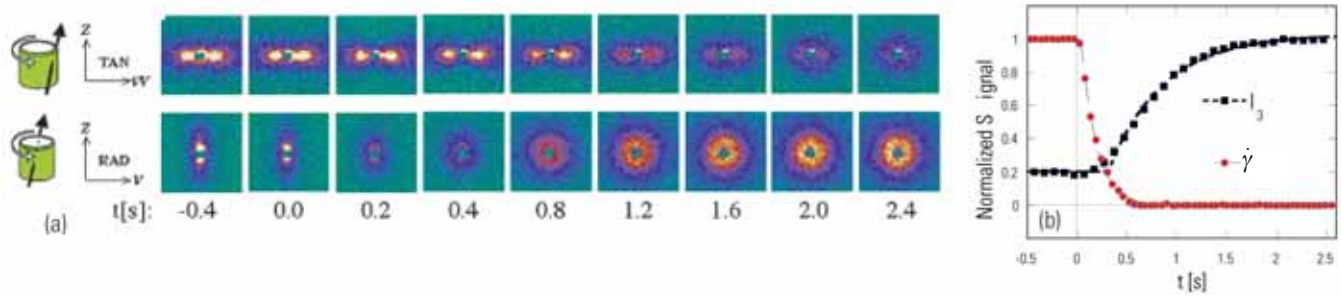

the intermittent operation of a Couette shear cell [6]. The cell was cycled through the process of shearing to a steady lamellar state, stopping, and relaxing fully to sponge equilibrium several thousand times for each sample. We thus accumulated statistically significant measurements on much shorter time scales than is possible for individual runs [7].

Fig. 2(a) shows some representative time-sliced SANS patterns accumulated at 0.1 s intervals during a relaxation series. Under shear the bilayers stack up normal to the direction of the applied shear gradient, giving rise to Bragg diffraction peaks in this direction and no signal in other directions. Fig. 2(a) shows the disappearance of the anisotropic signal from the stacked bilayers and the accompanying appearance of the sponge's isotropic ring of diffuse scattering over the course of a few seconds. Fig. 2(b) shows the growth in intensity of the isotropic scattering ring as function of time, which is directly related to the fusion of membranes to form channels and thus the structural relaxation time, τ_R. These data follow a simple exponential decay of the rate of growth of the signal as membrane fusion re-establishes the sponge with a relaxation time of approximately 0.40 s.

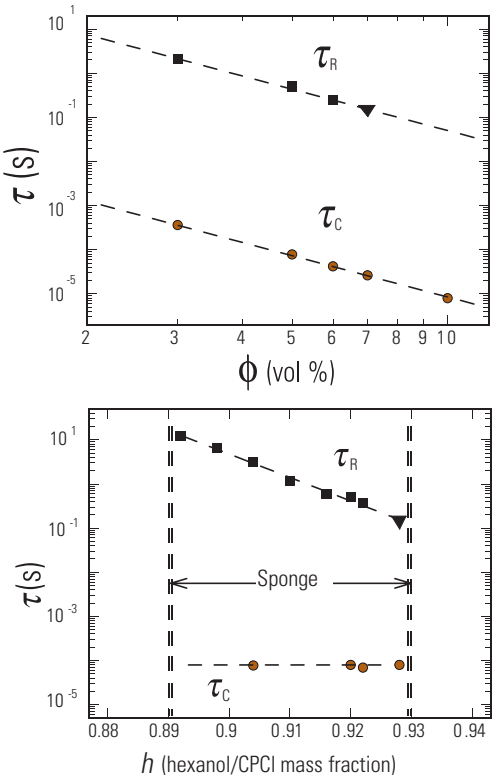

FIGURE 3.

Membrane contact time, τ_C, and structural relaxation time, τ_R, versus a) membrane volume fraction ϕ at constant membrane composition b) membrane composition, for ϕ = 5 % samples.

Membrane fusion is an activated process since it involves an energetically unfavorable intermediate state in which membranes are sharply curved and in close contact (Fig. 1(ii)). The activation energy, E_F, is the energy cost of forming this highly curved state, and relates the structural relaxation time to the interval between membrane contacts τ_C by an Arrhenius relation: $\tau_R = \tau_C \exp(E_F/k_BT)$.

The time required for membranes separated by a mean distance d_α to diffuse into contact may be obtained from dynamic light scattering, allowing the determination of E_F [2]. Figure 3a shows τ_R and τ_C determined for samples at various membrane volume fractions, but constant composition of membrane components (hexanol and CPCl) in a mass ratio h = 0.92. This composition is near the middle of the stability region of this sponge phase. Both τ_R and τ_C scale as ϕ^{-3}, as expected from the Arrhenius relation and the rheology of shear alignment [3], yielding an activation energy $E_F \approx$ 16 kJ mol^{-1} (6.7k_BT) that is independent of membrane concentration.

Variation of the membrane composition ratio h directly affects the relative stability of sponge and stacked bilayer states through the energy cost for bending the membrane into a "saddle-splay" that occurs throughout the sponge. At a constant membrane volume fraction of 5 %, Fig. 3b shows that the membrane contact time is independent of composition, but the structural relaxation time decreases by almost two decades as the hexanol content increases. This clearly demonstrates how hexanol reduces the energy cost of forming highly curved necking points in the membrane, reducing the activation energy for fusion from 25 kJ mol^{-1} (10.3 k_BT) for h = 0.892 to 14 kJ mol^{-1} (5.8 k_BT) for h = 0.928. This technique has interesting potential applications to biological membrane fusion using lipid systems with a suitable relaxation mode.

References:

[1] G. Porte, Curr. Opin. Colloid Interface Sci. **1**, 345 (1998), and references therein.

[2] S. T. Milner *et al.*, J. Phys. (Paris) **51**, 2629 (1990).

[3] L. Porcar *et al.*, Phys. Rev. Lett. **89**,168301 (2002).

[4] L. Porcar *et al.*, Langmuir **19**, 10779 (2003).

[5] M. E. Cates and S. T. Milner, Phys. Rev. Lett. **62**, 1856 (1989).

[6] L. Porcar *et al.*, Rev. Sci. Instrum. **73**, 2345 (2002).

[7] See also: W. A. Hamilton *et al.*, Phys Rev E **60**, R1146 (1999); and L. Porcar *et al.*, Physica B (in press).

Non-Lamellar Lipid Phases and the Membrane Fusion Problem

L. Ding[1], W. Liu[1], W. Wang[1], C. J. Glinka[2], D. L. Worcester[3], L. Yang[4], and H. W. Huang[1]

[1] Rice University
Houston, TX 77251

[2] NIST Center for Neutron Research
National Institute of Standards and Technology
Gaithersburg, MD 20899

[3] University of Missouri
Columbia, Missouri 65211

[4] National Synchrotron Light Source
Brookhaven National Laboratory
Upton, NY 11973

The lipid bilayers that compartmentalize the contents of living cells are flexible, robust structures that nevertheless at times must fuse to allow vital biochemical processes involving chemical transport between organelles to occur. How and under what conditions bilayers fuse has been a challenging scientific problem for many years. The primary experimental complication in studying this process has been the unstable and highly transient nature of intermediate fusion structures. We have been studying the phase behavior of substrate-supported multiple lipid bilayers by neutron and x-ray diffraction for several years, and recently discovered [1] a stable phase with features that are similar to the commonly postulated interbilayer state that is crucial to membrane fusion. In this intermediate state, two contacting monolayers become continuous via an hourglass-shaped structure called a stalk. The phase we found with x-ray diffraction consists of a three-dimensional hexagonal array of stalk-like structures.

To further validate and refine our observation of a membrane fusion intermediate structure, we have initiated complementary neutron diffraction measurements at the NCNR using a controlled humidity chamber constructed for this purpose. The objective was to measure diffraction intensities while varying the D_2O/H_2O ratio in the relative humidity as an independent method to solve the phase problem. As a first step we applied the method to the well known inverted hexagonal (H_{II}) phase of diphytanoyl phosphatidylcholine (DPhPC) depicted in Fig. 1. Aligned multilayer samples were prepared by direct deposition of lipid from an organic solution onto clean, flat silicon wafers, followed by evaporation of the solvent and hydration with saturated water vapor at room temperature. In this process the lipid spontaneously forms a stack of hydrated bilayers (in the L_α phase) parallel to the substrate. A set of six identically prepared substrates, interleaved with thin copper spacers, was held upright in a copper sample holder. The lipid sample on each wafer was in direct contact with the humidified air in the sample chamber.

The sample was pre-examined by x-ray diffraction. At 25 °C it showed three phases as a function of relative humidity (RH), namely: the lamellar L_α phase, for RH > 90 %; the rhombohedral (R) phase, which contains the stalk structure, for 80 % < RH < 90 %; and the inverted hexagonal (H_{II}) phase for RH below 80 %. In the HII phase, the diffraction pattern indicated that the lipid tubes formed periodic arrays of two-dimensional hexagonal symmetry, with the axes of the tubes lying parallel to the substrate. The sample formed domains having a definite tube orientation. The domain orientation in the plane of the substrate was random.

The neutron measurements were done on the NG-7 30 m SANS instrument in the geometry depicted in Fig. 2. The neutron wavelength was 0.5 nm, with 11 % wavelength resolution (FWHM), with the detector as close as possible to the sample, 0.875 m, resulting in a Q-range from 0.3 nm^{-1} to 7 nm^{-1}. The sample was aligned by adjusting its tilt and rotation about a vertical axis to maximize the intensity of the principal reflection from the inter-bilayer spacing. Attenuation of the incoherent scattering from the lipid by the silicon wafers cast a line shadow on the detector, which served as a reliable and convenient determination of the angle between the substrate and the incident beam. The measurements were conducted at 25 °C and 58 % RH at five D_2O/H_2O ratios: 0:1, 1:3, 1:1, 3:1, and 1:0.

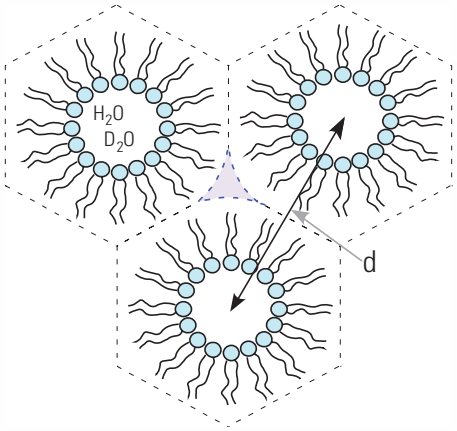

FIGURE 1.

Cross-section of the H_{II} phase in which lipid molecules self-assemble into rod-like, reverse micelle structures that form a 2D hexagonal lattice. The corresponding d-spacing of the related 1D lamellar phase, L_α, is indicated by the double-ended arrow.

Fig. 2. shows a typical SANS pattern for the DPhPC sample in the H_{II} phase, in this case for the substrate angle ω = 1.3 °. Eight independent off-specular peaks are visible, in addition to the first order specular peak (i.e., in the Q_z direction normal to the plane of the substrate) that has maximum intensity at this ω-angle. Patterns were recorded over three hours for each of five D_2O/H_2O ratios, and used to integrate the intensities of the non-specular peaks that arise from the in-plane structure of the multilayers. To obtain accurate intensities for the much stronger specular peaks, data were collected as ω was increased in steps, $\Delta\omega$ = 0.25 °, 3 minutes per step, from ω = 0 ° to 13 °.

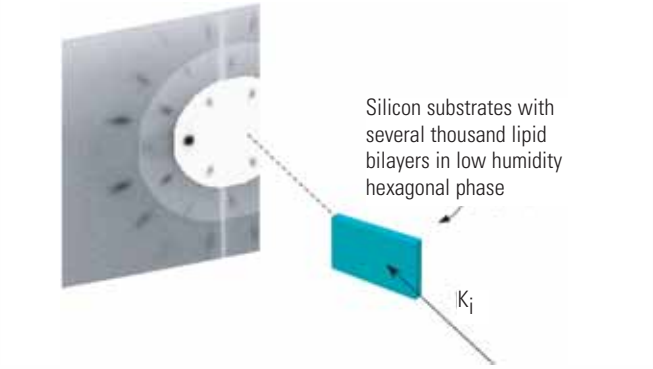

FIGURE 2.

Schematic of the sample geometry and corresponding diffraction pattern from the hexagonal phase of the phospholipid DPhPC recorded on the SANS instrument's area detector. To show all the peaks detected, the intensities of the three circular regions are on different scales. The white vertical line is the shadow of the silicon substrate that was utilized to determine the incident angle ω.

It is standard practice that one obtains integrated peak intensities from a single crystal by collecting the diffraction intensity while rotating the sample, as in the ω-scan described above. On the other hand one obtains integrated peak intensities directly in powder diffraction since the sample can be regarded as rotating without change. Here we have the unusual situation that one part of the diffraction pattern is obtained from an ω-scan while another part of the pattern, the off-specular reflections, is essentially independent of ω since it arises from powder diffraction by the domains that are randomly oriented in the plane of the sample. Therefore it was essential to verify the relative normalization between the two scans as set forth in Ref. 3. We then used the requirements of hexagonal symmetry to test our data reduction and normalization procedures. Within the estimated uncertainties in the integrated intensities, we found good agreement among all symmetry-related peaks.

The contrast variation measurements enabled us to determine, in a more direct way than the swelling method used in our previous x-ray work, the phase factors for the scattering amplitudes obtained from the integrated peak intensities. With both the amplitude and phase information available, the scattering length density distribution shown in Fig. 3 was obtained by Fourier inversion.

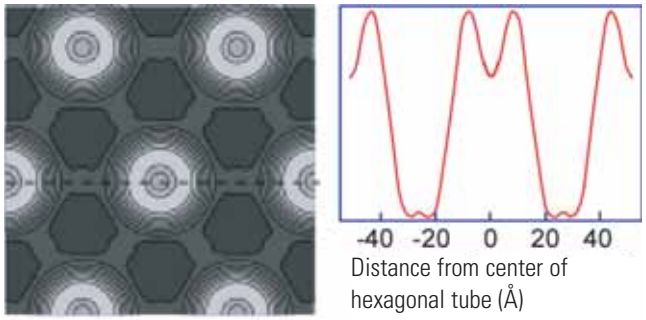

FIGURE 3.

Neutron scattering length density map (left) of pure DPhPC (d13) in the hexagonal phase hydrated with H_2O at 58 % relative humidity. The density profile along the dashed line in (a) is shown in (b).

The diffraction method used here has clear advantages over powder diffraction for detailed structure determination of lipid phases. Even for the relatively simple case described here, a powder diffraction pattern would have overlapping peaks making the measurement of intensity significantly more difficult. Perhaps the clearest advantage of the present method is the apparent lattice symmetry shown on the 2D detector. The R phase, that captures the membrane fusion intermediate structure, was readily identified by this method [2] and would have been very difficult to detect by powder diffraction. Finally the difficult phase problem can be solved very directly by this method using D_2O/H_2O exchange. We anticipate that these advantages will be highly beneficial to our continuing studies of non-lamellar lipid phases and their relation to membrane fusion structures.

References

[1] L. Ding, W. Liu, W. Wang, C.J. Glinka, D.L. Worcester, L. Yang and H.W. Huang, Langmuir (in press, 2004).

[2] L. Yang and H.W. Huang, Science **297**, 1877 (2002).

[3] L. Yang and H.W. Huang, Biophys. J. **84**, 1808 (2003).

Stabilizing Highly Immiscible Polymer Blends

J. H. Lee[1], M. L. Ruegg[1], N. P. Balsara[1,2], Y. Zhu[3], S. P. Gido[3], R. Krishnamoorti[4], M-H Kim[5]

[1] University of California
Berkeley, California 94720

[2] Lawrence Berkeley National Laboratory
Berkeley, California 94720

[3] University of Massachusetts
Amherst, Massachusetts 01003

[4] University of Houston
Houston, Texas 77204

[5] NIST Center for Neutron Research
National Institute of Standards and Technology
Gaithersburg, Maryland 20899
and University of Maryland
College Park, Maryland 20742

The word surfactant usually refers to a molecule that is used to modify the interfacial properties of aqueous systems. In their presence, mixtures of oil and water self-organize into a variety of structures such as vesicles, bilayers, lamellae, and microemulsions [1]. This rich phase behavior is due to the availability of different types of surface-active molecules such as ionic and non-ionic surfactants, cosurfactants, phospholipids, proteins, etc. In this short report we demonstrate that surfactant design concepts established in aqueous systems can be used to organize other immiscible fluids such as polymers [2]. Polymer recycling is one application that motivates our work. The immiscibility of all commercially important polymers precludes the possibility of using commingled plastic waste. If we can find surfactants to organize immiscible polymers, then these ideas may be extended to organize commingled plastic waste.

Alkyl polyglycol ether molecules (often referred to as nonionic surfactants) are examples of effective surfactants for 50/50 oil/water mixtures. Single-phase, microphase separated states are obtained in these systems in spite of the extremely low mutual solubility of oil and water. The hydrophobic and hydrophilic interactions of these nonionic surfactant molecules are comparable in magnitude [3]. They are thus often referred to as *balanced surfactants*. Our objective is to design and characterize balanced surfactants for mixtures of highly immiscible polymers. The immiscible polymers chosen for this study are polyethylene (PE) and polyisobutylene (PIB), and the surfactant is a polyethylene-*block*-head-to-head polypropylene diblock copolymer (PE-PP). We prepared four PE/PIB/PE-PP blend samples containing 10, 15, 20 and 30 volume % block copolymer, labeled B10, B15, B20 and B30, respectively. The ratio of the volume fractions of the homopolymers, ϕ_{PE}/ϕ_{PIB}, was fixed at 1.05 for all blends (approximately the critical composition of the binary homopolymer blend).

Oil/water/nonionic surfactant and PE/PIB/PE-PP mixtures are thermodynamically similar systems. Oil and water are grossly incompatible with each other. Similarly, PE and PIB are grossly incompatible polymers. Surfactant/oil interactions are generally simple and homogeneous solutions are obtained above the upper critical solution temperature (UCST). The interactions between PE and PP homopolymers are also simple and lead to a UCST. PE is thus our analog of oil. The key to balanced surfactants is the nature of surfactant/water interactions. The solubility of ethyleneoxide chains in water decreases with increasing temperature, leading to a lower critical solution temperature (LCST). Mixtures of PIB and PP homopolymers also exhibit an LCST. Thus, we chose PIB to mimic water and PE-PP to mimic the nonionic surfactant. Our conclusions regarding the phase behavior of

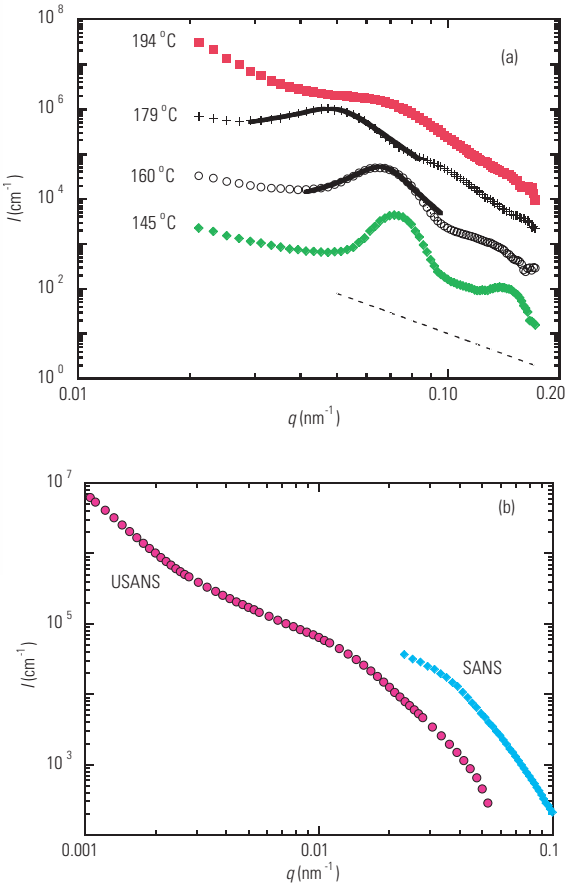

FIGURE 1.
(a) SANS profiles from B20. The dashed curve represents background. (b) SANS and USANS profiles from B10 at 145 °C.

PE/PIB/PE-PP mixtures are based on a combination of small- and ultra small-angle neutron scattering (SANS and USANS, respectively), polarized and depolarized small angle light scattering, and transmission electron microscopy (TEM). In this paper we highlight some of the SANS, USANS, and TEM results.

SANS intensity profiles, $I(q)$, where I is the scattering intensity and q is the scattering vector, for B20 at selected temperatures are shown in Fig. 1a. At 145 ˚C we see a primary scattering peak centered at $q_1 = 0.07$ nm^{-1} and a secondary scattering peak centered at $q_2 = 0.14$ nm^{-1}, corresponding to the first and second order peaks of the lamellar phase with characteristic length $d = 2\pi/q_1 = 90$ nm. At 160 ˚C and 179 ˚C, we see a broad primary peak with little or no evidence of a secondary peak (Fig. 1a). These scattering profiles are qualitatively consistent with those expected from droplet microemulsions. At 194 ˚C, we observe a sharp increase in the low angle SANS (0.02 nm$^{-1} \le q \le 0.04$ nm^{-1}), and the primary scattering peak is reduced to a shoulder (Fig. 1a). This indicates that the periodic structure obtained at the lower temperatures is lost at 194 ˚C. In Fig. 1b we show the SANS and USANS data obtained from sample B10 (filled symbols) at 145 ˚C. We find a broad but noticeable shoulder in the USANS profile in the vicinity of $q_1 = 0.01$ nm^{-1}. This indicates the possible presence of a weakly periodic structure with a characteristic length = $2\pi/q_1 = 630$ nm.

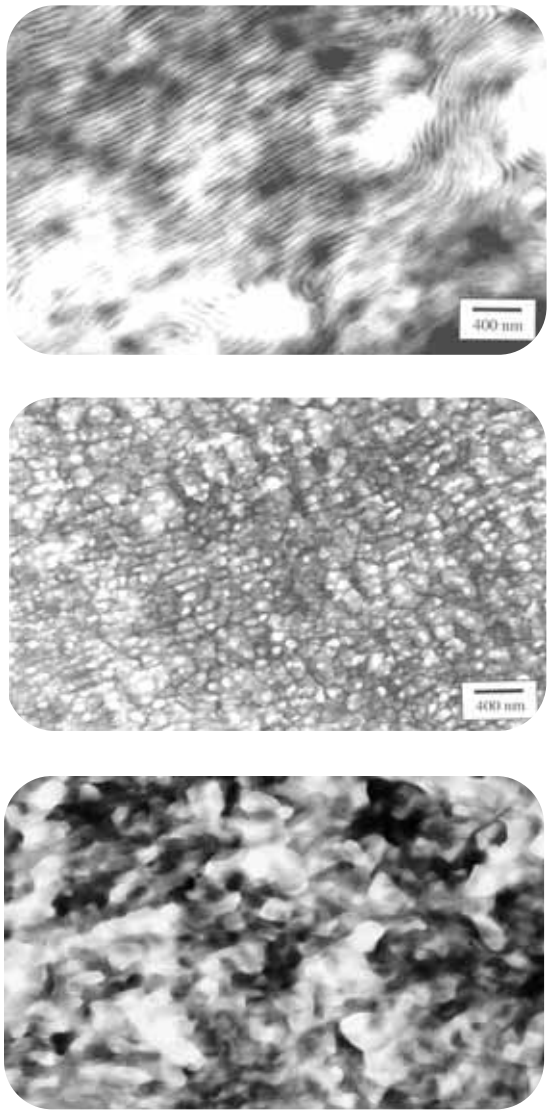

FIGURE 2.

Transmission electron micrographs of the (a) lamellar ($T = 145$ ˚C), (b) droplet microemulsion ($T = 160$ ˚C) phases of sample B20, and (c) bicontinuous microemulsion ($T = 145$ ˚C) phase of sample B10.

In Fig. 2a we show a micrograph obtained from B20 at 145 ˚C indicating clear evidence of a lamellar phase. The dark bands represent the location of the block copolymer and the bright broader bands represent alternating layers of PE and PIB. In Fig. 2b we show a micrograph obtained from B20 at 160 ˚C. It is clear that heating the sample from 145 ˚C to 160 ˚C results in a dramatic change in morphology: the lamellar phase gives way to a droplet microemulsion phase comprising nearly monodisperse droplets of PIB in a PE matrix. In Fig. 2c we show a TEM micrograph obtained from sample B10 at 145 ˚C. The structure observed is very similar to that obtained from bicontinuous oil/water microemulsions. We see white PIB-rich regions interspersed in gray PE-rich regions. We observe a broad distribution of distances between adjacent PIB-rich domains with an average of about 500 nm. The characteristic length scales of the microemulsion and lamellar phases obtained by TEM and SANS are in excellent agreement.

The phase behavior of mixtures of highly immiscible PE/PIB polymers stabilized by a PE-PP diblock copolymer was studied by a combination of experiments in both real and reciprocal space. At 145 ˚C, we found the existence of lamellar and bicontinuous microemulsion. Heating the lamellar phase leads to the formation of a droplet microemulsion at 160 ˚C. This kind of droplet microemulsion phase, wherein the volume fractions of both droplet and matrix phases are equal, has not previously been obtained in polymer blends. Our work represents the first application of surfactant design principles, proposed by Khalweit and coworkers for aqueous mixtures [3], to mixtures in which dipole-dipole and hydrogen bonding interactions are absent.

References:

[1] H. T. Davis, *Statistical Mechanics of Phases, Interfaces, and Thin Films*; Wiley-VCH: New York, 1996.

[2] J. H. Lee, *et al.*, Macromolecules, **36**, 6537 (2003).

[3] M. Kahlweit, R. Strey, Angew. Chem. Int. Ed. Engl. **24**, 654 (1985).

Neutron Reflectometry for Highly Accurate Nanometer Metrology

J. A. Dura
NIST Center for Neutron Research
National Institute of Standards and Technology
Gaithersburg, MD 20899

M. P. Seah
Quality of Life Division
National Physical Laboratory
Teddington, Middlesex, TW11 0LW, UK

Nanotechnology research and innovation require accurate measurement of features on the nanometer level, i.e. nanometrology. We report a comparison of techniques for measurements of 1.5 nm to 8 nm SiO_2 films on Si at the state of the art in precision and accuracy [1]. SiO_2 on Si is a well-understood system with high quality ultra-thin samples available. It is technologically relevant since at this thickness it serves as a gate oxide in Si electronics. The International Technology Roadmap for Semiconductors (ITRS) indicates the need for these measurements at a standard uncertainty of ≈ 1 %. The present comparison was organized under the auspices of the Consultative Committee for Amount of Substance (CCQM), the body authorized under the International Committee for Weights and Measures (CIPM) to oversee the framework for the SI system for amount of substance. Neutron reflectometry (NR), grazing incidence x-ray reflectometry (GIXRR), x-ray photoelectron spectroscopy (XPS) and ellipsometry were found to be the most accurate and precise methods.

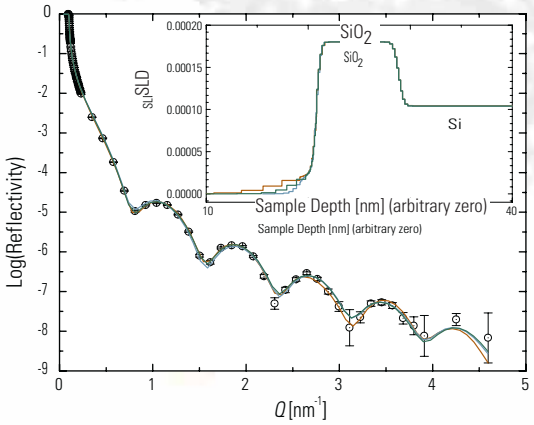

FIGURE 1. Neutron Reflectivity vs. Q (see text for details). The inset is the model depth profile of the scattering length density determined in each fit.

Sets of ten samples for (100) and (111) orientation Si were prepared by thermal oxidation. A sample from each wafer was characterized at the National Physical Laboratory (NPL) by XPS under carefully established reference conditions. Ellipsometry, providing relative differences in thickness across the wafer, was used to adjust the XPS data to determine the reference thickness d_{RT} for each sample. The SiO2 thicknesses determined by each technique at a given laboratory, d, were analyzed through the equation $d = md_{RT} + c$. Here, m scales the measurement against the XPS result, whereas c represents an offset, which incorporates the thickness of a

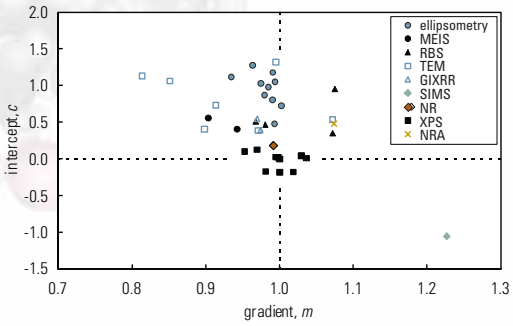

FIGURE 2. Plots of m, and c for various techniques. (from Ref 1, Fig. 20A.)

contamination layer containing adsorbed carbonaceous matter and water. In techniques that take into account the contamination, e.g. GIXRR and NR, the offset, c, can represent a misrepresentation of the contamination layer. XPS is unique in that the contamination has no effect on the result and c should be zero. It is also unique in that while being linear, its length scale has a high uncertainty and needs calibration. This calibration was an essential part of the study and showed that a 1.4 % correction was required. For all techniques, the RMS scatter of the data about the linear fit is an indication of precision. Accuracy is indicated by consistent m values near 1 and c values near 0.

NR was measured on 4 samples with d as follows: 1.65 ± 0.15 nm, 2.00 ± 0.05 nm, 5.55 ± 0.03 nm, and 8.04 ± 0.01 nm. The uncertainties encompass the full range of acceptable fits and therefore represent a 95 % confidence level. As an example, Fig. 1 shows the reflectivity vs. momentum transfer, $Q = 4\pi\sin\theta/\lambda$, for the 8 nm sample, the best fit (blue), and two poorer but acceptable fits.

XPS measurements from the 13 additional laboratories achieved excellent reproducibility when employing the reference geometry, the RMS scatter about the linear fit vs. d_{RT} ranged from 0.019 nm (NPL) to 0.136 nm. NR had the next lowest scatter of all measurements (0.026 nm), indicating high precision. For comparison, data from all techniques achieved mean RMS scatters of 0.15. A plot of m vs. c for all of the laboratories is reproduced in Fig. 2. The precision of XPS is further indicated by the small scatter of its data on this plot. The high degree of apparent accuracy of both NR and XPS is indicated by their proximity to $m = 1$, $c = 0$.

References

M. P. Seah, et al., Surface and Interface Analysis (in press).

Half-lives, Nuclear Data, and Analytical Accuracy

R. M. Lindstrom
Analytical Chemistry Division
National Institute of Standards and Technology
Gaithersburg, MD 20899

Industry depends on quality management of measurements and materials that are traceable to national or international standards. Because of its accuracy and reliability in detecting trace elements, instrumental neutron activation analysis (INAA) is generally recognized as a method of choice when new procedures are being developed or when other methods yield results that do not agree. Our continuing examination of the metrological basis of activation analysis has recently demonstrated the need for accurate nuclear data. Published high-precision measurements of decay half-lives were not in agreement with NIST values [1]. To date, the half-life of ^{76}As was redetermined and found indeed to be inconsistent with published compilations [2]. Measurements on other nuclides (^{24}Na, ^{42}K, and ^{198}Au) were found to be in satisfactory agreement with the previous consensus values [3].

A recent example of the need for accuracy arose as we attempted to determine the Ge content by INAA in a Ge:Si alloy, an important electronic material. Because the literature half-life did not match the observed decay, we proceeded to measure an irradiated specimen of pure Ge. The sample was counted continuously for 5 days (10 half-lives) in conjunction with a precision pulser. The half-life was determined separately for each of ten singlet and multiplet gamma peaks (^{77}Ge has 240 of them) using a chi-squared minimization method to fit the standard decay equation $A_i = A_0 e^{-\lambda t}$. The average of these measurements is 11.174 h ± 0.009 h, where the uncertainty is the standard deviation of the mean. By comparison, the 8th *Table of Isotopes* [4] gives the half-life as 11.30 h ± 0.01 h, differing by 13 standard deviations of the mean from the current measurement.

Plotting $A_i/e^{-\lambda t}$, where A_i is the measured activity and λ is the correct value of the decay constant, should yield a constant (A_0). Figure 1, showing measurements at one peak (416 keV), illustrates the consequence of putting the wrong decay time into the above formula. As can be seen, the value of λ taken from the literature (blue circles) leads to a serious discrepancy. (The half life is given by $ln(2)/\lambda$.)

In the most precise work, even the standard equation for the decay-corrected activity is inadequate to describe a measurement. When decay, pileup, and dead time are all important, a "coupled" approach giving a more adequate expression for pulse pileup has been derived [5] and applied [6] in this laboratory to the precise determination of half-life in aluminum. The pulse pileup correction factor is the continued function

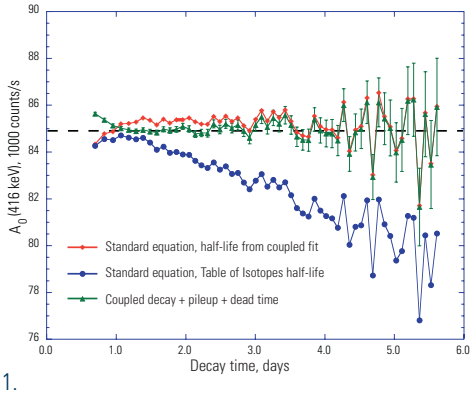

FIGURE 1.

The extrapolated activity $A_{0,sat}$ at 416 keV of a source of ^{77}Ge decaying over ten half-lives. The downturn of the red diamonds and blue circles at short decay time shows the effects of high dead time on using the standard equation for analysis. Varying λ, chi-squared minimization of the coupled approach data (see text) to a constant gives a half-life of 11.20 hours. The coupled approach also reveals the expected amount of residual 1.4-hour ^{75}Ge in the first day. The Table of Isotopes value of 11.3 hours (blue circles) is clearly too long to represent these data.

$f_{pileup} = \exp(\alpha I_0 \exp(\alpha I_0 \ldots)))$, where the parameter α is determined by calibration. Although the generalized treatment of coupled dead times is still a research topic [7] the latter expression describes the ^{77}Ge decay still better at high dead times, as shown by the green triangles in Fig. 1.

Assessing the quality of published nuclear data is becoming more important as formal quality specifications such as ISO/IEC 17025 are becoming required in more applications.

References

[1] R. R. Greenberg, R. M. Lindstrom, and D. S. Simons, J. Radioanal. Nucl. Chem. **245**, 57 (2000).

[2] R. M. Lindstrom, M. Blaauw, and R. F. Fleming, J. Radioanal. Nucl. Chem. **257**, 489 (2003).

[3] R. M. Lindstrom, M. Blaauw, and M. P. Unterweger, J. Radioanal. Nucl. Chem. **263** (2005(in press))

[4] R. B. Firestone, and V. S. Shirley, Table of Isotopes, 8th ed. (Wiley, New York, 1996).

[5] R. F. Fleming, Trans. Am. Nucl. Soc. **33**, 234 (1979).

[6] R. F. Fleming, and R. M. Lindstrom, J. Radioanal. Nucl. Chem. **113**, 35 (1987).

[7] J. W. Müller, Nucl. Instrum. Methods A**301** (1991) 543.

Proof of Concept for Thermal Neutron Laue Diffraction

B. H. Toby[1], T. D. Pike[1,2], C. Y. Jones[1], A. Santoro[1], D. Johnson[1], P. C. Brand[1], E. Prince[1], and D. L. Jacobson[3]

[1] NIST Center for Neutron Research
National Institute of Standards and Technology
Gaithersburg, MD 20899

[2] Johns Hopkins University
Baltimore, MD 21218

[3] Physics Laboratory
National Institute of Standards and Technology
Gaithersburg, MD 20899

To explore the possible advantages of neutron Laue diffraction, a prototype instrument has been developed. This instrument has allowed for extremely rapid data collection and suggests bright prospects for this type of measurements within the NCNR.

Neutron diffraction has many advantages over the corresponding x-ray technique. Neutrons generally provide better sensitivity to light atom positions and more structural detail, since data can be collected over a wider region of Q. Neutron measurements are typically less affected by experimental artifacts, such as absorption or sample container scattering, and structural models may also be more accurate. While the past few decades have seen a significant growth in neutron *powder* diffraction, this has not occurred in neutron *single-crystal* diffraction. The reasons for this are twofold: traditional neutron single-crystal measurements require samples in the range of 1 mm^3 to 10 mm^3, which are rarely available, and one or more weeks of beam time to collect a full dataset. Ironically, there has been a huge growth in *x-ray* single-crystal practice, both in the 1980's, and again in the current decade, due to significant advances in instrumentation.

For neutron single-crystal measurements to have any significant impact in science, data collection times should not exceed a few days, so that reasonable throughput becomes possible. Crystal sizes must drop to the < 0.1 mm^3 range, to increase the range of materials that can be studied. Laue diffraction is a technique that offers these possibilities. In this method, a stationary single crystal is placed in a "white" neutron beam—one with a wide range of wavelengths. This allows a large number of reflections to diffract so that the number of these reflections is limited only by the solid angle for the area detector. It is also the most effective use of a reactor neutron source, since the entire thermal spectrum is put to work.

The ILL has developed two Laue instruments, LADI and VIVALDI, for macromolecular and small molecule/inorganic materials, respectively; these instruments are revolutionizing the field. The ILL designs, however, are not appropriate for the NCNR, where gamma backgrounds can be expected to be comparable to the peak scattered neutron flux.

To explore how neutron Laue diffraction might be pursued at the NCNR, a prototype camera was developed for use at the thermal column. The initial design uses dysprosium foil as a cylindrical "film" to capture the neutron intensities and the autoradiogram from the Dy foil is then recorded using conventional image plates. The cylindrical geometry offers a very large solid angle that could even be extended through use of Dy foil on the cylinder top and bottom.

Initial measurements at the thermal column indicate that with a conventional, *circa* 10 mm^3 crystal of NaCl, a complete diffraction pattern may be collected in a 1/2 hour! This crystal is two orders of magnitude larger than what is needed, but significantly longer measurement times are certainly possible. It is also worth noting that the Dy foil technique has been estimated to have a quantum efficiency of less than < 0.1, so more efficient detection could also offer an order of magnitude improvement. Initial measurements were attempted with minimal collimation and shielding; improvements in this are expected to significantly improve sensitivity. Finally, if an instrument can be designed for a thermal beam-port use, at least another order of magnitude in flux can be gained. Based on this evidence, neutron Laue diffraction at the NCNR should be able to offer US researchers access to the power of neutron single-crystal diffraction.

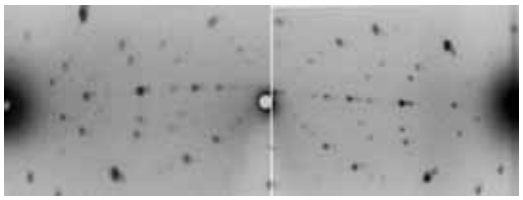

FIGURE 1.

An initial Laue diffraction image from a 35 minute neutron exposure using a ≈10 mm^3 NaCl crystal. The backscattering region is in the center of the image.

FIGURE 2.

Simulated Laue image for NaCl in approximately the same orientation as in the experimental image. Degree of reflection order superposition is indicated by color: three orders is shown in blue, two in red and those without any superposition are in green.

Determining Statistical Uncertainty in Models Fitted to Pair Distribution Functions

B. H. Toby
NIST Center for Neutron Research
National Institute of Standards and Technology
Gaithersburg, MD 20899

S. J. L. Billinge
Michigan State University
East Lansing, MI 48824

A recent collaboration between the NCNR and Michigan State University has established theory for statistical error estimation in results determined from pair distribution analysis. This advance will allow increased utilization of the technique for structural study. It can also be expected to result in improvements in the associated experimental techniques and data processing techniques.

Crystallography provides exquisite detail of atomic structure in crystalline materials through analysis of Bragg scattering intensities. However, Bragg scattering effectively superimposes columns of unit cells with lengths ≈ 100 Å in electron diffraction, and from superimposing all unit cells a volume > 10^6 Å^3 for x-ray and neutron scattering. At best, crystallographic methods will see localized deviations from long-range order as disorder due to this superposition. In contrast, spectroscopic methods are typically sensitive to atom arrangements over very short distances, usually limited to the first or second coordination sphere. The one technique that can be used to obtain information over a range of 2 Å to 50 Å, when local ordering is not reflected in the long-range structure of a material is to directly fit models to experimental pair distribution functions (PDF).

To determine the PDF, powder diffraction is measured over a wide range in Q; corrections are applied to obtain $S(Q)$; the entire data, including both Bragg and diffuse scattering is then Fourier transformed, resulting in a PDF, $G(r)$, which indicates the probability of finding pairs of atoms separated by distance r. The PDF contains information on both local and mid-range structure. PDF analysis is traditionally applied to glasses, liquids and amorphous materials, where no crystalline order is present. However, PDFs are used increasingly for structural analysis of local order in crystalline materials, to the level that the Los Alamos National Laboratory has recently developed a new moderately high-resolution powder diffractometer, NPDF, specifically for PDF determinations.

In contrast to crystallographic techniques, where accuracy levels are well established and statistical uncertainties are well understood, accuracy and precision have been open questions in PDF analysis. Limited statistical error theory for the PDF was developed a decade ago [1], but these methods do not yield error estimates for models fitted to the PDF, or even coordination numbers from integrating the PDF. The lack of error estimates has hampered acceptance of PDF results. While this lack has been much discussed over the last decade, only recently was this problem addressed. Building on results from decades of work in statistical crystallography done within the NCNR [2], theory for statistical error analysis of PDF results was developed and published this year [3]. These results are straightforward and are summarized in the box reproduced below.

$S(Q_j)$,$\sigma[S(Q_j)]$ are known from experiment.
Model predicts observation y_i as $M_i(\mathbf{p})$ where $\mathbf{p}$ is a vector of parameters.
Design matrix, A, is defined as $A_{ij} = \frac{\partial M_i(\mathbf{p})}{\partial P_j}$
PDF is $G(r_k) = \frac{2}{\pi^2} \sum_j Q_j [S(Q_j) - 1]\sin(Q_j r_k)\Delta Q_j$.
Covariance matrix for $G(r)$ is,
$V_{G,jk} = \frac{4}{\pi^2} \sum_i Q_i^2 \sin(Q_i r_j)\sin(Q_i r_k)\Delta Q_i^2 \{\sigma[s(Q_i)]\}^2$.
Linear functions of $G(r)$, $f\{G(r)\} = \mathbf{f}^T\mathbf{g}$ and $\sigma[\{G(r)\}] = \mathbf{f}^T\mathbf{V}_G\mathbf{f}$.
The best fit to PDF is obtained by solving $\mathbf{A}^T\mathbf{V}_G^{-1}\mathbf{A}\mathbf{p} = \mathbf{A}^T\mathbf{g}$.
Resulting covariance matrix for model is $V_p = (\mathbf{A}^T\mathbf{V}_G^{-1}\mathbf{A})^{-1}$ so that uncertainty on parameter p_j is given by $\sigma[p_j] = V_{p,jj}$.

These equations allow experimental uncertainties to be established for parameters fitted to a PDF in exactly the same manner as that used for crystallographic studies. In fact, PDF analysis can be expected to have smaller statistical uncertainties than Rietveld results, since PDF data will normally utilize a greater range of data. Modifications will be needed to PDF computation software to generate and save the covariance matrix for the PDF. Likewise changes will also be needed to software that fits models to a PDF. However, considerable interest in these adaptations is apparent. The development of statistical uncertainty theory for the PDF can also be expected to result in improved experimental methods and of data treatment, as it will be possible to identify systematic errors when deviations exceed statistical limits, so that the underlying reason for the discrepancy can be identified and addressed.

References

[1] B. H. Toby and T. Egami, Acta. Cryst. A **48**, 336 (1992).
[2] E. Prince, *Mathematical Techniques in Crystallography and Materials Science*, Second ed.(Springer-Verlag, New York, 1994).
[3] B. H. Toby and S. J. L. Billinge, Acta. Cryst. A **A60**, 315 (2004).

Development of a Sensitive Fast-Neutron Spectrometer

B. M. Fisher
Tulane University
New Orleans, LA 70118

J. S. Nico, A. K. Thompson, D. M. Gilliam
Physics Laboratory, Ionizing Radiation Division
National Institute of Standards and Technology
Gaithersburg, MD 20899

The Neutron Interactions and Dosimetry Group of the Ionizing Radiation Division is engaged in the development of a new class of fast-neutron spectrometers that are expected to be both sensitive and relatively compact. This development is motivated primarily by needs for measurement services and standards for homeland security applications, such as personnel radiation dose measurements in the vicinity of active interrogation devices (used for inspection of packages and cargo). In addition, this spectrometry development may find applications in low-background/underground science. In the course of this work, it has been necessary to revive lost technology for lithium-loaded liquid scintillators. We have recently had success in finding an effective scintillation cocktail based on a mixture of an aqueous LiCl solution and an experimental di-isopropyl naphthalene scintillator with surfactants. This solution was obtained with help from the British Division of Zinsser Analytic; it has extremely good clarity, light output, and stability. We are studying segmented arrays of this liquid scintillator to improve its energy resolution and are using delayed coincidence with thermal neutron capture in the ^{6}Li to reduce ambient and cosmic-ray backgrounds.

We have been collaborating with a Russian group led by V.N. Gavrin on neutron spectrometer development for more than four years [1]. Gavrin's team had used a 15 liter liquid scintillator requiring delayed coincidence with thermal neutron capture to measure extremely low levels of neutron fluence rates for a selection of materials to be used in the construction of the underground laboratory for the Russian-American Gallium Experiment (SAGE) solar neutrino experiment. With the 15 liter detector, Gavrin *et al.* were able to measure neutron fluence rates as low as 10^{-7} cm^{-2} s^{-1}, in spite of much higher fluence rates of gamma-ray background radiation. However the energy resolution of this spectrometer was a rather modest 40 % and the efficiency was only about 9 %. The Russian team proposed improving both of these performance parameters by breaking up the 15 liter volume into smaller segments and replacing the ^{3}He tubes with dissolved ^{6}Li for the thermal neutron capture detection. The energy resolution should be improved by segmentation because of the nonlinearity of scintillation light production as a function of proton recoil energy; e.g., a 4 MeV recoil event gives more light than two 2 MeV recoils. With sufficiently fine segmentation, a given neutron will usually produce only one recoil in any particular segment so that these can be observed separately and properly interpreted using the known nonlinear light production function. The efficiency for delayed neutron capture coincidence is improved by incorporation of the capturing nuclide within the liquid scintillator solution, because of reduced parasitic capture in hydrogen and reduced neutron leakage prior to thermalization.

The figures show recently obtained proton recoil spectra, the delayed coincident lithium capture events, and the time-distribution of the capture events. These spectra have been obtained using NIST-developed data acquisition software, based on digitization and time-stamping of all pulses. Monte Carlo simulations are also ongoing for optimally scaling up the current results from a single 125 ml detector to a large 16-segment array.

Reference:

[1] J.N. Abdurashitov, V.N. Gavrin, A.V. Kalikhov, V.L. Matushko, A.A. Shikhin, V.E. Yants, O.S. Zaborskaia, J.M. Adams, J.S. Nico, and A.K. Thompson, Nucl. Instrum. Meth. A **476**, 318 (2002).

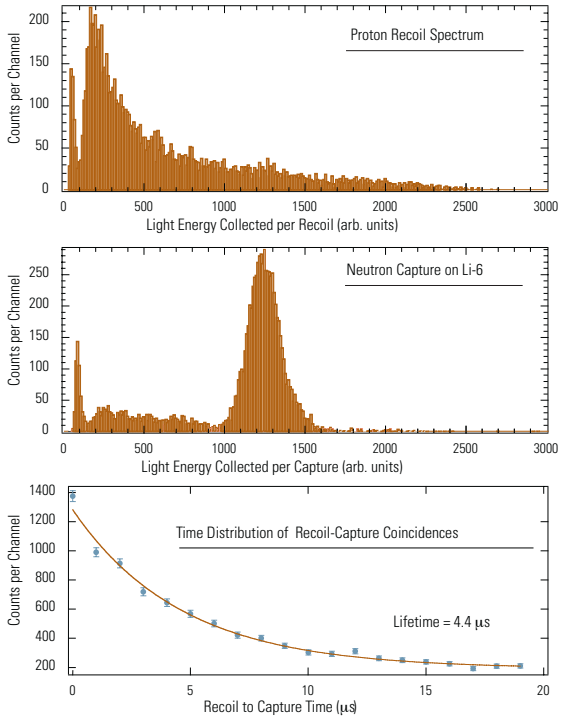

Serving the Science and Technology Community

Dynamic equilibrium may be the best way to describe the current status of the NCNR user program. New instruments continue to come on line, existing ones are being upgraded to remain at an internationally competitive level, while older ones are being withdrawn from general user service. The AND/R instrument (Advanced Neutron Reflectometer/Diffractometer), primarily intended for reflectometry studies in the biosciences, is now fully functional. The CNBT consortium is heavily involved in using its capabilities to full advantage in research on the structure of membranes. The first call for proposals including AND/R is in progress. The NCNR User's Group has carried out an independent survey of our user base, indicating a high level of user satisfaction, with many useful comments on possible improvements (see details below). The number of participants, as shown in the figure, continues to grow, but at a slower rate than in past years. The first of two Calls for Proposals in Fiscal year 2004 stimulated the submission of 200 proposals, a number similar to those for the three previous calls. 58 % of the proposals were approved, with a total beam-time allocation of 569 instrument days. The second Call is in progress at the time of this writing. Despite budgetary constraints that forced the withdrawal of the Fermi Chopper Spectrometer and the Filter Analyzer Spectrometer from the general user program, and curtailment of time on two neutron reflectometers, the number and quality of the accepted proposals ensures that scientific productivity will be maintained at a high level.

A Survey of NCNR Users

Our user group, headed by Nitash Balsara of the University of California at Berkeley, recently made an independent survey of our community. The results were both gratifying and informative. The survey covered seven main subjects: the proposal process for obtaining beam time, health physics training, user support facilities, sample environments, instrument performance and support, and software performance and support. Participants were asked to rate their experiences on a scale of 1 to 3 (1 = poor, 2 = adequate, 3 = excellent). Of the 160 responders, 41 % were professors, 31 % were graduate students and post-docs, and 23 % were staff scientists. The proposal process received a rating of 2.7, health physics training rated 2.5, user support facilities 2.5, sample environment 2.7, primary NCNR instrument used 2.8, and data analysis and software 2.5. In the cases of sample environments and major instrumentation, a majority felt that performance was excellent. 67 % of users felt that the instrument they used was excellent, while 94 % rated support from the NCNR staff as excellent. 66 % of users felt that the sample environment, another key aspect of the user experience, was excellent, while 87 % rated the staff support in this area excellent. These data indicate that while the NCNR provides access to world-class instruments, its real strength lies in the support provided by dedicated staff scientists. It is also clear that users with well-written proposals gain access to the NCNR facilities: 81 % of users rated the proposal submission process as excellent. The responses provided a number of good ideas for new instruments and sample environments. 56 % of the users felt that remote viewing of instrument status and data would be useful. These inputs provide specific avenues for improving the effectiveness of the NCNR.

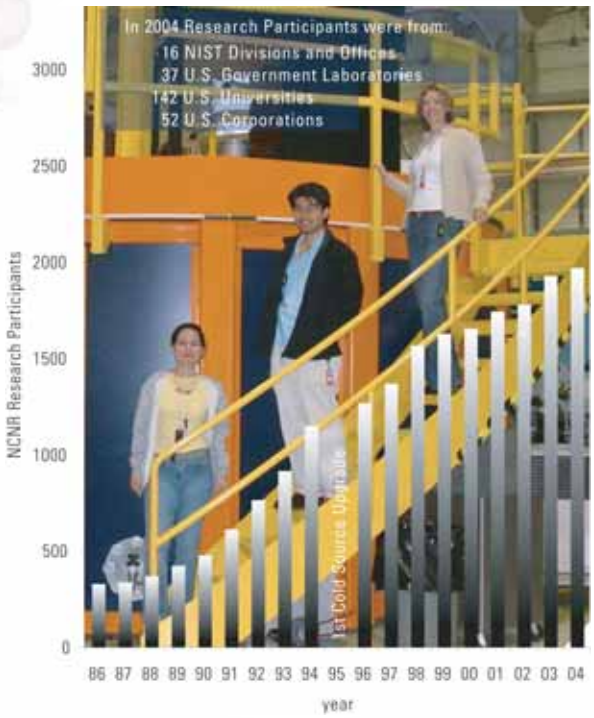

Tenth Annual Summer School

Educating young scientists in the practice of neutron scattering science is an important component of CHRNS activities. Each summer, a week-long course on neutron methods is held, with the emphasis on spectroscopy or SANS and reflectometry in alternating years. The latter topics were the theme of this year's course, held at the NCNR in early June 2004. A one-day schedule of lectures preceded three days of hands-on instruction, including six experiments and the associated

data analysis. Divided into groups of six to eight, the 35 students carried out SANS studies of tri-block copolymer solutions, surfactant-coated colloidal particles, and latex microspheres, as well as reflectometry experiments on GaMnAs magnetic films, lecithin/cholesterol membranes, and polymer monolayers at an air-liquid interface. On the final day, the student groups presented their results to their compatriots and the summer school staff. The student evaluations of the course indicate that the school continues to be a very effective method of introducing advanced neutron methods to agile young minds.

Center for High Resolution Neutron Scattering

The Center (CHRNS) is a partnership between NIST and the National Science Foundation (NSF) that has been crucial to the development and operation of user instruments at the NCNR. It offers a suite of instruments unmatched in North America for the investigation of the structure and dynamics of solids by neutron scattering, probing length scales from 1 nm to ≈ 10 μm and energies from ≈ 30 neV to ≈ 100 meV. Most of the proposals we receive ask for time on one of the CHRNS instruments, which include a 30 m SANS diffractometer, the high-resolution USANS diffractometer, the backscattering spectrometer (HFBS), the disk-chopper spectrometer (DCS), the neutron spin-echo spectrometer (NSE), and the cold-neutron triple-axis spectrometer (SPINS). An upgraded 10 m SANS diffractometer will be included among the CHRNS instruments in 2005. CHRNS also plays a major role in the NCNR's educational activities, through its annual weeklong summer school on neutron scattering, and its other outreach efforts.

Cold Neutrons for Biology and Technology

A new instrument for structural biology, the Advanced Neutron Diffractometer/ Reflectometer, AND/R, is now fully operational. This instrument and other facilities dedicated to studies of biological membrane systems are part of the Cold Neutrons for Biology and Technology (CNBT) research initiative, a consortium funded by the National Institutes of Health (NIH-NCRR), with contributions from NIST, the University of California at Irvine, the University of Pennsylvania and the Johns Hopkins University. In addition to the above-mentioned institutions, the CNBT partnership encompasses investigators from Rice University, Carnegie Mellon, Duke, and the NIH-NIAAA, as well as collaborators from the Los Alamos National Laboratory. Other CNBT resources include 10 % of the time on the NG-7 30 m SANS diffractometer, a fully equipped biology laboratory, and two state of the art computer clusters—one at NCNR and one at UC Irvine—for molecular dynamics simulations. This combination provides a powerful set of capabilities for US researchers interested in structural biology problems that involve membrane systems, largely due to the first major NIH investment in years into neutron scattering.

Independent Programs

The Neutron Interactions and Dosimetry Group (Physics Laboratory) provides measurement services, standards, and fundamental research in support of NIST's mission as it relates to neutron technology and neutron physics. The national and industrial interests served include homeland security, neutron imaging, scientific instrument calibration, nuclear-electric power production, radiation protection, defense nuclear energy systems, radiation therapy, and magnetic resonance imaging. The group's research comprises three major activities. The first is Fundamental Neutron Physics, including magnetic trapping of ultracold neutrons, operation of a neutron interferometry and optics facility, development of neutron spin filters based on laser polarization of 3He, measurement of the beta decay lifetime of the neutron, and investigations of other coupling constants and symmetries of the weak interaction. This project involves a large number of collaborators from universities and national laboratories. The second is Standard Neutron Fields and Applications, using both thermal and fast neutron fields for materials dosimetry in nuclear reactor applications, neutron spectrometry development, and for personnel dosimetry in radiation protection. The third is Neutron Cross Section Standards, including experimental advancement of the accuracy of such standards, as well as their evaluation, compilation and dissemination.

The Smithsonian Institution's Nuclear Laboratory for Archeological Research is part of the Anthropology Department at the American Museum of Natural History. During its 27 year partnership with NCNR, it has chemically analyzed over 28 900 archaeological artifacts by Instrumental Neutron Activation Analysis (INAA), drawing extensively on the collections of the Smithsonian, as well as on those of many institutions world-wide. The analyses provide a means of linking these diverse collections together to study continuity and change in the production of ceramic objects. INAA data are used to determine if groups of ceramics have been made from the same or different raw materials. They can then be attributed to geographic regions, specific sources, workshops and even individual artists. The ability to link pottery groups found in archaeological contexts to specific production locations is currently being used to examine trade and cultural exchange between the Valley of Mexico and the Maya Civilization through analysis of ceramics from the city of Teotihuacan.

The Polymers Division of the Materials Science and Engineering Laboratory works with the NCNR in research on electronics materials, nanomanufacturing, polyelectrolyte solutions, and biomaterials. The variety of methods employed in these studies include small angle neutron scattering (SANS), neutron reflectometry and neutron spin echo (NSE) spectroscopy. In the electronics materials research, the NCNR provides unique measurements that impact next-generation photolithography, including the in-situ distribution of

aqueous base and water in ultrathin polymer films, the segmental dynamics of polymers, and measurement of the spatial form of the deprotection reaction. In the nanomanufacturing program, neutron techniques are used to elucidate the underlying principles of dispersing and manipulating advanced materials such as carbon nanotubes and block copolymer solutions. For polyelectrolyte solutions, the chain dynamics and equilibrium structure differ from those of neutral polymers due to the presence of long-ranged electrostatic interactions. Measuring the local structure and dynamics requires new experimental methods, such as SANS to characterize the equilibrium structure and NSE spectroscopy to study the dynamics occurring at lengths between 3 nm and 60 nm, and times from 45 ps to 100 ns. In the biomaterials program, NCNR instruments provide important structure and dynamics information for tissue engineering, regenerative medicine, and protein preservation.

The Nuclear Methods Group (Analytical Chemistry Division, Chemical Sciences and Technology Laboratory) develops and applies nuclear analytical techniques for the determination of elemental compositions, striving for improvements in accuracy, sensitivity, and selectivity. The group has pioneered the use of cold neutrons as analytical probes in two methods, prompt-gamma activation analysis (PGAA) and neutron depth profiling (NDP). In PGAA, the amount of a particular analyte is measured by detecting characteristic gamma rays emitted by the sample while it is being irradiated in an intense cold-neutron beam. NDP is another in-beam method that can characterize the concentration of several elements as a function of depth in the first few microns below a surface. It accomplishes this by energy analysis of the charged particles emitted promptly during neutron bombardment. In addition to NDP and PGAA, the group has a high level of capability in two more conventional methods, instrumental and radiochemical neutron activation analysis (INAA and RNAA). In aggregate, the techniques used by the group are a powerful set of complementary tools for addressing analytical problems for both in-house and user programs, and are used to help certify a large number of NIST Standard Reference Materials.

The Center for Food Safety and Applied Nutrition, U.S. Food and Drug Administration (FDA), directs and maintains a neutron activation analysis (NAA) facility at the NCNR. This facility provides agency-wide analytical support for special investigations, and emergency response, complementing other analytical techniques used at FDA with instrumental, neutron-capture prompt-gamma, and radiochemical NAA procedures, radioisotope x-ray fluorescence spectrometry (RXRFS), and low-level gamma-ray detection. This combination of analytical techniques enables diverse multi-element and radiological information to be obtained for foods and related materials. The NAA facility supports agency quality assurance programs by developing in-house reference materials, by characterizing food-related certified reference materials with NIST and other agencies, and by verifying analyses for FDA's Total Diet Study Program. Studies include development of RXRFS methods for screening food ware and food packaging materials for the presence of Pb, Cd and other potentially toxic elements, use of instrumental NAA to investigate bromate residues in bread products, development of Compton suppression techniques for instrumental NAA, and use of prompt-gamma NAA to determine elemental compositions of NIST Ephedra Standard Reference Materials and commercial dietary supplements.

The ExxonMobil Research and Engineering Company is a member of the Participating Research Team (PRT) that operates, maintains, and conducts research at the NG-7 30 m SANS instrument and the NG-5 Neutron Spin Echo Spectrometer. Their mission is to use those instruments, as well as other neutron scattering techniques available to them at NCNR, in activities that complement research at ExxonMobil's main laboratories as well as at its affiliates' laboratories around the world. The aim of these activities is to deepen understanding of the nature of ExxonMobil's products and processes, so as to improve customer service and to improve the return on shareholders' investment. Accordingly, and taking full advantage of the unique properties of neutrons, most of the experiments we conduct here at NCNR use SANS or other neutron techniques to study the structure and dynamics of hydrocarbon materials, especially in the fields of polymers, complex fluids, and petroleum mixtures. ExxonMobil regards its participation in the NCNR and collaborations with NIST and other members of the scientific community not only as an excellent investment for the company, but also as a good way to contribute to the scientific health of the nation.

Scientists and engineers based at the nation's universities contribute substantially to the development of state-of-the-art neutron beam instruments, as well as maintaining collaborative research programs of exceptional quality at the NCNR. The University of Maryland stations a number of scientists at our facility, performing research with our most advanced instruments, as well as contributing to their operation. The development of the SPINS and MACS spectrometers owes much to the leadership of personnel from The Johns Hopkins University, who also carry out an outstanding neutron scattering program at the NCNR. The CNBT consortium, as described previously, is led by a group including the University of California at Irvine, The University of Pennsylvania and The Johns Hopkins University, with participation from Rice, Carnegie Mellon, and Duke Universities.

For more than thirty years, the U.S. Army Research Laboratory (USARL) has conducted a neutron scattering program at the NCNR, investigating materials at high pressures, the dynamics of molecular solids, and texture and stresses in engineering materials. The USARL group has also contributed significantly to NCNR instrumentation, most notably by initiating the development of a residual stress diffractometer.

Operations

The NIST reactor (NBSR) operated for 211 full power (20 MW) days or 85 % of the scheduled time during FY2004. A cycle has 38 days of continuous full power operation, followed by 11 days of shutdown for maintenance, refueling, and startup preparations. The operating license for the NBSR expired on May 16, 2004 and U.S. Nuclear Regulatory Commission (NRC) regulations allow for continued operation after submittal of a timely application for license renewal. At the completion of the NRC review process, a 20 year renewal may be granted from the date of the completed review. To gain regulatory approval for those additional years of facility operation, the first phase of a rigorous license renewal process was completed on April 9, 2004, when the NCNR submitted to the NRC the application for license renewal. The application consisted of a Safety Analysis Report (SAR), Technical Specifications, an environmental report, and a letter certifying that congressional appropriations for funding the decommissioning of the NBSR will be requested when necessary.

The SAR was written in collaboration with Brookhaven National Laboratory, with preliminary and final reviews performed by personnel drawn from reactor engineering, reactor operations, research facility operations, health physics, and facility management. The safety analyses within the SAR used state-of-the-art calculational methods to confirm the conservatism of the analyses of the previous SAR and showed that no fuel damage is predicted for any of the events required to be considered.

The Reactor Operations and Engineering Group also worked on a variety of activities to prepare the NCNR for reliable long-term operation. To assure the availability of a long-term disposal site for activated waste material, the Operations group performed a comprehensive assessment of the NBSR's disposal capabilities and needs. This was followed by extensive discussions with the disposal site operator and

Senior operations supervisors Dan Wilkison and Bill Mueller inspect a new control rod to be inserted during 2004.

resulted in an understanding that the existing material disposal process would continue for at least fifteen more years. Secondary cooling water pumps, motors, and one set of control rods were acquired for installation in the near future. We also purchased heavy water and additional control rods so that these vital resources would be available when needed in the future. Cooling tower equipment was upgraded to increase the efficiency of the tower and plans were made to upgrade secondary and experimental water systems.

Dr. Wade Richards, who has many years of experience as a nuclear engineer and reactor manager, was hired to enhance the analytical strengths of the Reactor Operations and Engineering group and to contribute to the on-going license renewal effort. In addition, all licensed operators were requalified this year and two operator candidates were hired with the expectation of each completing an NRC license examination by the end of the year.

Facility Developments

Data Analysis, Visualization, and Modeling Software

Numerous developments in user software have occurred over the past year. Many improvements and extensions have been made to the DAVE (Data Analysis and Visualization Environment) package including the addition of data reduction modules for Neutron Spin-Echo and Triple-Axis spectrometers, a new Fourier Transformation Toolkit, and significant enhancements to DCS-MSLICE that enable unprecedented visualization capabilities for single crystal diffuse scattering phenomena. New experiment planning and analysis tools have been added that help users get the most out of their beam-time, including a new module that calculates self-shielding corrections for samples with slab and annular geometries, and a simple-to-use scattering and absorption cross-sections calculator. The popularity of this software package continues to grow and NIST users are exploiting the power of DAVE with data from other institutions. Moreover, scientists from disciplines that do not use neutron scattering are finding the general-purpose visualization and analysis utilities in DAVE quite useful. In the past year the DAVE software was downloaded over 2900 times and the web pages were viewed nearly 30 000 times.

The Igor Pro-based SANS data reduction and analysis software developed at the NCNR continues to be very popular with facility users. In October of 2003, a significant update of the SANS data reduction package was released. Nearly all of the added features were in direct response to users' needs and feedback. Increasingly complex experimental setups and anisotropic materials have made it necessary to manipulate 1D and 2D data sets in non-standard ways. New tools are provided to allow users easier access to both 1D and 2D data sets for viewing and manipulation. To facilitate interpretation of SANS data, approximately 24 additional model functions are being added to the existing SANS Analysis package.

In collaboration with scientists at the University of Maryland, Baltimore County, we are developing software to calculate model SANS intensities from high-resolution x-ray crystal or NMR structures. Our program, XTAL2SAS, was originally written for protein structures and reads structural coordinate files in standard PDB (Protein Data Bank) format. First, each amino acid in the structure is replaced by a sphere of the appropriate volume and scattering length density, with its center of mass at the alpha carbon coordinate position. Then, the total protein volume is filled randomly with points using a Monte Carlo method. The distance distribution function, P(r), is determined by calculating all possible distances between points in the molecule, each point weighted by its appropriate scattering length density value. The scattered intensity is then obtained by a Fourier transform of P(r). The intensities can be calculated for proteins in H_2O, D_2O or mixed solutions.

In the past year XTAL2SAS has been modified to allow the user to model the distribution of bound water at the surface, using a solvent-accessible surface area approach that agrees well with molecular dynamics simulation results. The program has been extended to include the prediction of model SANS intensities from nucleic acid structures. Since nucleic acid bases cannot be represented by spherical shapes, an entirely different method for representing their structure was developed. We have now successfully predicted the SANS intensity from a 10-mer DNA duplex in H_2O solution containing 0.3 mol/L NaCl.

Over the past year, our suite of reflectometry programs, Reflpak, has continued to improve. It is now equally functional and convenient to install on four platforms, Windows, Macintosh OS X, Linux and SGI/IRIX and is available for download from the NCNR website. Improvements include the ability to reduce polarized datasets, support for front and back reflectivity, and support for pluggable file formats and three new instruments including a reflectometer at the Australian facility, ANSTO. Numerous user interface improvements are in place including increased interactivity with graphs, expanded user help, and snapshots and an undo stack that make exploring the parameter space of the fit much easier. Improved analysis program development is underway with genetic algorithm optimization available, though not yet exposed in the user interface. A collaboration with the DANSE (Distributed Data Analysis for Neutron Scattering Experiments) team at CalTech has been initiated to create a distributed fitting engine.

The CMPR package (www.ncnr.nist.gov/xtal/software/cmpr/), a collection of tools for powder diffraction data display, manipulation, unit cell visualization and peak fitting was extended in 2004 to include access to the ICDD-JCPDS database via incorporation of the program LOGIC. These programs run on virtually all computer platforms and there are self-installation tools available for Windows and Macintosh. The entire GSAS crystallographic package and the NCNR's front-end package, EXPGUI (www.ncnr.nist.gov/xtal/software/expgui/), were also ported to the Macintosh in 2004, so that this package may now

be used on that platform, in addition to Windows, Linux and Silicon Graphics. A self-installation tool is available for the Macintosh and Windows.

BT-7 Double Focusing Triple Axis Spectrometer Installation

A major milestone in the modernization of the NCNR's thermal neutron instruments was reached this year with the installation of the incident beam components of a state-of-the-art triple-axis spectrometer at the BT-7 beam port. The monochromator drum for the spectrometer (see Fig. 1) houses two doubly-focusing mechanisms for supporting segmented monochromator crystals. Individually aligned Cu(220) and PG(002) crystals have been installed providing over 400 cm^2 in reflecting area for each monochromator. Built into the drum are magnetic guide fields for the option of installing polarizing crystals in the future. The spectrometer's sample stage is cantilevered from the monochromator drum and features two coaxial rotary tables, one for sample rotation and one for the independent rotation of magnetic field coils, and a fully motorized sample goniometer. Also completed this year, and visible in Fig. 1, is the instrument's 30 m^2 air pad floor system. Composed of anodized aluminum tiles over a bed of self-leveling epoxy, the floor is level to within +/- 0.75 mm over its entire area. This type of air pad flooring was developed at the NCNR and will be the standard for future instrument construction at the NCNR.

The BT-7 spectrometer is designed to be used with interchangeable customized analyzer/detection systems supported on air pads. The first of these, to house a multi-strip horizontally focusing PG(002) analyzer array and a linear position-sensitive detector, is at an advanced stage of development and will be installed when the assembly and testing currently underway is completed.

FIGURE 1.

Engineer Colin Wrenn (right, standing) and machinist Mike Rinehart keep a watchful eye as engineer Mike Murbach (left) test drives the air-pad-supported under-carriage (loaded with lead bricks, in foreground) for the analyzer/detector section of the new thermal neutron triple-axis spectrometer at BT-7.

Status of the Multi Axis Crystal Spectrometer (MACS)

A third generation cold neutron spectrometer with unprecedented capabilities is under development at the NCNR. The instrument will use focusing Bragg optics to produce the most intense cold monochromatic neutron beam worldwide ($\Phi > 10^8$ n/cm^2/s for $\Delta E = 0.2$ meV). The multi-channel detection system will analyze neutrons scattered into a solid angle of 0.15 Sr, which is an order of magnitude more than for conventional triple axis instrumentation. The combination of enhancements in beam flux and detection efficiency yields almost two orders of magnitude gain in efficiency for experiments that require an overview of Q-space in a selected range of energy transfer.

The scientific goal of the MACS project is greater insight into nanoscale dynamic phenomena in materials science. Specific research enabled by MACS includes direct measurements of interactions in magnetic thin films, determination of spin density wave structure in organic metals, elucidation of spin and charge polarons in oxides, studies of dynamic correlations at pressure and field driven quantum phase transitions, and studies of composite spin in frustrated and doped magnets.

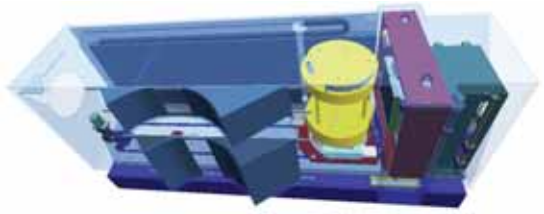

FIGURE 2.

CAD image of the monochromating system for the MACS spectrometer. The "golden" doubly focusing monochromator was built and tested at The Johns Hopkins University.

Fig. 2 shows the helium filled cask, which houses the 1428 cm^2 PG monochromator. By translating this device along the beam-line a large range of incident energies (2.5 meV to 20 meV) can be accessed with limited motion of the sample and detector. Fig. 3 shows the centerpiece of the MACS detector system. A patent is pending for this design which translates and rotates two vertically focusing analyzers and orients a background suppressing collimator with a single stepping motor. Twenty such devices will operate in parallel in the MACS detector system.

Much of the mechanical design work for MACS was completed over the last year. Beam-line shielding for the initial installation that will occur in the fall of 2004 has been received and many other parts are in various stages of manufacturing. Commissioning will start in the summer of 2005. An exciting period of discovery will follow as this new tool for probing dynamic correlations in condensed matter becomes available to the scientific community through CHRNS in the summer of 2006.

10 meter SANS Instrument

The NCNR's two high resolution, 30 m long, pinhole collimation Small-Angle Neutron Scattering (SANS) instruments are consistently over-subscribed by factors of 2 to 3. To alleviate this situation, the NCNR, with partial support from the NSF through CHRNS, is rebuilding a 20-year-old, medium resolution 8 m long SANS instrument. A thorough design study, aimed at optimizing performance within the available space at the end of the NG-1 neutron guide, has resulted in an engineering model (see Fig. 4) for a 10 m SANS instrument having all the operational features and ease of use of the 30 m instruments, and a measurement range (0.002 Å^{-1} < Q < 0.7 Å^{-1} compared with 0.0005 Å^{-1} < Q < 0.7 Å^{-1} for the 30 m instruments) that would satisfy the requirements of roughly one-half to two-thirds of SANS user experiments. Although modeled after the 30 m SANS instruments, the 10 m SANS instrument has some distinctive features, including the computer-controlled insertion of multiple pinhole collimation (with 7 converging beams) to achieve the instrument's best resolution (Q_{min} = 0.002 Å^{-1}), and a retractable sample chamber, to accommodate easily large pieces of sample environment equipment without reducing the Q-range of the instrument. An outside engineering firm is doing the detailed engineering design and fabrication of the instrument with completion scheduled for April 2005. When operational, 50 % of the beam time will be available through the NCNR's user program, and an additional 20 % will be set aside for graduate student training and early stage thesis research. This allocation of beam time represents a novel approach to enhancing the NCNR's educational and outreach efforts.

FIGURE 3.

CAD image of the double crystal analyzer of which there will be 20 in the MACS detector system.

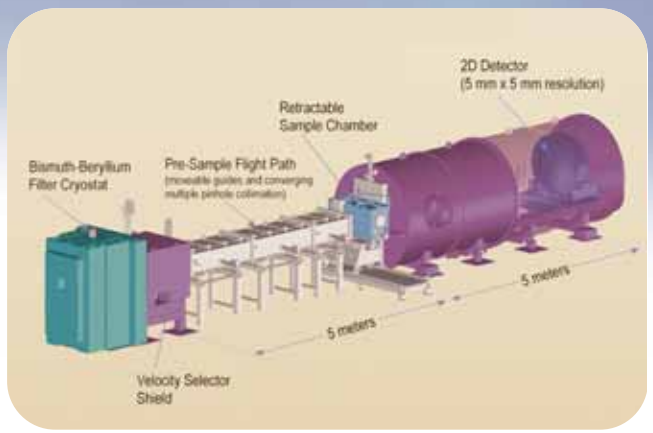

FIGURE 4.

3D engineering model of the 10 m SANS instrument currently under construction for installation at the end of the NG-1 neutron guide.

Origin and Removal of Spurious Background Peaks in Vibrational Spectra Measured by the Filter-Analyzer Neutron Spectrometer (FANS)

The ultimate sensitivity of the Filter-Analyzer Neutron Spectrometer (FANS), which is invaluable for measuring the vibrational spectra of materials, is typically limited by spurious features ubiquitous in all measured spectra. Recently we demonstrated that these spurious features, occurring between 50 meV and 85 meV, reflect the phonon excitations of beryllium excited by neutrons elastically scattered from the sample. We further determined that the addition of an auxiliary polycrystalline bismuth filter, in front of the main beryllium-graphite-beryllium filter analyzer, could significantly reduce such undesirable features. The test bismuth filter resulted in only a minor attenuation in sample scattering intensity concomitant with a reduction in the thermal- and fast-neutron background from the sample. An optimal bismuth filter requires a high-purity, low-hydrogen-content material with a sufficiently small crystallite grain size distribution to ensure a sharp Bragg cutoff in the energy dependence of the neutron total cross section. As a first instance, we were able to produce an acceptable material by melt-casting radial Bi wedges. At present, we have successfully installed a prototype, room-temperature Bi filter (15 cm thick) comprised of such melt-cast wedges in front of the original FANS filter analyzer. This filter essentially eliminates the spurious beryllium phonons in the critical 50 meV to 85 meV region, replacing them with Bi phonons, which occur only at 12 meV and below. This filter greatly enhances the capability of FANS for probing smaller mass, more dilute, and more weakly scattering systems. We plan to replace this first-generation Bi filter with an improved material synthesized by the room-temperature compression of high-purity, finely polycrystalline (with an average crystallite grain size of ≈ 240 μm) bismuth needles. Tests have shown that this pressed material results in a somewhat improved filter performance (due to a relatively sharper Bragg cutoff energy) compared to that of the melt-cast material.

American Conference on Neutron Scattering Hosted by NCNR

Nearly 500 participants from the Americas and abroad attended a remarkably successful second American Conference on Neutron Scattering (ACNS 2004) in College Park, Maryland, June 6 - 10, 2004. The ACNS was sponsored by the Neutron Scattering Society of America (NSSA) and hosted by the NCNR. A total of 389 abstracts were received, a 40 % increase over the very successful first ACNS held two years ago in Knoxville, TN.

Participation of graduate students, postdoctoral researchers, and new faculty was particularly encouraged—funding was made available to help defray travel expenses (the US Departments of Energy and Commerce, through their neutron scattering facilities, as well as the National Science Foundation and the University of Maryland, provided generous support as sponsors). Educational endeavors organized within the Conference included three different tutorials on neutron scattering: the NCNR Summer School Lectures, talks on Residual Stress and Mechanical Behavior, and an introduction to Pair Distribution Function Analysis of Diffraction Data. About a dozen commercial enterprises exhibited wares. The meeting was also the occasion for the presentation of several awards that are reported in another section.

The scope of the Meeting is far too large to adequately cover in this article. Instead, a few selected topics will be highlighted in shortened contributed perspectives. Those interested in specific topics can view all of the abstracts at the ACNS web site: www.ncnr.nist.gov/acns. The names referred to below can be traced through the website. A more extensive report is to be published in an upcoming issue of Neutron News.

Ferroelectrics (P. Gehring, NCNR)

A strong resurgence of interest in ferroelectricity was reflected in a session devoted to the subject on the first day of the conference. Research groups submitted abstracts that covered a broad range of ferroelectric materials and different scattering techniques. The emphasis of almost all of the presentations was on elastic and diffuse scattering, as only two talks dealt with inelastic scattering. The topics could be grouped into three categories pertaining to the so-called "relaxor" ferroelectrics, lead-oxides with quenched chemical disorder that exhibit record-setting piezoelectric properties, the venerable doped ferroelectric compound $KTa_{1-x}Nb_xO_3$, and discoveries of new multiferroics, uncommon systems in which magnetic and ferroelectric order are coupled. Two new examples of multiferroics, arguably the hottest topic in ferroelectrics today, were presented. Neutron diffraction data on $DyMn_2O_5$, a magnetoelectric switch, was used to correlate anomalies in the dielectric constant and polarization with magnetic transitions induced by field or temperature. Similarly, anomalies in the dielectric constant of $HoMnO_3$ at magnetic transitions indicated a coupling of the ferroelectric and magnetic order, and inelastic scattering measurements on the same material revealed a two-dimensional excitation spectrum.

Instrumentation (K. Crawford, Spallation Neutron Source)

Two oral sessions were devoted to instrumentation, and there were many instrumentation-related posters. In addition, some of the talks in the science sessions prominently displayed impressive instrumentation developed to carry out the science discussed. A number of innovative instrument concepts were presented. One idea being developed at IPNS is the use of a statistical chopper to discriminate against inelastic scattering on a time-of-flight (TOF) instrument for measuring elastic diffuse scattering (Osborn). The TISANE technique proposed by Gaehler, under development and testing at NIST (Glinka), uses TOF at a steady-state SANS instrument to enable time-resolved SANS studies of effects at the sub-millisecond time scale. Another effort under development at IPNS combines the properties of a TOF SANS instrument with a MIEZE-type neutron resonance spin-echo spectrometer to obtain high quasielastic energy resolution with SANS q-resolution (Bleuel). A poster demonstrated the use of a double-crystal diffractometer to obtain tomographic images with refracted neutrons, enabling a quite different contrast from that obtained with conventional transmission tomography (Strobl). A number of new instruments are in various stages of design and construction for the SNS, and status updates for most of these were covered in posters as well.

There were a number of presentations on the development of components for instruments. These included the use of a ^3He polarization analyzer for studying diffuse magnetic scattering from thin films (Chen), continued development of polycapillary lenses for focusing neutrons onto small samples (Gibson), the ongoing work at HMI on solid-state neutron optical elements (collimators, polarizers, benders) based on stacked Si wafers each coated as appropriate for the specific application (Krist), and a high-resolution gas area-detector for neutrons (Kampmann).

Magnetism (S.-H. Lee, NCNR)

The fields of magnetism and superconductivity were well represented with a variety of oral and poster presentations. Among topics performed with conventional instruments were spin-wave studies in a two-dimensional frustrated magnet, and unusual phase transitions in oxides due to spin, electronic, orbital and lattice couplings. The high magnetic fields now available at neutron facilities expand the accessible region in (*H-T*) phase space and are used to investigate the competition and coexistence of magnetism and superconductivity. Examples include studies of high-Tc cuprates, a field-induced Bose-condensation of magnons in an S = 1 alternating quantum chain, and field-induced bound spinons in an S = 1/2 spin chain. The contribution of these recent neutron scattering results to theory was underscored in several other talks.

Recent developments at research facilities around the world have extended the accessible dynamical scattering region into unexplored (Q, ω) regimes, both at low and high energies. Investigations of high energy magnetic excitations in superconducting and non-superconducting cuprates, performed at the MAPS spectrometer at ISIS, have revealed new features and refueled the debate about the roles of weakly interacting quasiparticles and/or stripes in high-T_c superconductivity. Another example is spin relaxation processes in spin-ice that have been studied using spin echo spectroscopy.

Mechanical Behavior and Residual Stress

(T. Gnaeupel-Herold and H.J. Prask, NCNR)

During the past five years there has been significant progress in the instrumentation of engineering diffractometers and the science performed.. The most substantial improvements were achieved at the recently commissioned instruments SMARTS in Los Alamos and ENGIN-X at ISIS. The specific strength of these pulsed-source instruments is the full-pattern acquisition that was demonstrated in a number of presentations on in *situ* polycrystal deformation experiments. Reactor instruments made a strong showing in pushing spatial resolution and penetrations to new limits.

The two major areas of research at engineering/stress instruments were presented in two invited talks, one on the micromechanics of polycrystal deformation (Ustundag), and the other on stress measurements in safety-critical components (Root). Both presentations underlined a trend towards more specialization and more efficient use of neutron beams for specific research.

Chemical Physics (C. Brown, NCNR)

Chemical physics at the ACNS was split into several sessions including 'Zeolites and Clathrates', 'Dynamics in Chemical Systems' and 'Confinement'. In the 'zeolites and clathrates' session Lobo illustrated the necessity for dual refinement of pair distribution functions from x-ray and neutron data of disordered materials, in much the same manner that is routine for standard powder diffraction. He also provided evidence that motion of rigid tetrahedral Si-O units provides the mechanism for the negative thermal expansion of chabazite.

After lunch (photo), the session of 'dynamics in chemical systems' was rounded out by Íñiguez who extended one-phonon *ab initio* calculations of neutron inelastic scattering spectra to include a general two-phonon term, and studied the structure, energetics and dynamics of a promising hydrogen storage material, sodium alanate (see highlight this issue.) The ensuing session on confinement phenomena mainly focused on recent results concerning the behavior of water and hydrogen in carbonaceous and siliceous materials with notable results coming from Chen *et al.*'s work on a kinetic glass transition in supercooled water confined in nanoporous silica glasses (see highlight this issue.)

Biology (S. Krueger, NCNR)

The meeting included two biology sessions, a session on thin films and membranes, and a number of biology-related posters. The first biology session on Proteins and Membranes included topics such as employing SANS for the characterization of standard viruses used in clinical diagnostic assays, studying the dynamical transition in proteins and DNA, using reflectivity to study the self-assembly of membrane protein arrays and studies of model membrane structure and bending rigidity.

The second biology session on Protein Structure and Hydration featured talks describing the neutron protein crystallography facility at LANL, the modeling of macromolecular structure from SANS intensities using both low and high resolution techniques, and the role of anchoring molecules and residual water on the stability of biological molecules and water dynamics at the surface of a protein. The session on Thin Films and Membranes included topics such as the use of neutron and x-ray reflectivity to determine the structure of synthetic peptides tethered to surfaces and the detection of lateral organization in model membranes using SANS.

Awards 2004

Shull Prize Awarded to Mike Rowe at the 2004 American Conference on Neutron Scattering, June 6-10, in College Park, MD

Richard Kayser, acting Deputy Director of NIST, Robert Shull (son of Nobelist Clifford Shull) of NIST, Mike Rowe, and Robert Briber, president of NSSA at the Shull Award ceremony.

"For his seminal vision, leadership, and contributions to the field of neutron scattering."

Dr. J. Michael Rowe of the NCNR is the first recipient of the Clifford G. Shull Prize of the Neutron Scattering Society of America (NSSA). The Shull Prize, which is awarded once every two years, was established by the NSSA to recognize outstanding research in neutron science and leadership promoting the North American neutron scattering community. The prize is named in honor of Prof. Clifford G. Shull, who shared the Nobel Prize in Physics in 1994 with Prof. Bertram Brockhouse for their seminal developments in the field of neutron science. The establishment of the prize was announced at the inaugural American Conference on Neutron Scattering (ACNS) in 2002. The prize, and a $5,000 honorarium, was awarded at the 2004 ACNS, which took place June 6-10, in College Park, MD.

Early in his scientific career, Mike Rowe was at the forefront of research on the dynamics, structure, and fundamental properties of materials, and published influential work on hydrogen in metals, orientationally disordered solids, and monatomic liquids. In addition, Mike Rowe has made significant contributions to the development of neutron spectrometers and other instruments that utilize cold neutrons, and he is an international leader in the design of the latest generation of cold neutron sources, including the most efficient hydrogen cold source currently operating in the world at the NCNR. Dr. Rowe's talents and his profound impact on American neutron science reach far beyond his individual contributions to research and instrumentation. Through his leadership and engineering creativity over the past 15 years, the NCNR has become the most important and widely used neutron research facility in North America.

Dr. Rowe received his Ph.D. in 1966 from McMaster University where he worked with Nobel Laureate B. N. Brockhouse. From 1966-72 he worked at Argonne National Laboratory before joining the National Bureau of Standards (now NIST) in 1973. Dr. Rowe retired as Director of the NCNR in March 2004, after heading the facility for 16 years.

APS 2004 Polymer Prize to Tim Lodge

Professor Tim Lodge of the University of Minnesota, a frequent visitor to the NCNR using neutrons to study polymer dynamics, was awarded the American Physical Society 2004 Polymer Physics Prize with the citation:

"For outstanding contributions to the fundamental understanding of polymer chain diffusion and segmental-chain dynamics."

Lodge has been on the faculty at Minnesota since 1982, where he is currently a Distinguished McKnight University Professor in the Departments of Chemistry and Chemical Engineering & Materials Science. After completing his Ph.D. in chemistry from Wisconsin in 1980, he spent 20 months as a National Research Council Postdoctoral Fellow at NIST, collaborating in neutron scattering and other experiments with Charles Han. His research interests center on the structure and dynamics of polymer liquids, including solutions, melts, blends, and copolymers, with particular emphases on rheology, diffusion, and scattering techniques. He has authored or co-authored over 160 refereed articles in the field of polymer science, and advised or co-advised 30 Ph.D. theses. Lodge is a fellow of the APS and serves on editorial boards of several journals. He is currently the Editor-in-Chief of *Macromocules*.

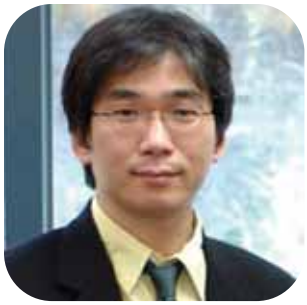

Sigma Xi Award Recognizes Outstanding Young NIST Scientist for 2004

Each year the NIST Chapter of Sigma Xi recognizes original basic or applied research by a NIST Gaithersburg staff member no more than ten years beyond their highest degree. This year Dr. Seung-Hun Lee of the NCNR has been awarded the 2004 NIST Sigma Xi Young Scientist Award, in recognition of his:

"Outstanding leadership in the use of inelastic neutron scattering to probe the magnetic properties of highly-correlated electron systems."

The award consists of a framed certificate, presented at the 28th annual banquet where Dr. Lee and spouse were the guests of honor. Dr. Lee will also be invited to present a Sigma Xi lecture at NIST.

Seung-Hun Lee has had a longstanding relationship with neutron scattering at the NCNR, beginning when he was a graduate student from The Johns Hopkins University where he finished a physics Ph.D. in 1996. Before being promoted to the permanent staff in the Condensed Matter Physics Team, he was Instrument Responsible for the SPINS cold neutron spectrometer, where he developed the instrumentation and carries out his award-winning research.

NSSA Prize for Outstanding Student Research

Rob Briber, NSSA president, presenting awards to Owen Vajk (top) and Tim Rappl (bottom)

The Neutron Scattering Society of America initiated an award for outstanding work presented by students at the 2004 ACNS meeting. From the 51 candidates in the Monday evening poster session, nine finalists were selected by the Program Committee and received a finalist certificate. Two full prizes, each of which consists of a certificate, a plaque, and $500 were awarded to: Owen Vajk (Stanford University) for *Quantum Percolation in a Two-Dimensional Heisenberg Antiferromagnet* and Timothy J. Rappl (University of California, Berkeley) for *Nucleation of Phase separation in Polymer Blends*. In both cases the neutron scattering work was carried out at the NCNR. The other finalists included Kapil Gupta (Johns Hopkins), Sylvia Ellen McLain (University of Tennessee), Markus Strobl (Hahn-Meitner Institut Berlin), Hans Pieter Mumm (University of Washington), Ronald G. Egres (University of Delaware), Robert C. Rogan (Caltech), and Matthew B. Stone (Johns Hopkins).

Owen Vajk, who is currently working at the NCNR and who worked with Martin Greven at Stanford, was also among the three recipients of the first Outstanding Dissertation in Magnetism awards announced by the American Physical Society topical group on magnetism. Vajk gave an invited talk on their work at the APS 2004 March Meeting, where he was presented with the $500 award.

Publications

Abbiendi, G., *et al.*, "Measurement of the Partial Widths of the Z into Up and Down Type Quarks," Phys. Lett. B **586**, 167 (2004).

Akbarzadeh, A. R., Bellaiche, L., Leung, K., Íñiguez, J., Vanderbilt, D., "Atomistic Simulations of the Incipient Ferroelectric $KTaO_3$," Phys. Rev. B **70**, 054103 (2004).

Aldridge, L. P., Bordallo, H. N., Desmedt, A., "Water Dynamics in Cement Pastes," Physica B, in press.

Allis, D. G., Hudson, B. S., "Inelastic Neutron Scattering Spectra of $NaBH_4$: Reproduction of Anion Mode Shifts Via Periodic DFT," Chem. Phys. Lett. **385** (3-4), 166 (2004).

Angell, C. A., Wang, L., Mossa, S., Yue, Y., Copley, J. R. D., "Vibrational Dynamics and Thermodynamics, Ideal Glass Transitions and Folding Transitions, in Liquids and Biopolymers," in *Slow Dynamics in Complex Systems*, edited by Tokuyama, M., and Oppenheim, I., AIP Conf. Proc. **708**, 473 (2004).

Arlen, M. J., Dadmun, M. D., "The Reinforcement of Polystyrene and Poly(Methyl Methacrylate) Interfaces Using Alternating Copolymers," Polymer **44** (22), 6883 (2003).

Bai, F., Wang, N., Li, J. F., Viehland, D., Gehring, P. M., Xu, G., Shirane, G., "X-Ray and Neutron Diffraction Investigations of the Structural Phase Transformation Sequence Under Electric Field in $0.7Pb(Mg_{1/3}Nb_{2/3})$-$0.3PbTiO_3$ Crystals," J. Appl. Phys. **96**, 1620 (2004).

Balsara, N. P., Rappl, T. J., Lefebvre, A. A., "Does Conventional Nucleation Occur During Phase Separation in Polymer Blends?," J. Poly. Sci. B **42** (10), 1793 (2004).

Bang, J., Lodge, T. P., "Mechanisms and Epitaxial Relationships Between Close-Packed and BCC Lattices in B Copolymer Solutions," J. Phys. Chem. B **107** (44), 12071 (2003).

Banovic, S. W., Vaudin, M. D., Gnäupel-Herold, T. H., Saylor, D. M., Rodbell, K. P., "Studies of Deformation Induced Texture Development in Sheet Materials Using Diffraction Techniques," Mater. Sci. Eng. A **380**, 155 (2004).

Bao, W., Chen, Y., Qiu, Y., Sarrao, J. L., "Novel Dynamic Scaling Regime in Hole- Doped La_2CuO_4," Phys. Rev. Lett. **91** (12), 127005 (2003).

Batra, A., Hedden, R. C., Schofield, P., Barnes, A., Cohen, C., Duncan, T. M., "Conformational Behavior of Guest Chains in Unaixially Stretched Poly(Diethylsiloxane) Elastomers: ^2H NMR and SANS," Macromol. **36** (25), 9458 (2003).

Berk, N. F., Majkrzak, C. F., "Wavelet Analysis of Neutron Reflectivity," Langmuir **19**, 7811 (2003).

Biggs, S., Kline, S. R., Walker, L. M., "The Absorption of Polymerized Rodlike Micelles at the Solid–Liquid Interface," Langmuir **20** (4), 1085 (2004).

Bishop, R. L., Blackman, M. J., "Instrumental Neutron Activation Analysis of Archaeological Ceramics: Scale and Interpretation," Acc. Chem. Res. **35** (8), 603 (2002).

Blaauw, M., "Hydrogen Precipitation in Titanium Observed with Neutron Incoherent Scattering and Prompt Gamma Neutron Activation Analysis," Nucl. Instrum. Methods Phys. Res. A **505** (1-2), 20 (2003).

Blackman, M. J., "Chemical Characterization of Tablets, Sealing Clays and Source Clays from Tell Leilan, Syria," Subartu **IX**, 455 (2004).

Borodin, O., Douglas, R., Smith, G. D., Trouw, F., Petrucci, S., "MD Simulations and Experimental Study of Structure, Dynamics, and Thermodynamics of Poly(Ethylene Oxide) and its Oligomers," J. Phys. Chem. B **107**, 6813 (2003).

Bossev, D. P., Ferdinand, S., Paulaitis, M. E., "Effect of Pressure on Microstructure in Water-in-Oil and Oil-in-Water Microemulsions for $C_{12}E_5$ n-Octane/D_2O Mixtures," Langmuir, in press.

Boukari, H., Chernomordik, V., Krueger, S., Nossal, R., Sackett, D. L., "Small-Angle Neutron Scattering Studies of Tubilin Ring Polymer," Physica B, in press.

Broholm, C., Aeppli, G., "Dynamic Correlations in Quantum Magnets," in *Strong Interactions in Low Dimensions*, edited by Baeriswyl, D., Degiorgi, L., (Kluwer Acedemic Publishers), in press.

Bromberg, L., Temchenko, M., Moeser, G. D., Hatton, T. A., "Thermodynamics of Temperature-Sensitive Polyether-Modified Poly(Acrylic Acid) Microgels," Langmuir **20** (14), 5683 (2004).

Burgess, I., Zamlynny, V., Szymanski, V., Lypkowski, J., Majewski, J., Satija, S., "Neutron Reflectivity Studies of Field Driven Transformations in a Monolayer of 4 Pentadecyl Pyridine at an Au Electrode Surfaces," J. Electroanal. Chem. **550**, 187 (2003).

Burgess, I., Li, M., Horswell, S. L., Szymanski, G., Lipkowski, J., Majewski, J., Satija, S., "Electric Field-Driven Transformation of a Supported Model Biological Membrane- An Electrochemical and Neutron Reflectivity Study," Biophys. J. **86** (3), 1763 (2004).

Caliskan, G., Mechtani, D., Roh, J. H., Kisliuk, A., Sokolov, A. P., Azzam, S., Cicerone, M. T., Lin-Gibson, S., Peral, I., "Protein and Solvent Dynamics: How Strongly are they Coupled?," J. Chem. Phys. **121**, 1978 (2004).

Cappelletti, R. L., "MSEL, FY 2003 Programs and Accomplishments," NIST IR, 7128 (2003).

Cappelletti, R. L., "NCNR 2003 NIST Center for Neutron Research Accomplishments and Opportunities," NIST SP 1006 (2003).

Cassells, M., Raby, T., McDonald, M., "The Use of Plate-Type Heat Exchangers," in *Proc. of International Conference on Nuclear Technology,* Am. Nucl. Soc. Trans. **89**, 63 (2003).

Chakoumakos, B. C., Rawn, C. J., Rondinone, A. J. Marshall, S. L., Stern, L. A., Circone, S., Kirby, S. H., Jones, C. Y., Toby, B. H., Ishii, Y., "The use of rigid body constraints in Rietveld refinements of neutron diffraction data of clathrate hydrates," in *Proceedings of the Fourth International Conference on Gas Hydrates*, vol. 2, p. 655, (2002).

Champion, J. D. M., Harris, M. J., Holdsworth, P. C. W., Wills, A. S., Balakrishnan, G., Bramwell, S. T., Čižmár, E., Fennell, T., Gardner, J. S., Lago, J., McMorrow, D. F., Orendáč, M., Orendáčová, A., Paul, D. McK., Smith, R. I., Telling, M. T. F., Wildes, A., "$Er_2Ti_2O_7$: Evidence of Quantum Order by Disorder in a Frustrated Antiferromagnet," Phys. Rev. B **68**, 020401 (2003).

Chari, K., Seo, Y.–S., Satija, S., "Competitive Adsorption at the Air-Water Interface from a Self-Assembling Polymer-Surfactant Mixture," J. Phys. Chem. B, in press.

Chen, C., Neelakanta, A., Sakai, V. G., Maranas, J. K., "On the Assesment of Interchain Packing Distances in Polymer Melts Using Neutron Diffraction," Macromol., in press.

Chen, S.–H., Chen, W.–R., Mallamace, F., "Observation of Liquid-to-Glass and Glass-to-Glass Transitions in L64/D2O Triblock Copolymer Micellar System," Molecular Simulation **29**, 10 (2004).

Chen, W. C., Gentile, T. R., O' Donovan, K. V., Borchers, J. A., Majkrzak, C. F., "Polarized Neutron Reflectometry of a Patterned Magnetic Film with a ^{3}He Analyzer and a Position-Sensitive Detector," Rev. Sci. Instrum., in press.

Chen, X. J., Zhang, C. L., Gardner, J. S., Sarrao, J. L., Almasan, C. C., "Variable-Range-Hopping Conductivity of the Half-Doped Bilayer Manganite $LaSr_2Mn_2O_7$," Phys. Rev. B **68**, 064405 (2003).

Cheng, X., Fisher, J. W., Yen, B. T., Roy, S., Prask, H. J., Gnäupel-Herold, T., "Residual Stress Modification by Post-Weld Treatment and its Beneficial Effect on Fatigue Strength of Welded Structures," Int. J. Fatigue **25**, 1259 (2003).

Chen-Mayer, H. H., Heward, W. J., Paul, R. L., Klug, F. J., Gao, Y., "Distribution of Chlorine in Quartz Determined by Neutron Beam Focusing Prompt Gamma Activation Analysis and Micro-X-Ray Fluorescence," J. Mater. Res. **18** (10), 2486 (2003).

Choi, H. D., Firestone, R. B., Lindstrom, R. M., Molnar, G. L., Reddy, A. V. R., Tan, V. H., Zhou, C. M., Paviottia-Corcuera, R. A., Trkov, A., "Development of a Database for Prompt Gamma-Ray Neutron Activation Analysis," J. Nucl. Sci. Technol., in press.

Chong, K. P., Sung, L., Ho, D. L., Van Landingham, M. R., "Solid Micromechanics: Research and Challenges," in *Proceedings of the 13th Micromechanics Europe (MME 2002) Workshop*, p. 347 (2002).

Chowdhuri, Z., Hansen, G. L., Jane, V., Keith, C. D., Lozowski, W. M., Snow, W. M., Dewey, M. S., Gilliam, D. M., Greene, G. L., Nico, J. S., Thompson, A. K., Wietfeldt, F. E., "A Cryogenic Radiometer for Absolute Neutron Rate Measurement," Rev. Sci. Instrum. 74, 4280 (2003)

Ciraci, S., Dag, S., Yildirim, T., Gülseren, O., Senger, R. T., "Functionalized Carbon Nanotubes and Device Applications," J. Phys.: Condens. Matter **16** (29), R901 (2004).

Ciraci, S., Gulseren, O., Dag, S., Yildirim, T., "Theoretical Models for Nanodevices and Nanomagnets Based on Carbon Nanotubes," in *Nanoengineered Nanofibrous Materials*, NATO-ASI Science Series II **169**, 4 (2004).

Cicerone, M. T., Soles, C. L., "Fast Dynamics and Stabilization of Proteins: Binary Glasses of Trehalose and Glycerol," Biophys. J. **86**, 3836 (2004).

Clarke, W. B., Guscott, R., Lindstrom, R. M., "Binding of Lithium and Boron to Human Plasma Proteins II: Results for a Bipolar not on Lithium Therapy," Biol. Trace Elem. Res. **97**, 117 (2004).

Cremer, J. T., Piestrup, M. A., Gary, C. K., Pantell, R. H., Glinka, C. J., "Biological Imaging with a Neutron Microscope," Appl. Phys. Lett. **85** (3), 494 (2004).

Cohen, R. E., Gehring, P. M., "Fundamental Physics of Ferroelectrics 2004," Colonial Williamsburg, VA, February 8-11, 2004, NIST IR 7106.

Coleman, M., Chandra, P., Dhanesh, D., Wermer, J., Udovic, T. J., "Zirconium Iron Disproportionation During Hydriding Reactions in Nuclear Gettering Operations," in *Adv. Mater. for Energy Conversion II*, edited by Chandra, D., Bautista, R. F., Shlapbach, L., (TMS, Warrendale, PA) p. 429 (2004).

Cook, J. C., Copley, J. R. D., "Simulations and Measurements of the Performance of a Channeled Neutron Guide for a Time-of-Flight Spectrometer at the NIST Center for Neutron Research," Rev. Sci. Instrum. **75** (2), 430 (2004).

Copley, J. R. D., "An Acceptance Diagram Analysis of the Contaminant Pulse Removal Problem with Direct Geometry Neutron Chopper Spectrometers," Nucl. Instrum. Methods A **510**, 318 (2003).

Crawford, M. K., Harlow, R. L., Lee, P. L., Zhang, Y., Hormadaly, J., Flippen, R., Huang, Q., Lynn, J. W., Stevens, R., Woodfield, B. F., Boerio-Goates, J., Fisher, R. A., "Coupled Magnetic and Structural Transitions in the Frustrated Spin-3/2 Antiferromagnetic $GeCo_2O_4$," Phys. Rev. B, in press.

Crawford, M. K., Harlow, R. L., Lee, P. L., Zhang, Y., Hormadaly, J., Flippen, R., Huang, Q., Lynn, J. W., Stevens, R., Woodfield, B. F., Boerio-Goates, J., Fisher, R. A., "Structure and Properties of the Integer Spin Frustrated Antiferromagnet $GeNi_2O_4$," Phys. Rev. B **68** (22), 220408 (2003).

Curtis, J. E., Tarek, M., Tobias, D. J., "Methyl Group Dynamics as a Probe of the Protein Dynamical Transition," J. Am. Chem. Soc., in press.

Dag, S., Gulseren, O., Ciraci, S., Yildirim, T., "Electronics Structure of the Contact Between Carbon Nanotube and Metal Electrodes," Appl. Phys. Lett. **83** (15), 3180 (2003).

Dag, S., Gulseren, O., Ciraci, S., Yildirim, T., "Physisorption of Oxygen Molecule on Carbon Nanotubes," NATO-ASI Science Series, p. 181 (2004).

Dai, P., Kang, H. J., Mook, H. A., Matsuura, M., Lynn, J. W., Kurita, Y., Komiya, S., Ando, Y., "Electronic Inhomogeneity and Competing Phases in Electron-Doped Superconducting $Pr_{0.88}LaCe_{0.12}CuO_{4-\delta}$," Phys. Rev. Lett., in press.

Danilkin, S. A., Hölzel, M., Fuess, H., Wipf, H., Udovic, T. J., Rush, J. J., Antonov, V. E., Gavriljuk, V. G., "Crystal Structure and Lattice Dynamics of Hydrogen-Loaded Austenitic Steel," J. Phys. IV, **112**, 407 (2003).

DeBruyn, H., Gilbert, R. G., White, J. W., Schulz, J. C., "Characterization of Electrosterically Stabilized Polystyrene Latex: Implications for Radical Entry Kinetics" Polymer **44** (16), 4411 (2003).

DeSanto, P., Buttrey, J., Grasselli, R. K., Lugmair, C. G., Volpe, A. F., Toby, B. H., Vogt, T., "Structural Aspects of the M1 and M2 Phases in MoVNbTeO Propane Ammoxidation Catalyst," Z. Kristallogr. **219**, 152 (2004).

Diallo, S. O., Pearce, J. V., Azuah, R. T., Glyde, H. R., "Quantum Distribution and Kinetic Energy in Solid ^{4}He," Phys. Rev. Lett., in press.

Ding, L., Liu, W., Wang, W., Glinka, C. J., Worcester, D. L., Yang, L., Huang, H. W., "Diffraction Techniques for Non-Lamellar Phases of Phospholipids," Langmuir, in press.

DiNoia, T. P., van Zanten, J. H., Kline, S. R., Garach-Domech, A., McHugh, M. A., Wright, P. J., Fetters, L. J., "Impact of Supercritical Fluid Solvent Quality on Polymer Conformation in Semidilute Solutions: SANS Data for Poly(ethylene-co-1-butene) in Dimethyl Ether to Kilobar Pressures," Macromol. **36** (19), 7372 (2003).

Diwekar, M., Borchers, J. A., O'Donovan, K. V., Johnston-Halperin, E., Awschalom, D. D., Shi, J., "Magnetic Properties of (Ga, Mn) as Digital Ferromagnetic Heterostructures," J. Appl. Phys. **95** (11), 6509 (2004).

Dominiak, P. M., Herold, J., Kolodziejski, W., Woźniak, K., "H-Bonding Dependent Structures of $(NH_4^+)3H^+(SO_4^{2-})_2$. Mechanisms of Phase Transition," Inorg. Chem. **42** (5), 1590 (2003).

Dzhosyuk, S. N., Mattoni, C. E. H., McKinsey, D. N., Thompson, A. K., Yang, L., Doyle, J. M., Huffman, P. R., "Neutron-Induced Luminescence and Activation in Neutron Shielding and Scintillation Detection Materials at Cryogenic Temperatures," Nucl. Instrum. Methods B **217** (3), 457 (2004).

Ehlers, G., Cornelius, A. L., Orendac, M., Kajnakova, M., Fennell, T., Bramwell, S. T., Gardner, J. S., "Dynamical Crossover in 'Hot' Spin Ice," J. Phys.: Condens. Matter, **15** (2), L9 (2003).

Ehlers, G., Cornelius A. L., Fennell, T., Koza, M., Bramwell, S. T., Gardner, J. S., "Evidence for Two Distinct Spin Relaxation Mechanisms in 'Hot' Spin Ice $Ho_2Ti_2O_7$," J. Phys.: Condens. Matter **16**, S635 (2004).

Elliot, J., Meuse, C. W., Silin, V., Krueger, S., Woodward, J. T., Petralli-Mallow, T., Plant, A. L., "*Biomimetic Membranes on Metal Supports: Opportunities and Challenges*," in Biomolecular Films: Design, Function, and Application, edited by Rusling, J., (Marcel Dekker Inc., New York) p. 99 (2004).

Esker, A. R., Grüll, H., Satija, S. K., Han., C. C., "Polymer Dynamics in Hydrogenous Systems by Neutron Reflectivity," J. Poly. Sci. B, in press.

Faraone, A., Liu, L., Mou, C.-Y., Shih, P.-C., Brown, C. M., Copley, J. R. D., Dimeo, R. M., Chen, S.-H., "Dynamics of Supercooled Water in Mesoporous Silica Matrix MCM-48-S," Eur. Phys. J. E **12** (s01), S59 (2003).

Fedeyko, J. M., Rimer, J. D., Lobo, R. F., Vlachos, D. G., "Spontaneous Formation of Silica Nanoparticles in Basic Solutions of Small Tetraalkylammonium Cations," J. Phys. Chem. B, in press.

Fitzsimmons, M. R., Bader, S. D., Borchers, J. A., Felcher G. P., Furdyna, J. K., Hoffmann, A., Kortright, J. B., Schuller, I. K., Schulthess, T. C., Sinha, S. K., Toney, M. F., Weller, D., Wolf, S., "Neutron Scattering Studies of Nanomagnetism and Artificially Structured Materials," J. Magn. Magn. Mater. **271**, 103 (2004).

Fratini, E., Chen, S.-H., Baglioni, P., "Investigation of the Temporal Evolution of Translational Dynamics of Water Molecules in Hydrated Calcium Aluminate Pastes," J. Phys. Chem. B **107** (37), 10057 (2003).

Gallagher, P. D., Satija, S. K., Karim, A., Douglas, J. F., Fetters, L. J., "Swelling of a Polymer Brush by a Poor Solvent," J. Poly. Sci. B, in press.

García-Sakai, V., Chen, C., Maranas, J. K., Chowdhuri, Z., "Effect of Blending with Poly(Ethylene Oxide) on the Dynamics of Poly(Methacrylate): A Quasielastic Neutron Scattering Approach," Macromol., in press.

Gardner, J. S., Ehlers, G., Bramwell, S. T., Gaulin, B. D., "Spin Dynamics in Geometrically Frustrated Antiferromagnets," J. Phys.: Condens. Matter **16**, S643 (2004).

Gardner, J. S., Gaulin, B. D., "Bringing Order to a Dynamic Magnet," in *ISIS 2003 Annual Report Highlights*, RAL-TR-2003-050 (2003).

Gehring, P. M., "Summer School on Methods and Applications of Neutron Spectroscopy Held at NIST," Neutron News **14** (4), 9 (2003).

Gehring, P. M., Chen, W., Ye, Z.–G., Shirane, G., "The Non-Rhombohedral Low-Temperature Structure of PMN-10%PT," J. Phys.: Condens. Matter, in press.

Gehring, P. M., Ohwada, K., Shirane, G., "Electric Field Effects on the Diffuse Scattering in $PbZn_{1/3}Nb_{2/3}O_3$ Doped with 8% $PbTiO_3$," Phys. Rev. B **70**, 014110 (2004).

Gentile, T. R., Hayden, M. E., Barlow, M. J., "Comparison of Metastability Optical Pumping Sources," J. Opt. Soc. Am. B: Opt. Phys. **20** (10), 2068 (2003).

George, M., Snyder, S. L., Terech, P., Glinka, C. J., Weiss, R. G., "N-Alkyl Perfluoroalkanamides as Low Molecular-Mass Organogelators," J. Am. Chem. Soc. **125**, 10275 (2003).

Gibson, W. M., Schultz, A. J., Richardson, J. W., Carpenter, J. M., Mildner, D. F. R., Chen-Mayer, H. H., Miller, M. E., Maxey, E., Prask, H. J., Gnäupel-Herold, T., Youngman, R., "Convergent Beam Neutron Crystallography," in Proc. SPIE Int. Soc. Opt. Eng. **5199**, 75 (2004).

Gibson, W. M., Schultz, A. J., Richardson J. W., Carpenter, J. M., Mildner, D. F. R., Chen-Mayer, H. H., Miller, M. E., Maxey, E. R., Youngman, R., " Convergent Beam Neutron Crystallography," J. Appl. Crystallogr. **37**, in press.

Gilliam, S. B., Gidcumb, S. M., Parikh, N. R., Patnaik, B. K., Hunn, J. D., Snead, L. L., Lamaze, G. P., "A Study of Helium Retention and Surface Blistering Characteristics of Tungsten with Regard to First Wall Conditions in an Inertial Fusion Energy Reactor," J. Nucl. Mater., in press.

Gnäupel-Herold, T., Foecke, T., Prask, H. J., Fields, R. J., "An Investigation of Springback Stresses in an AISI-1010 Deep Drawn Cup," Mater. Sci. Eng. A, in press.

Gnäupel-Herold, T., Prask, H. J., Biancaniello, F. S., "Residual Stresses and Elastic Constants in Thermal Deposits," in *Recent Advances in Experimental Mechanics—In Honor of Isaac M. Daniel*, edited by E.E. Gdoutos, (Kluwer Academic Publishers, Dordrecht 2002) p. 507.

Gnäupel-Herold, T., Prask, H. J., Fields, R. J., Foecke, T. J., Shi, M. F., Lienert, U., "A Synchrotron Study of Residual Stresses in a A16022 Deep Drawn Cup," Mater. Sci. Eng. A **366**, 104 (2004).

Gnezdilov, V. P., Pashkevich, Yu. G., Tranquada, J. M., Lemmens, P., Güntherodt, G., Yeremenko, A. V., Barilo, S. N., Shiryaev, S. V., Kurnevich, L. A., Gehring, P. M., "Interplay of Structural and Electronic Phase Separation in Single-Crystalline $La_2CuO_{4.05}$ Studied by Neutron and Raman Scattering," Phys. Rev. B **69**, 174508 (2004).

Goodrich, R. G., Young, D. P., Hall, D., Balicas, L., Fisk, Z., Harrison, N., Betts, J., Migliori, A., Woodward, F. M., Lynn, J. W., "Extension of the Temperature-Magnetic Field Phase Diagram of CeB_6," Phys. Rev. B **69** (5), 054415 (2004).

Goremychkin, E. A., Osborn, R., Bauer, E. D., Maple, M. B., Frederick, N. A., Yuhasz, W. M., Woodward, F. M., Lynn, J. W., "Crystal Field Potential of $PrOs_4Sb_{12}$: Consequences for Superconductivity," Phys. Rev. Lett., in press.

Granado, E., Ling, C. D., Neumeier, J. J., Lynn, J. W., Argyriou, D. N., "Inhomogeneous Magnetism in La-doped $CaMnO_3$: (I) Nanometric-Scale Spin Clusters and Long-Range Spin Canting," Phys. Rev. B **68** (13), 134440 (2003).

Grohol, D., Huang, Q., Toby, B., Lynn, J. W., Lee, Y. S., Nocera, D. G., "Powder Neutron Diffraction Analysis and Magnetic of Kagome-Type Vanadium Jarosite $NaV_3(OD)_6(SO_4)_2$," Phys. Rev. B **68** (9), 094404 (2003).

Gu, X., Nguyen, T., Sung, L., Ho, D. L., Vanlandingham, M. R., Jean, Y. C., Martin, J. W., "Advanced Techniques for Nanocharacterization of Polymeric Coating Surfaces," in *Proc. of the 81st Annual Meeting: Program of the Federation of Societies for Coatings Technology* (2003).

Gu, X., Raghavan, D., Ho, D. L., Sung, M. R., Van Landingham, M. R., Nguyen, T., "Nanocharacterization of Surface and Interface of Different Epoxy Networks," Mat. Res. Soc. Symp. Proc. **740**, DD10.9.1 (2002).

Gu, X., Sung, L., Ho, D. L., Michaels, C. A., Nguyen, D., Jean, Y. C., Nguyen, T., "Surface and Interface Properties of UV-Exposed PVDF/PMMA-CO-PEA Blends," in *Proceedings of 26th Annual Meeting of the Adhesion Society*, edited by Koberstein, J. T., Anderson, G. L., p. 505 (2003).

Gu, X., Sung, L., Ho, D. L., Michaels, C. A., Nguyen, D., Jean, Y. C., Nguyen, T., "Surface and Interface Properties of PVDF/Acrylic Copolymer Blends Before and After UV Exposure," in *Proc. of the 80th Annual Meeting: Program of the Federation of Societies for Coating Technologies*, (2002).

Gulseren, O., Yildirim, T., Ciraci, S., "Formation of Quantum Structures on a Single Nanotube by Modulation Hydrogen Adsorption," Phys. Rev. B **68** (11), 115419 (2003).

Hammouda, B., Ho, D. L., Kline, S., "Insight into Chestering in Poly(ethylene oxide) Solutions" Macromol., in press.

Han, S.-W., Gardner, J. S., Booth, C. H., "Structural Properties of the Geometrically Frustrated Pryochlore $Tb_2Ti_2O_7$," Phys. Rev. B **69**, 024416 (2004).

Hansen, F. Y., Criswell, L., Fuhrmann, D., Herwig, K. W., Diama, A., Dimeo, R. M., Neumann, D. A., Volkmann, U. G., Taub, H., "Intramolecular Diffusive Motion in Alkane Monolayers Studied by High-Resolution Quasielastic Neutron Scattering and Molecular Dynamics Simulations," Phys. Rev. Lett. **92** (4), 46103 (2004).

Harris, A. B., Aharony, A., Entin-Wohlman, O., Korenblit, I. Ya., Yildirim, T., "Landau Expansion for the Kugel-Khomskii t_{2g} Hamiltonian," Phys. Rev. B **69** (9), 094409 (2004).

Harris, A. B., Yildirim, T., Aharony, A., Entin-Wohlman, O., Korenblit, I. Ya., "Hidden Symmetries and their Consequences in t_{2g} Cubic Perovskites," Phys. Rev. B **69** (3), 035107 (2004).

Harris, A. B., Yildirim, T., Aharony, A., Entin-Wohlman, O., Korenblit, I. Ya., "Unusual Symmetries in the Kugel-Khomskii-Hamiltonian," Phys. Rev. Lett. **91** (8), 087206 (2003).

Hauer, B., Hempelman, R., Udovic, T. J., Rush, J. J., Kocklemann, W., Jansen, E., Scafer, W., Richter, D., "Neutron Scattering Studies on the Vibrational Excitations and the Structure of Ordered Niobium Hydrides: The λ Phases," Phys. Rev. B, in press.

Hedden, R. C., Bauer, B. J., "Structure and Dimensions of PAMAM/PEG Dendrimer-Star Polymers," Macromol. **36**, 1829 (2003).

Hedden, R. C., Lee, H. J., Bauer, B. J., Soles, C. L., Wu, W. L., Lin, E. K., "Measurement of Pore Size and Matrix Characteristics in Low-k Dielectrics by Neutron Contrast Variation," in *Characterization and Metrology for ULSI Technology*, AIP Conf. Proc. **683**, 567 (2003).

Hedden, R. C., Lee, H.-J., Bauer, B. J., "Characterization of Nanoporous Low-k Thin Films by Small-Angle Neutron Scattering Contrast Variation," Langmuir **20** (2), 416 (2004).

Hedden, R. C., Lee, H. J., Soles, C. L., Bauer, B. J., "Pore Size Distributions in Low-k Dielectric Thin Films from SANS Porosimetry," in ACS Polymeric Materials: Science and Engineering Preprints **90**, 494 (2004).

Heller, W. T., Vigil, D., Brown, S., Blumenthal, D. K., Taylor, S. S., Trewhella, J., "C Subunits Binding to the Protein Kinase A RIα Dimer Induce a Large Conformational Change," J. Biol. Chem. **279**, 19084 (2004).

Ho, D. L., Hammouda, B., Kline, S. R., "Unusual Phase Behavior in Mixtures of Poly(ethylene oxide) and Ethyl Alcohol," Phys. Rev. E, in press.

Hobbie, E. K., Lin-Gibson, S., Wang, H., Pathak, J. A., Kim, H., "Ubiquity of Domain Patterns in Sheared Viscoelastic Fluids," Phys. Rev. E **69** (6), 061503 (2004).

Hoelzel, M., Danilkin, S., Ehrenberg, H., Toebbens, D., Udovic, T. J., Fuess, H., Wipf, H., "Effects of High-Pressure Hydrogen Charging on the Structure of Austenitic Stainless Steels," Mater. Sci. Eng. A, in press.

Huang, Q., Foo, M. L., Lynn, J. W., Zandbergen, H. W., Lawes, G., Wang, Y., Toby, B. H., Ramirez, A. P., Ong, N. P., Cava, R. J., "Low Temperature Phase Transitions and Crystal Structure of $Na_{0.5}CoO_2$," J. Phys.: Condens. Matter, in press.

Hudson, B. S., Braden, D. A., Allis, D. G., Jenkins, T., Baronov, S., Middleton, C., Withnall, R., Brown, C. M., "The Crystalline Enol of 1, 3-Cyclohexanedione and its Complex with Benzene: Vibrational Spectra, Simulation of Structure and Dynamics and Evidence for Cooperative Hydrogen Bonding," J. Phys. Chem. A, in press.

Huffman, P. R., Coakley, K. J., Dzhosyuk, S. N., Golub, R., Korobkina, E., Lamoreaux, S. K., Mattoni, C. E. H., McKinsey, D. N., Thompson, A. K., Yang, G. L., Yang, L., Doyle, J. M., "Progress Towards Measurement of the Neutron Lifetime Using Magnetically Trapped Ultracold Neutrons," in "*Quark-Mixing, CKM Unitarity*" edited by Abele, H., Mund, D., (Mattes Verlag, Heidelberg, 2003) p. 77.

Indrakanti, A. N., Jones, R. L., Kumar, S. K., "' Do Nonequilibrium Effects Control Thin Film Phase Behavior?," Macromol. **37**, 9 (2004).

Íñiguez, J., Yildirim, T., Udovic, T. J., Sulic, M., Jensen, C. M., "Structure and Hydrogen Dynamics of Pure and Ti-doped Sodium Alanate," Phys. Rev. B **70**, 060101 (2004).

Jach, T., Dura, J. A., Nguyen, N. V., Swider, J., Cappello, G., Richter, C., "Comparative Thickness Measurements of SiO_2/Si Films for Thicknesses Less Than 10 nm," Surf. Interface Anal. **36**, 23 (2004).

Jacobson, D. L., Allman, B. E., McMahon, P. J., Nugent, K. A., Paganin, D., Arif, M., Werner, S. A., "Thermal and Cold Neutron Phase-Contrast Radiography," Appl. Radiat. Isotop., in press.

Jones, C. Y., Chen, G., Dai, S., Singh, P. M., "Solubility in the NaOH-Na_2CO_3-Na_2SO_4-$Na_2S_2O_3$-Na_2S-H_20 System, a Simulated Black Liquor Recovery Boiler Smelt," Ind. Eng. Chem. Res. **42** (18), 4228 (2003).

Jones, C. Y., Peral, I., "Dynamics of Trimethylene Oxide in a Structure II Clathrate Hydrate," Am. Mineral. **89**, 1176 (2004).

Jones, R. L., Hu, T. J., Prabhu, V. M., Soles, C. L., Lin, E. K., Wu, W.-L., Goldfarb, D. L., Angelopoulos, M., "Form of Deprotection in Chemically Amplified Resists," in *Characterization and Metrology for ULSI Technology*, AIP Conf. Proc. **683**, 429 (2003).

Jones, R. L., Hu, T., Lin, E. K., Wu, W.-L., Casa, D. M., Orji, N. G., Vorburger, T. V., Bolton, P. J., Barclay, G., "Sub-Nanometer Wavelength Metrology of Lithographically Prepared Structures: A Comparison of Neutron and X-Ray Scattering," in Proc. SPIE Int. Soc. Opt. Eng. **5038**, 191 (2003).

Jones, R. L., Prabhu, V. M., Goldfarb, D. L., Lin, E. K., Soles, C. L., Lenhart, J. L., Wu, W. L., Angelopoulos, M., "Correlation of the Reaction Front with Roughness in Chemically Amplified Photoresists," in *Polymers for Microelectronics and Nanoelectronics*, ACS Symp. Proc. **874**, 86 (2004).

Kamazawa, K., Park, S., Lee, S.–H., Sato, T. J., Tsudoda, Y., "Dissociation of Spin Objects in Geometrically Frustrated $CdFe_2O_4$," Phys. Rev. B **70**, 024418 (2004).

Kang, H. J., Dai, P., Lynn, J. W., Matsuura, M., Thompson, J. R., Zhang, S.-C., Argyriou, D. N., Onose, Y., Tokura, Y., Reply to Comment on "Antiferromagnetic Order as the Competing Ground State in Electron Doped $Nd_{1.85}Ce_{0.15}CuO_4$," Nature **426**, 140 (2003).

Karen, P., Kjekshus, A., Huang, Q., Karen, V. L., Lynn, J. W., Rosov, N., Natali-Sora, I., Santoro, A., "Neutron Powder Diffraction Study of Nuclear and Magnetic Structures of Oxidized and Reduced $YBa_2Fe_3O_{8+w}$" J. Solid State Chem. **174** (1), 87 (2003).

Keith, C. D., Chowdhuri, Z., Rich, D. R., Snow, W. M., Bowman, J. D., Penttilä, S. L., Smith, D. A., Leuschner, M. B., Pomeroy, V. R., Jones, G. L., Sharapov, E. I., "Neutron Cross Sections for ^3He at Epithermal Energies," Phys. Rev. C **69** (3), 034005 (2004).

Kent, M. S., Yim, H., Sasaki, D. Y., Satija, S., Majewski, J., Gog, T., "Analysis of Myoglobin Adsorption to Cu(II)-IDA and Ni(II)-IDA Functionalized Langmuir Monolayers by Grazing Incidence Neutron and X-Ray Techniques," Langmuir **20** (7), 2819 (2004).

Kenzelmann, M., Chen, Y., Broholm, C., Reich, D. H., Qiu, Y., "Bound Spinons in an Antiferromagnetic S=1/2 Chain with a Staggered Field," Phys. Rev. Lett. **93**, 017204 (2004).

Kepa, H., Khoi, L., V., Brown, C. M., Dietl, T., Furdyna, J. K., Giebultowicz, T. M., "Determination of Hole-Induced Ferromagnetic Mn-Mn Exchange in p-Type $Zn_{1-x}Mn_xTe$ by Inelastic Neutron Scattering," Physica B **350**, 36 (2004).

Kepa, H., Khoi, L. V., Brown, C. M., Dietl, T., Furdyna, J. K., Giebultowicz, T. M., "Determination of Hole-Induced Ferromagnetic Exchange Between Nearest-Neighbor Mn Spins in p-Type $Zn_{1-x}Mn_xTe$," J. Magn. Magn. Mater. **272-276** Supp. 1, E1545 (2004).

Kepa, H., Majkrzak, C. F., Sipatov, A. Y., Giebultowicz, T. M., "Polarized Neutron Reflectometry Studies of Magnetic Semiconductor Superlattices," Physica B **335** (1-4), 44 (2003).

Kepa, H., Majkrzak, C. F., Sipatov, A. Y., Giebultowicz, T. M., "Domain Structure of EuS/Pbs and EuS/YbSe Superlattices Studied by Polarized Neutron Reflectometry," Physica B **345** (1-4), 193 (2004).

Kepa, H., Sankowski, P., Kacman, P., Sipatov, A. Yu., Majkrzak, C. F., Giebultowicz, T. M., "Antiferromagnetic Interlayer Coupling in EuS/YbSe Superlattices," J. Magn. Magn. Mater. **272-276**, 323 (2004).

Kepa, H., Springholz, G., Giebultowicz, T. M., Goldman, K. I., Majkrzak, C. F., Kacman, P., Blinowski, J., Holl, S., Krenn, H., Bauer, G., "Magnetic Interactions in EuTe Epitaxial Layers and EuTe/PbTe Superlattices," Phys. Rev. B **68** (2), 024419 (2003).

Kepa, H., Van Khoi, L., Brown, C. M., Sawicki, M., Furdyna, J. K., Giebultowicz, T. M., Dietl, T., "Probing Hole-Induced Ferromagnetic Exchange in Magnetic Semiconductors by Inelastic Neutron Scattering," Phys. Rev. Lett. **91** (8), 087205 (2003).

Keren, A., Gardner, J. S., Ehlers, G., Fukaya, A., Segal, E., Uemura, Y. J., "Dynamic Properties of a Diluted Pyrochlore Cooperative Paramagnet $(Tb_pY_{1-p})_2Ti_2O_7$," Phys. Rev. Lett. **92** (10), 107204 (2003).

Khan, A., Heath, C. H., Dieregsweiler, U. M., Wyslouzil, B. E., "Homogeneous Nucleation Rates for D_2O in a Supersonic Laval Nozzle," J. Chem. Phys. **119** (6), 3138 (2003).

Kidwell, C. B., Ondov, J. M., "Elemental Analysis of Sub-Hourly Ambient Aerosol Collections," Aerosol Sci. Technol. **38** (3), 205 (2004).

Kim, H.-C.,Volksen, W., Miller, R. D., Huang, E., Yang, G. Y., Briber, R. M., Shin, K., Satija, S. K., "Neutron Reflectivity on Nanoporous Poly(Methylsilsesquioxane) Thin Films," Chem. Mater. **15**, 609 (2003).

Kim, M.-H., "Modified Porod's Law to Estimate the Transition Layer Thickness Between Two Phases: Test of Triangular Smoothing Function," J. Appl. Crystallogr. **37**, 643 (2004).

Kim, H., Foster, M. D., Jiang, H., Tullis, S., Bunning, T. J., Majkrzak, C. F., "Interface Structure of Photonic Multilayers Prepared by Plasma Enhanced Chemical Vapor Deposition," Polymer **45** (10), 3175 (2004).

Kim, Y. J., Wyslouzil, B. E., Wilemski, G., Wölk, J., Strey, R., "Isothermal Nucleation Rates in Supersonic Nozzles and the Properties of Small Water Clusters," J. Phys. Chem. A **108** (20), 4365 (2004).

Kirby, B. J., Borchers, J. A., Rhyne, J. J., te Velthuis, S. G. E., Hoffmann, A., O'Donovan, K. V., Wojtowic, T., Liu, X., Lim, W. L., Furdyna, J. K., "Annealing- Dependent Magnetic Depth Profile in Ga1-xMnxAs," Phys. Rev. B **69** (8), 081307 (2004).

Kishi, Y., De Graef, M., Craciunescu, C., Lograsso, T. A., Neumann, D. A., Wuttig, M., "Microstructures and Transformation Behavior of CoNiGa Ferromagnetic Shape Memory Alloys," J. Phys. IV **112**, 1021 (2003).

Kluthe, C., Al-Kassab, T., Barker, J., Pyckhout- Hintzen, W., Kirchheim, R., "Segregation of Hydrogen at Internal Ag/MgO (metal/oxide)-Interfaces as Observed by Small Angle Neutron Scattering," Acta Mater. **52** (9), 2701 (2004).

Koga, T., Ji, Y., Seo, Y. S., Gordon, C., Qu, F., Rafailovich, M. H., Sokolov, J. C., Satija, S.K., "Neutron Reflectivity Study of Glassy Polymer Brushes in Density Fluctuating Supercritical Carbon Dioxide," J. Poly. Sci. B, in press.

Koubi, L., Saiz, L., Tarek, M., Scharf, D., Klein, M. L., "Influence of Anesthetic and Nonimmobilizer Molecules on the Physical Properties of a Polyunsaturated Lipid Bilayer," J. Phys. Chem. B **107** (51), 14500 (2003).

Kreyssig, A., Stockert, O., Reznik, D., Woodward, F. M., Lynn, J. W., Reichart, W., Souptel, D., Behr, G., Loewenhaupt, M., "Low-Energy Phonons in $TbNi_2B_2C$ and $HoNi_2B_2C$," Physica B: Condens. Matter **350** (1-3), 69 (2004).

Krishnamurthy, V. V., Bhandar, A. S., Piao, M., Zoto, I., Lane, A. M., Nikles, D. E., Wiest, J. M., Mankey, G. J., Porcar, L., Glinka, C. J., "Shear and Magnetic Field-Induced Ordering in Magnetic Nanoparticle Dispersion from Small-Angle Neutron Scattering," Phys. Rev. E **67** (5), 051406 (2003).

Krueger, S., Perez-Salas, U. A., Gregurick, S. K., Kuzmanovic, D., "SANS from Proteins, Nucleic Acids, and Viruses," in *Neutron in Biology—Techniques and Applications*, Springer Biological Physics Series, Springer Publishing, New York, NY, edited by Fitter, J., Gutberlet, T., Katsaras, J., in press.

Kulkarni, A., Goland, A., Herman, H., Allen, A., Ilavsky, J., Long, G., Johnson, C. A., Ruud, J. A., "Microstructure Property Correlations in Industrial Thermal Barrier Coatings," J. Am. Ceram. Soc. **87** (7), 1294 (2004).

Kulkarni, A., Gutleber, J., Sampath, S., Goland, A., Lindquist, W. B., Herman, H., Allen, A. J., Dowd, B., "Studies of the Microstructure and Properties of Dense Ceramic Coatings Produced by High-Velocity Oxygen-Fuel Combustion Spraying," Mater. Sci. Eng. A **369** (1-2), 124 (2004).

Kuppa, V., Menakanit, S., Krishnamoorti, R., Manias, E., "Simulation Insights on the Structure of Nanoscopically Confined Poly(ethylene oxide)," J. Poly. Sci. B **41**, 3285 (2003).

Kutteruf, M. R., Brown, C. M., Iwaki, L. K., Campbell, M. B., Korter, T. M., Heilweil, E. J., "Terahertz Spectroscopy of Short-Chain Polypeptides," Chem. Phys. Lett. **375** (3-4), 337 (2003).

Kuzmanovic, D. A., Elashvili, I., Wick, C., O'Connell, C., Krueger, S., "Bacteriophage MS2: Molecular Weight and Spatial Distribution of the Protein and RNA Components by Small-Angle Neutron Scattering and Virus Counting," Struct. **11**, 1339, 2004.

Lamaze, G. P., Chen-Mayer, H. H., Soni, K. K., "Analysis of Thin Films and Surfaces by Cold Neutron Depth Profiling," App. Surf. Sci., in press.

Lavrov, A. N., Kang, H. J., Kurita, Y., Suzuki, T., Komiya, S., Lynn, J. W., Lee, S.-H., Dai, P., Ando, Y., "'Spin-Flop' Transition and Anisotropic Magnetoresistance in $Pr_{1.3-x}La_{0.7}Ce_xCuO_4$: Unexpectedly Strong Spin-Charge Coupling in Electron-Doped Cuprates," Phys. Rev. Lett. **92** (22), 227003 (2004).

Lee, H. J., Soles, C. L., Liu, D. W., Bauer, B. J., Lin, E. K., Wu, W. L., "Structural Characterization of Methylsilsesquioxane-Based Porous Low-k Using X-Ray Porosimetry," in *Proc. of the International Interconnect Technology Conference (IITC)*, p. 103 (2003).

Lee, H. J., Soles, C. L., Liu, D. W., Bauer, B. J., Lin, E. K., Wu, W. L., Grill, A., "Structural Characterization of Porous Low-k Thin Films Prepared by Different Processing Techniques Using X-Ray Porosimetry," J. App. Phys. **95**, 2355 (2004).

Lee, J. H., Ruegg, M. L., Balsara, N. P., Zhu, Y., Gido, S. P., Krishnamoorti, R., Kim, M.-H., "Phase Behavior of Highly Immiscible Polymer Blends Stabilized by Balanced Surfactants," Macromol. **36** (17), 6537 (2003).

Lee, S.–H., Louca, D., Ueda, H., Park, S., Sato, T. J., Isobe, M., Ueda, Y., Rosenkranz, S., Zscack, P., Íñiguez, J., Qiu, Y., Osborn, R., "Orbital and Spin Chains in ZnV_2O_4," Phys. Rev. Lett., in press.

Lee, Y. S., Chou, F. C., Tewary, A., Kastner, M. A., Lee, S.–H., Birgeneau, R. J., "Neutron Scattering Study of the Effect of Dopant Disorder on the Superconductivity and Magnetic Order in Stage-4 La_2CuO_{4+y}," Phys. Rev. B **69**, 020502 (2004).

Leheny, R. L., Lee, Y. S., Shirane, G., Birgeneau, R. J., "Spin Wave Propagation in the Domain State of a Random Field Magnet," Euro. Phys. J. B **32** (3), 287 (2003).

Lesemann, M., Nathan, H., DiNoia, T. P., Kirby, C. F., McHugh, M. A., van Zanten, J. H., Paulaitis, M. E., "Self-Assembly at High Pressures: SANS Study of the Effect of Pressure on Microstructure of C_8E_5 Micelles in Water," Indus. Eng. Chem. Res. **42** (25), 6425 (2003).

Levin, I., Amos, T. G., Bell, S. M., Farber, L., Roth, R. S., Vanderah, T. A., Roth, R. S., Toby, B. H., "Phase Equilibria, Crystal Structures, and Dielectric Anomaly in the $BaZrO_3$-$CaZrO_3$ System", J. Solid State Chem. **175** (2), 170 (2003).

Li, J., Sleight, A. W., "Structure of β-$AgAlO_2$ and Structural Systematics of Tetrahedral $MM'X_2$ Compounds," J. Solid State Chem. 177 (3), 889 (2004).

Li, J., Yokochi, A. F. T., Sleight, A. W., "Oxygen Intercalation of Two Polymorphs of $CuScO_2$," Solid State Sci., in press.

Lin, E. K., Lee, H. J., Bauer, B. J., Wang, H., Wetzel, J. T., Wu, W.-L., "Structure and Property Characterization of Low-k Dielectric Porous Thin Films Determined by X-Ray Reflectivity and Small-Angle Neutron Scattering," in *Low Dielectric Constant Materials for IC Applications*, edited by Ho, P. S., Leu, J., Lee, W. W., (Springer Publishing Inc) **11**, 1339 (2003).

Ling, C. D., Granado, E., Neumeier, J. J., Lynn, J. W., Argyriou, D. N., "Magnetic Inhomogeneities in Electron-Doped $Ca_{1-x}La_xMnO_3$," J. Magn, Magn. Mater. **272-276**, Part 1, 246 (2004).

Ling, C. D., Granado, E., Neumeier, J. J., Lynn, J. W., Argyriou, D. N., "Inhomogeneous Magnetism in La-Doped $CaMnO_3$: (II) Phase Separation due to Lattice-Coupled Ferromagnetic Interactions," Phys. Rev. B **68**, 134439 (2003).

Lin-Gibson, S., Jones, R. L., Washburn, N. R., Horkay, F., "Structure-Property Relationships of PEGDM Hydrogels," in ACS Polymer Preprints, in press.

Lin-Gibson, S., Kim, H., Schmidt, G., Han, C. C., Hobbie, E. K., "Shear-Induced Structure in Polymer-Clay Nanocomposite Solutions," J. Colloid Interface Sci. **274**, 515 (2004).

Lin-Gibson, S., Schmidt, G., Kim, H., Han, C. C., Hobbie, E. K., "Shear-Induced Mesostructure in Nanoplatelet-Polymer Networks," J. Chem. Phys. **119**, 8080 (2003).

Liu, Q. T., Diamond, M. L., Gingrich, S. E., Ondov, J. M., Maciejczyk, P., Stern, G. A., "Accumulation of Metals, Trace Elements and Semi-Volatile Organic Compounds in Films on an Urban Impervious Surface," Environ. Pollut. **122**, 51 (2003).

Liu, L., Faraone, A., Mou, C.–Y., Shih, P.–C., Shen, S.–H., "Slow Dynamics of Supercooled Water Confined in Nanoporous Silica Materials," J. Phys.: Condens. Matter, in press.

Livingston, R. A., Bumrongjaroen, W., Neumann, D. A., "Inelastic Neutron Scattering Measurements of Pozzolan Performance in Portland Cement," in *Nondestructive Characterization of Materials XI,* edited by Green, R. E., Djordjevic, B. B., Hentschel, M. P., (Springer, Berlin, Germany), p. 615 (2003).

Lobanov, M. V., Greenblatt, M., Caspi, E. N., Jorgensen, J. D., Sheptyakov, D. V., Toby, B. H., Botez, C. E., Stephens, P. W., "Crystal and Magnetic Structure of the $Ca_3Mn_2O_7$ Ruddlesden-Popper Phase: Neutron and Synchrotron X-Ray Diffraction Study," J. Phys.: Condens. Matter **16**, 5339 (2004).

Lu, C., Richardson, R., Pelton, R., Cosgrove, T., Dalnoki-Veress, K., "PEO Penetration into Water-Plasticized Poly(vinylphenol) Thin Films," Macromol. **37**, 494 (2004).

Lufaso, M. W., "Crystal Structures, Modeling, and Dielectric Property Relationships of 2:1, Ordered $Ba_3MM'_2O_9$ (M = Mg, Ni, Zn; M' = Nb, Ta) Perovskites," Chem. Mater. **16**, 2148 (2004).

Lufaso, M. W., Woodward, P. M., Goldberger, J., "Crystal Structures of Disordered $A_2Mn^{3+}M^{5+}O_6$ (A=Sr, Ca; M=Sb, Nb, Ru) Pervoskites," J. Solid State Chem. **177** (4-5), 1651 (2004).

Lynn, J. W., "ACNS 2004," ACNS 2004 Program Booklet **1**, 1 (2004).

Lynn, J. W., Huang, Q., Brown, C. M., Miller, V. L., Foo, M. L., Schaak, R. E., Jones, C. Y., Mackey, E. A., Cava, R. J., "Structure and Dynamics of Superconducting Na_xCoO_2 Hydrate and its Unhydrated Analog," Phys. Rev. B **68**, 214516 (2003).

Mackay, M. E., Dao, T. T., Tuteja, A., Ho, D. L., Van Horn, B., Kim, H.-C., Hawker, C. J., "Nanoscale Effects Leading to Non-Einstein-Like Decrease in Viscosity," Nature Mater. **2**, 762 (2003).

Mackey, E. A., Anderson, D. L., Liposky, P. J., Lindstrom, R. M., Chen-Mayer, H. H., Lamaze, G. P., Simons, D. S., Thompson, P.E., "New Thermal Neutron Prompt Gamma-Ray Activation Analysis Instrument at the National Institute of Standards and Technology Center for Neutron Research," Nucl. Instrum. Methods B, in press.

Mackey, E. A., Becker, D. A., Oflaz, R. D., Paul, R. L., Greenberg, R. R., Lindstrom, R. M., Yu, L. L., Wood, L. J., Long, S. E., Kelly, W. R., Mann, J. L., MacDonald, B. S., Wilson, S. A., Brown, Z. A., Briggs, P. H., Budhan, J., "Certification of NIST Standard Reference Material 1575a Pine Needles and Results of an International Laboratory Comparison," NIST SP260-156, (2004).

Majkrzak, C. F., Berk, N. F., Perez-Salas, U. A., "Phase Sensitive Neutron Reflectometry," Langmuir **19** (19), 7796 (2003).

Majkrzak, C. F., Berk, N. F., "Phase Sensitive Reflectometry and the Unambiguous Determination of Scattering Length Density Profiles," Physica B **336** (1-2), 27 (2003).

Malwitz, M. M., Butler, P. D., Porcar, L., Angelette, D. P., Schmidt, G., "Orientation and Relaxation of Polymer-Clay solutions as Studied by Rheology and SANS," J. Poly. Sci. B, in press.

Malwitz, M. M., Lin-Gibson, S., Hobbie, E. K., Butler, P. D., Schmidt, G., "Orientation of Platelets in Multilayered Nanocomposite Polymer Films," J. Poly. Sci. B **41** (24), 3237 (2003).

Mamontov, E., "Comment on "Quasielastic Neutron Scattering of Two-Dimensional Water in a Vermiculite Clay" [J. Chem. Phys. **113**, 2873 (2003)] and "A Neutron Spin-Echo Study of Confines Water" [J. Chem Phys. **115**, 11299 (2001)]," J. Chem. Phys., in press.

Mamontov, E., Branzy, R., Koranne, M., Egami, T., "Nanoscale Heterogeneities and Oxygen Storage Capacity of $Ce_{0.5}Zr_{0.5}O_2$," J. Phys. Chem. B **107** (47), 13007 (2003).

Mang, P. K., Vajk, O. P., Arvanitaki, A., Lynn, J. W., Greven, M., "Spin Correlations and Magnetic Order in Nonsuperconducting $Nd_{2-x}Ce_xCuO_{4\pm\delta}$," Phys. Rev. Lett. 93 (2), 027002 (2004).

Manson, J. L., Chapon, L. C., Bordallo, H. N., Feyerherm, R., Argyriou, D. N., Loose, A., "Spin Ordering in the Mixed-Ligand Antiferromagnet $Mn(dca)_2$(Pyrazine)," J. Magn. Magn. Mater. **260**, 462 (2003).

Martter, T. D., Foster, M. D., Yoo, T., Xu, S., Lizarraga, G., Quirk, R. P., "Thermodynamic Interaction Parameter of Star-Star Polybutadiene Blends," J. Poly. Sci. B **41** (3), 247 (2003).

Martínez-Iñesta, M. M., Peral, I., Lobo, R. F., Proffen, T., "A Pair Distribution Function Analysis of Zeolite Beta," Microporous Mesoporous Mater., in press.

Martinho, H., Granado, E., Moreno, N. O., Garcia, A., Toniani, I., Rettori, C., Neumeier, J. J., Oseroff, S. B., "Strong Charge Carrier Effect on the Magnetic Coupling of La-Doped $CaMnO_3$," Physica B **320** (1-4), 40 (2002).

Matějíček, J., Brand, P. C., Drews, A. R., Krause, A., Lowe-Ma, C., "Residual Stresses in Cold-Coiled Helical Compression Springs for Automotive Suspensions Measured by Neutron Diffraction," Mater. Sci. Eng. A **367**, 306 (2004).

Matsuura, M., Dai, P., Kang, H. J., Lynn, J. W., Argyriou, D. N., Onose, Y., Tokura, Y., "Magnetic Field Effect on Static Antiferromagnetic Order Above the Upper Critical Field in $Nd_{1.85}Ce_{0.15}CuO_4$," Phys. Rev. B **69** (10), 104510 (2004).

Matsuura, M., Dai, P., Kang, H. J., Lynn, J. W., Argyriou, D. N., Prokes, K., Onose, Y., Tokura, Y., "Effect of a Magnetic Field on the Long-Range Magnetic Order in Insulating Nd_2CuO_4 and Superconducting $Nd_{1.85}Ce_{0.15}CuO_4$," Phys. Rev. B **68**, 144503 (2003).

Mattoni, C. E. H., Adams, C. P., Alvine, K. J., Doyle, J. M., Dzhosyuk, S. N., Golub, R., Korobkina, E., McKinsey, D. N., Thompson, A. K., Yang, L., Zabel, H., Huffman, P. R., "A Long Wavelength Neutron Monochromator for Superthermal Production of Ultracold Neutrons," Physica B **344** (1-4), 343 (2004).

McKinsey, D. N., Brome, C. R., Butterworth, J. S., Dzhosyuk, S. N., Golub, R., Habicht, K., Huffman, P. R., Mattoni, C. E. H., Yang, L., Doyle, J. M., "Detecting Ionizing Radiation in Liquid Helium Using Wavelength Shifting Light Collection," Nucl. Instrum. & Methods A **516** (2-3), 475 (2004).

Michels, A., Viswanath, R. N., Barker, J. G., Birringer, R., Weissmüller, J., "Range of Magnetic Correlations in Nanocrystalline Soft Magnets," Phys. Rev. Lett. **91** (26), 267204 (2003).

Mildner, D. F. R., Brand, P. C., Clem, D. L., "Cold Pressing of Copper Single Crystals for a Large Area Doubly-Focusing Monochromator," J. Appl. Crystallogr. **37**, 455 (2004).

Miller, C. E., Majewski, J., Faller, R., Satija, S., Kuhl, T. L., "Cholera Toxin Assault on Lipid Monolayers Containing Ganglioside GM1," Biophys. J. **86**, 3700 (2004).

Miller, M. K., Wirth, B. D., Odette, G. R., "Precipitation in Neutron-Irradiated Fe-Cu and Fe-Cu-Mn Model Alloys: A Comparison of APT and SANS Data," Mater. Sci. Engin. A **353** (1-2), 133 (2003).

Moeser, G. D., Green, W. H., Laibinis, P. E., Linse, P., Hatton, T. A., "Structure of Polymer-Stabilized Magnetic Fluids: Small-Angle Neutron Scattering and Mean-Field Lattice Modeling," Langmuir **20** (13), 5223 (2004).

Mook, H. A., Dai, P., Hayden, S. M., Hiess, A., Lee, S.–H., Dogan, F., "Polarized Neutron Measurement of Magnetic Order in $YBa_2Cu_3O_{6.45}$," Phys. Rev. B **69**, 134509 (2004).

Moyer, R. O., Toby, B. H., "Ca_2IrD_5 - An Order-Disorder Transition," J. Alloys Compnds. **363**, 99 (2004).

Mukherjee, S., Cohen, R. E., Gülseren, O., "Vacancy Formation Enthalpy at High Pressures in Tantalum," J. Phys: Condens. Matter **15**, 855 (2003).

Nakatani, A. I., Chen, W., Schmidt, R. G., Gordon, G. V., Han, C. C., "Chain Dimensions in Polysilicate-Filled Poly(Dimethyl Siloxane)," Int. J. Thermophys. **23** (1), 199 (2002).

Nair, S., Dimeo, R. M., Neumann, D. A., Horsewill, A. J., "Methyl Rotational Tunneling Dynamics of *p*-xylene Confined in a Crystalline Zeolite Host," J. Chem. Phys., in press.

Nieh, M.-P., Harroun, T. A., Raghunathan, V. A., Glinka, C. J., Katsaras, J., "Concentration Independent Spontaneously Forming Biomimetic Vesicles," Phys. Rev. Lett. **91** (15), 158105 (2003).

Nieh, M.-P., Harroun, T. A., Raghunathan, V. A., Glinka, C. J., Katsaras, J., "Spontaneously Formed Monodispersed Biomimetic Unilamellar Vesicles: The Effect of Charge, Dilution and Time," Biophys. J. **86** (4), 2615 (2004).

Nieh, M.-P., Raghunathan, V. A., Glinka, C. J., Harroun, T., Katsaras, J., "Structural Phase Behavior of High-Concentration, Alignable Biomimetic "Bicelle" Membranes," Macromolecular Symp., in press.

Nieh, M.-P., Raghunathan, V. A., Wang, H., Katsaras, J., "Highly Aligned Lamellar Lipid Domains Induced by Macroscopic Confinement," Langmuir **19**, 6936 (2003).

Noakes, D. R., Arrott, A. S., Belk, M. G., Deevi, S. C., Huang, Q. Z., Lynn, J. W., Shull, R. D., Wu, D., "Incommensurate Spin Density Waves in Iron Aluminides," Phys. Rev. Lett. **91** (21), 217201 (2003).

Noakes, D. R., Arrott, A. S., Belk, M. G., Deevi, S. C., Lynn, J. W., Shull, R. D., Wu, D., "Properties of Incommensurate Spin Density Waves in Iron Aluminides," J. Appl. Phys. **95** (11), 6574 (2004).

Norman, A. I., Cabral, J. T., Ho, D. L., Amis, E. J., Karim, A., "Scattering Methods Applied to High Throughput Materials Science," ACS Polymeric Mater. Sci. Eng. **90**, 339 (2004).

O'Donovan, K. V., Borchers, J. A., Maat, S., Carey, M. J., Gurney, B. A., "Neutron Reflectivity on $CoFe_2O_4$ Exchange Springs for Spin Valve Applications," J. Appl. Phys. **95** (11), 7507 (2004).

Otano-Rivera, W., Messier, R., Pilione, L. J., Santiago, J. J., Lamaze, G. P., "Effect of Al Additions and AlN Interlayers on the Stablization of cBN Sputtered Thin Films," J. Diamond & Rel. Mater., in press.

Ozoliņš, V., Majzoub, E. H., Udovic, T. J., "Electronic Structure anf Rietveld Refinement Parameters of Ti-doped Sodium Alanates," J. Alloys Compnds. **375**, 1 (2004).

Paglia G., Buckley, C. E., Udovic, T. J., Rohl, A. L., Jones, F., Maitland, C. F., Connolly, J., "Boehmite Derived γ-Alumina System. 2. Consideration of Hydrogen and Surface Effects," Chem. Mater. **16** (10), 1914 (2004).

Pakstis, L. M., Ozbas, B., Hales, K. D., Nowak, A. P., Deming, T. J., Pochan, D., "Effect of Chemistry and Morphology on the Biofunctionality of Self-Assembling Diblock Copolypeptide Hydrogels," Biomacrom. **5** (2), 312 (2004).

Park, S. R., Choi, S. M., Dender, D. C., Lynn, J. W., Ling, X. S., "Fate of the Peak in a Type-II Superconductor: Multicriticality in the Bragg Glass Transition," Phys. Rev. Lett. **91** (16), 167003 (2003).

Park, S.–H., Liu, H., Kleinsorge, M., Grey, C. P., Toby, B. H., Parise, J. B., "[Li-Si-O]-MFI: A New Microporous Lithosilicate with the MFI Topology," Chem. Mater. **16** (13), 2605 (2004).

Parker, D. R., Green, M. A., Bramwell, S. T., Wills, A. S., Gardner, J. S., Neumann, D. A., "Positive and Negative Colossal Magnetoresistance in a Spin Glass Selenide Spinel," J. Am. Chem. Soc. **126**, 2710 (2004).

Paul, R. L., "Determination of Hydrogen in Semiconductors and Related Material by Cold Neutron Prompt Gamma-Ray Activation Analysis," in *Hydrogen in Semiconductors*, MRS Symp. Proc. **813**, H2.2 (2004).

Paul, R. L., Chen-Mayer, H. H., Myneni, G. R., Lanford, W., "Hydrogen Uptake by High Purity Niobium Studied by Nuclear Analytical Methods," Materiaux & Techniques **7-8-9**, 23 (2003).

Paul, R. L., Simons, D. S., "Radiochemical Neutron Activation Analysis for Certification of Ion-Implanted Phosphorus in Silicon," Anal. Chem. **75**, 4028 (2003).

Pearce, J. V., Diallo, S. O., Glyde, H. R., Azuah, R. T., Arnold, T., Larese, J. Z., "Enhanced Bose-Einstein Condensation and Kinetic Energy of Liquid ^{4}He Near a Free Surface," J. Phys.: Condens. Matter **16**, 4391 (2004).

Peral, I., Jones, C. Y., Varkey, S. P., Lobo, R. F., "Structural Comparison of Two EUO-type Zeolites Investigated by Neutron Diffraction," Microporous Mesoporous Mater. **71**, 125 (2004).

Perez-Salas, U., Faucher, K. M., Majkrzak, C. F., Berk, N. F., Chaikof, E. L., Krueger, S., "Characterization of a Biomimetic Polymeric Lipid Bilayer by Phase Sensitive Neutron Reflectometry," Langmuir **19** (19), 7688 (2003).

Perez-Salas, U., Rangan, P., Krueger, S., Briber, R. M., Thirumalai, D., Woodson, S. A., "Compaction of a Bacterial Group I Ribozyme Coincides with the Assembly of Core Helices," Biochem. **43** (6), 1746 (2004).

Phair, J. W., Schulz, J. C., Aldridge, L. P., Smith, J. D., "Small-Angle Neutron Scattering (SANS) and Rheological Characterization of Aluminosilicate Hydrogels," J. Am. Ceram. Soc. **87** (1), 129 (2004).

Phair, J. W., Schulz, J. C., Bertram, W., Aldridge, L. P., VanDeventer, J. S. J., "Investigation of the Microstructure of Alkali Activated Cements by Neutron Scattering," Cem. Concr. Res. **33**, 1811 (2003).

Popov, G., Lobanov, M. V., Tsiper, E. V., Greenblatt, M., Caspi, E. N., Borissov, A., Kiryukhin, V., Lynn, J. W., "Crystallographic and Magnetic Structure of the Sr_2MnReO_6 Double Perovskite," J. Phys.: Condens. Matter **16**, 135 (2004).

Porcar, L., Hamilton, W. A., Butler, P. D., Warr, G. G., "Relaxation of a Shear-Induced Lamellar Phase Measured with Time Resolved Small Angle Neutron Scattering," Physica B, in press.

Porcar, L., Hamilton, W. A., Butler, P. D., Warr, G. G., "Scaling of Structural and Rheological Response of L3 Sponge Phases in the "Sweetened" Cetylpyridinium-Hexanol/dextrose-brine System," Langmuir **19** (26), 10779 (2003).

Pozzo, D. C., Walker, L. M., "Reversible Shear Gelation of Polymer-Clay Dispersions," Colloids Surf. A **240** (1-3), 187 (2004).

Prabhu, V. M., Amis, E. J., Bossev, D. P., Rosov, N., "Organic Counterion Statics and Dynamics Studied by Small-Angle Neutron Scattering and Neutron Spin Echo Spectroscopy," J. Chem. Phys., in press.

Prodi, A., Gilioli, E., Gauzzi, A., Licci, F., Marezio, M., Bolzoni, F., Huang, Q., Santoro, A., Lynn, J. W., "Charge, Orbital and Spin Ordering Phenomena in $(NaMn^{3+}_3)(Mn^{3+}_2Mn^{4+}_2)O_{12}$, a Doping-Free Model System," Nature Mater. **3**, 48 (2004).

Proffen, T., Billinge, S. J. L., Toby, B. H. "Structure of Complex Materials Special Edition," Z. Kristallogr. **219** (3), III-IV (2004).

Radlinski, A. P., Ioannidis, M. A., Hinde, A. L., Hainbuchner, M., Baron, M., Rauch, H., Kline, S. R., "Angstrom to Millimeter Characterization of Sedimentary Rock Microstructure,"J. Colloid Interf. Sci. **274** (2), 607 (2004).

Rajca, A., Wongsriratanakul, J., Rajca, S., "Organic Spin Clusters: Macrocyclic-Macrocyclic Polyarymethyl Polyradicals with Very High Spin S= 5-13," J. Am. Chem. Soc. **126** (21), 6608 (2004).

Rajca, S., Rajca, A., Wongsriratanakul, J., Butler, P. D., Choi, S.-M., "Organic Spin Clusters: A Dendritic-Macrocyclic Poly(arylmethyl) Polyradical with Very High Spin of S = 10 and its Derivatives: Synthesis, Magnetic Studies, and Small-Angle Neutron Scattering," J. Am. Chem. Soc. **126** (22), 6972 (2004).

Ramaswamy, A. L., Kaste, P., Trevino, S. F., "A 'Micro Vision' of the Physio-Chemical Phenomena Occurring in Nanoparticles of Aluminum," J. Energetic Mater. **22**, 1 (2004).

Rao, G. H., Huang, Q., Yang, H. F., Ho, D. L., Lynn, J. W., Liang, J. K., "Magnetic Phase Transitions of Pr5Ge4," Phys. Rev. B. **69** (9), 094430 (2004).

Ratcliff, W., Lee, S.-H., Broholm, C., Cheong, S. W., Huang, Q., "Freezing of Spin-Correlated Nano-Clusters in a Geometrically Frustrated Magnet," Phys. Rev. B **65**, 220406 (2002).

Rawn, C. J., Rondinone, A. J., Chakoumakos, B. C., Marshall, S. L., Stern, L. A., Circone, S., Kirby, S. H., Jones, C. Y., Toby, B. H., & Ishii, Y., "Neutron powder diffraction studies as a function of temperature of structure II hydrate formed from methane plus ethane gas mixture," in *Proceedings of the Fourth International Conference on Gas Hydrates*, vol. 2, p. 595 (2002).

Reynolds, B. J., Ruegg, M. L., Balsara, N. P., Radke, C. J., Schaffer, T. D., Lin, M. Y., Shull, K. R., Lohse, D. J., "Thermodynamics of Polymer Blends Organized by Balanced Block Copolymer Surfactants Studied by Mean-Field Theories and Scattering," Macromol., in press.

Richter, D., Neumann, D. A., "Neutron-Scattering Studies of Dynamics: A New Frontier in Materials Science," Mater. Res. Soc. Bull. **28**, 913 (2003).

Richter, D., Rowe, J. M., "New Frontiers in the Application of Neutron Scattering to Materials Science," Mater. Res. Soc. Bull., **28** (12), 903 (2003).

Ruegg, M. L., Newstein, M. C., Balsara, N. P., Reynolds, B. J., "Small-Angle Neutron Scattering From Nonuniformly Labeled Block Copolymers," Macromol. **37** (5), 1960 (2004).

Russo, D., Hura, G., Head-Gordon, T., "Hydration Dynamics Near a Model Protein Surface," Biophys. J. **86**, 1852 (2004).

Saiz, L., Bandyopadhyay, S., Klein, M. L., "Effect of the Pore Region of a Transmembrane Ion-Channel on the Physical Properties of a Simple Membrane," J. Phys. Chem. B. **108** (8), 2608 (2004).

Sakai, V. G., Chen, C., Maranas, J. K., Chowdhuri, Z., "Effect of Blending with Poly(Ethylene Oxide) on the Dynamics of Poly (Methacrylate): A Quasi-Elastic Neutron Scattering Approach," Macromol., in press.

Sampath, S., Jiang, X. Y., Matějíček, J., Prchlik, L., Kulkarni, A., Vaidya, A., "Role of Thermal Spray Processing Method on the Microstructure, Residual Stress and Properties of Coatings: An Integrated Study for Ni-5 wt. % Al Bond Coats," Mater. Sci. Engin. A. **364** (1-2), 216 (2004).

Satija, R., Jacobson, D. L., Arif, M., Werner, S. A., "In Situ Neutron Imaging Technique for Evaluation of Water Management Systems in Operating PEM Fuel Cells," J. Power Sources **129** (2), 238 (2004).

Sato, T. J., Lee, S.–H., Katsufuji, T., Masaki, M., Park, S., Copley, J. R. D., Takagi, H., "Unconventional Spin Fluctuations in the Hexagonal Antiferromagnet $YMnO_3$," Phys. Rev. B **68**, 014432 (2003).

Sato, T. J., Lynn, J. W., Hor, Y. S., Cheong, S.-W., "First-Order Transition in the Itinerant Ferromagnet $CoS_{1.9}Se_{0.1}$," Phys. Rev. B **68**, 214411 (2003).

Schleier-Smith, M. H., van Buren, L. D., Doyle, J. M., Dzhosyuk, S. N., Gilliam, D. M., Mattoni, C. E. H., McKinsey, D. N., Yang, L., Huffman, P. R., "The Production of Nitrogen-13 by Neutron Capture in Boron Compounds," Nucl. Instrum. Methods B **215** (3-4), 531 (2004).

Seah, M. P., Spencer, S. J., Bensebaa, F., Vickridge, I., Danzebrink, H., Krumrey, M., Gross, T., Oesterle, W., Wendler, E., Rheinländer, B., Azuma, Y., Kojima, I., Suzuki, N., Suzuki, M., Tanuma, S., Moon, D. W., Lee, H. J., Cho, H. M., Chen, H. Y., Wee, A.T. S., Osipowicz, Y., Pan, J. S., Jordaan, W. A., Hauert, R., Klotz, U., van der Marel, C., Verheijen, M., Tamminga, Y., Muller, D., Dura, J. A., "Ultra-thin SiO2 on Si: Part V, Results of a CCQM Study of Thickness Measurements," J. Surf. Inter. Anal., in press.

Shi, H. T., Lederman, D., O' Donovan, K. V., Borchers, J. A., "Exchange Bias and Enhancement of the Néel Temperature in Thin NiF_2 Films," Phys. Rev. B **69**, 214416 (2004).

Shin, K., Wang, H., Satija, S. K., Han, C.C., Josell, D., Bonevich, J. E., "Rapid Deformation of Thin Gold Layers in Polymer Matrices Studied by X-Ray Reflectivity," J. App. Phys. **94** (3), 2115 (2003).

Shirane, G., Xu, G., Gehring, P. M., "Dynamics and Structure of PMN and PZN," Ferroelectr., in press.

Silverstein, M. S., Bauer, B. J., Lee, H. J., Hedden, R. C., Landes, B., Lyons, J., Kern, B., Niu, J., Kalantar, T., "The Structural Evolution of Pore Formation in Low-k Dielectric Thin Films," in *Characterization and Metrology for ULSI Technology*, AIP Conf. Proc. **683**, 572 (2003).

Simmons, B., Agarwal, V., Singh, M., McPherson, G., John, V., Bose, A., "Phase Transition Dynamics and Microstructure Evolution in a Crystalline Surfactant Mesophase Using Time-Dependent Small-Angle Neutron Scattering," Langmuir **19**, 6329 (2003).

Singh, M., Agarwal, V., De Kee, D., McPherson, G., John, V., Bose, A., "Shear- Induced Orientation of a Rigid Surfactant Mesophase," Langmuir **20** (14), 5693 (2004).

Singh, M., Tan, G., Agarwal, V., Fritz, G., Maskos, K., Bose, A., John, V., McPherson, G., "Structural Evolution of a Two Component Organogel," Langmuir, in press.

Smith, L. J., Price, D. L., Chowdhuri, Z., Brady, J. W., Saboungi, M. L., "Molecular Dynamics of Glucose in Solution: A Quasielastic Neutron Scattering Study," J. Chem. Phys. **120**, 3527 (2004).

Soles, C. L., Cicerone, M. T., "Fast Dynamics and Stabilization of Proteins: Binary Glasses of Trehalose and Glycerol," Biophys. J. **86**, 3836 (2004).

Soles, C. L., Douglas, J. F., Wu, W.-L., Peng, H., Gidley, D. W., "Comparative Specular X-Ray Reflectivity, Positron Annihilation Lifetime Spectroscopy Incoherent Neutron Scattering Measurements of the Dynamics in Thin Polycarbonate," Macromol. **37** (8), 2890 (2004).

Soles, C. L., Douglas, J. F., Wu, W.-L., "The Dynamics of Thin Polymer Films: Recent Insights from Incoherent Neutron Scattering," J. Polym. Sci. B, in press.

Soles, C. L., Jones, R. L., Lenhart, J. L., Prabhu, V. M., Wu, W.-L., Lin, E. K., Goldfarb, D. L., Angelopoulos, M., "Polymer Dynamics and Diffusive Properties in Ultra Thin Photoresist Films," in Proc. SPIE Int. Soc. Opt. Eng. **5039**, 366 (2003).

Soles, C. L., Vogt, B. D., Jones, R. L., Prabhu, V. M., Wu, W.–L., Lin, E. K., Goldfarb, D. L., Angelopoulos, M., "Dynamics, Diffusion and Dissolution in Ultrathin Photoresist Films," Proc. SPIE Int. Soc. Opt. Eng., in press.

Spiecker, P. M., Gawrys, K. L., Kilpatrick, P. K., "Aggregation and Solubility Behavior of Asphaltenes and Their Subfractions," J. Colloid Interf. Sci. **267** (1), 178 (2003).

Spiecker, P. M., Gawrys, K. L., Trail, C. B., Kilpatrick, P. K., "Effects of Petroleum Resins on Asphaltene Aggregation and Water-in-Oil Emulsion Formation," Colloids Surf. A **220** (1-3), 9 (2003).

Stadler, S., Idzerda, Y. U., Dvorak, J., Borchers, J. A., "Using Circularly Polarized Soft X- Rays to Probe Antiferromagnetically Correlated Co/Cu Multilayers," J. Appl. Phys. **95** (11), 6672 (2004).

Stancik, C. M., Lavoie, A. R., Schütz, J., Achurra, P. A., Lindner, P., Gast, A. P., Waymouth, R., "Micelles of Imidazolium-Functionalized Polystyrene Diblock Copolymers Investigated with Neutron and Light Scattering," Langmuir **20** (3), 596 (2004).

Stancik, C. M., Pople, J. A., Trollsås, M., Linder, P., Hedrick, J. L., Gast, A. P., "Impact of Core Architecture on Solution Properties of Dendrimer-Like Star Copolymers," Macromol. **36**, 5765 (2003).

Stewart, J. R., Ehlers, G., Wills, A. S., Bramwell, S. T., Gardner, J. S., "Phase Transitions, Partial Disorder and Multi-K Structures in $Gd_2Ti_2O_7$," J. Phys.: Condens. Matter **16**, L321 (2004).

Stock, C., Birgeneau, R. J., Wakimoto, S., Gardner, J. S., Chen, W., Ye, Z.-G., Shirane, G., "Universal Static and Dynamic Properties of the Structural Transition in $Pb(Zn_{1/3}Nb_{2/3})O_3$," Phys. Rev. B **69**, 094104 (2004).

Stone, M. B., Reich, D. H., Broholm, C., Lefmann, K., Rischel, C., Landee, C. P., Turnbull, M. M., "Extended Quantum Critical Phase in a Magnetized Spin-$\frac{1}{2}$ Antiferromagnetic Chain," Phys. Rev. Lett. **91** (3), 037205 (2003).

Strzalka, J., Gibney, B. R., Satija, S., Majkrzak, C. F., Blasie, J. K., "Specular Neutron Reflectivity and the Structure of Artificial Protein Maquetts Vectorially Oriented at Interfaces," Langmuir, in press.

Sung, L., Scierka, S., Baghai-Anaraki, M., Ho, D. L., "Characterization of Metal-Oxide Nanoparticles: Synthesis and Dispersion in Polymeric Coatings," in *Nanomaterials for Structural Applications*, edited by Berndt, C., Fischer, T. E., Ovid'ko, I., Skandan, G., Tsakalakos, T., MRS Symp. Proc. **740**, I5.4.1 (2003).

Sung, L., Vicini, S., Ho, D. L., Hedhli, L., Olmstead, C., Wood, K. A., "Effect of Microstructure of Fluorinated Acrylic Coatings on UV Degradation Testing," Polymer, in press.

Talon, C., Smith, L. J., Brady, J. W., Lewis, B. A., Copley, J. R. D., Price, D. L., Saboungi, M.-L., "Dynamics of Water Molecules in Glucose Solutions," J. Phys. Chem. B. **108**, 5120 (2004).

Tande, B. M., Wagner, N. J., Mackay, M. E., "Phase Behavior of Hybrid Dendron-Linear Copolymers and Blends With Linear Homopolymer," Comptes Rendus Chimie, **6** (8-10), 853 (2003).

Tang, F., Gnäupel-Herold, T., Prask H. J., Anderson, I. E., "Neutron Diffraction Study of Residual Stresses in Al/AlCuFe Composites," in *Advances in Powder Metallurgy & Particulate Materials 2003*, edited by R. Lawcock and M. Wright, Part 6, p. 1.

Tang, F., Meeks, H., Spowart, J. E., Gnäupel-Herold, T., Prask, H. J., Anderson, I., "Consolidation Effects on Tensile Properties of a Pure Al Matrix Composites," Metall. Trans. A, in press.

Taub, H., Hansen F. Y., Criswell, L., Fuhrmann, D., Herwig, K. W., Diama, A., Mo, H., Dimeo, R. M., Neumann, D. A., Volkmann, U. G., "Slow Diffusive Motions in a Monolayer of Tetracosane Molecules Adsorbed on Graphite," in *Slow Dynamics in Complex Systems* edited by Tokuyama, M., and Oppenheim, I., AIP Conf. Proc. **708**, 201 (2004).

Thomas, J. J., Chen, J. J., Jennings, H. M., Neumann, D. A.,"Ca-OH Bonding in the C-S-H Gel Phase of Tricalcium Silicate and White Portland Cement Pastes Measured by Inelastic Neutron Scattering," Chem. Mater. **15** (20), 3813 (2003).

Thornton, J., "Enhanced Radiography for Aircraft Materials and Components," Engineering Failure Anaylsis **11** (2), 207 (2004).

Toby, B. H., Billinge, S. J. L., "Determination of Standard Uncertainties in Fits to Pair Distribution Functions," Acta Crystallogr. A **60**, 315 (2004).

Toby, B. H., "A Program for Viewing and Editing CIF's," J. Appl. Crystallogr. **36**, 1288 (2003).

Toby, B. H., "Inspecting Rietveld Fits from pdCIF: pdCIFplot," J. Appl. Crystallogr. **36**, 1285 (2003).

Toby, B. H., Von, Dreele, R. B., Larson, A. C., "Reporting of Rietveld Results Using pdCIF: GSAS2CIF," J. Appl. Crystallogr. **36**, 1290 (2003).

Toney, M. F., Rubin, K. A., Choi, S.–M., Glinka, C. J., "Small Angle Neutron Scattering Measurements of Magnetic Cluster Sizes in Magnetic Recording Disks," Appl. Phys. Lett. **82** (18), 3050 (2003).

Tremsin, A. S., Mildner, D. F. R., Feller, W. B., Downing, R. G., "Very Compact High Performance Microchannel Plate Neutron Collimators," in IEEE Trans. Nucl. Sci. **51**, 1020 (2004).

Treviño, S. F., Mildner, D. F. R., "Hot Pressing Germanium Monochromator Crystals," J. Appl. Crystallogr. **37**, 339 (2004).

Trouw, F. R., Borodin, O., Cook, J. C., Copley, J. R. D., Smith, G. D., "Quasielastic Neutron Scattering Study of the Local Dynamics of Poly(Ethylene Glycol) Dimethyl Ether in Aqueous Solution," J. Phys. Chem. B **107** (38), 10446 (2003).

Tsao, F. C., Huang, P. J., Yang, C. C., Wu, S. Y., Li, W.-H., Lee, K. C., Lynn, J. W., Ku, H. C., "Mn Magnetic Ordering in Fully Oxygenated $LuMnO_3$," J. Magn. Magn. Mater. **272-276**, 1778 (2004).

Udovic, T. J., Arif, M., Majkrzak, C. F., Jacobson, D. L., Yildirim, T., Neumann, D. A., Rush, J. J., Pivovar, A. M., "Neutron Metrology for the Hydrogen Economy," in *Adv. Mater. For Energy Conversion II*, edited by Chandra, D., Bautista, R. G., Schlapbach, L., (TMS, Warrendale PA (2004)) p. 101.

Udovic, T. J., Neumann, D. A., Leao, J., Brown, C. M., "The Origin and Removal of Spurious Background Peaks in Vibrational Spectra Measured by Filter-Analyzer Neutron Spectrometers," Nucl. Instrum. Methods A **517**, 189 (2004).

Ueda, M., Sakurai, K., Okamoto, S., Lohse, D. J., MacKnight, W. J., Shinkai, S., Sakurai, S., Nomura, S., "Spherulite Formation From Microphase-Separated Lamellae in Semi-Crystalline Diblock Copolymer Comprising Polyethylene and Atactic Polypropylene Blocks," Polymer **44** (22), 6995 (2003).

Unterwger, M. P., Lindstrom, R. M., "Ionization Chamber Measurements of the Half-Lives of ^{24}Na, ^{42}K, ^{76}As and ^{198}Au," Appl. Radiat. Isot. **60**, 325 (2004).

Vogt, B. D., Soles, C. L., Prabhu, V. M., Jones, R. L., Wu, W.–L., Lin, E. K., Goldfarb, D. L., Angelopoulos, M., "Measurements of Water Distribution in Thin Lithographic Films," Proc. SPIE Int. Soc. Opt. Eng. **5376**, 56 (2004).

Vogt, B. D., Soles, C. L., Jones, R. L., Wang, C.–Y., Lin, E. K., Wu, W.–L., Satija, S. K., Goldfarb, D. L., Angelopoulos, M., "Interfacial Effects on Moisture Absorption in Thin Polymer Films," Langmuir **20** (13), 5285 (2004).

Waldron, J. E. L., Green, M. A., Neumann, D. A., "Structure and Electronic Properties of Monoclinic $Nb_{12}O_{29}$," J. Phys. Chem. Solids **65** (1), 79 (2004).

Wang, C. Y., Prabhu, V. M., Soles, C. L., Vogt, B. D., Wu, W. L., Lin, E. K., Satija, S. K., "Interdiffusion in Polystyrene and End-Functional Polystyrene Thin Films near a Solid Surface," in ACS Polymeric Materials: Science and Engineering **89**, 258 (2003).

Wang, H., Zhou, W., Ho, D. L., Winey, K. I., Fisher, J. E., Glinka, C. J., Hobbie, E. K., "Dispersing Single-Walled Carbon Nanotubes with Surfactants: A Small Angle Neutron Scattering Study," Nano Lett., in press.

Wiebe, C. R., Gardner, J. S., Kim, S. J., Luke, G. M., Wills, A. S., Gaulin, B. D., Greedan, J. E., Swainson, I., Qiu, Y., Jones, C. Y., "Magnetic Ordering in the Spin-Ice Candidate $Ho_2Ru_2O_7$," Phys. Rev. Lett. **93** (7), 076403 (2004).

Wiebe, C. R., Greedan, J. E., Kyriakou, P. P., Luke, G. M., Gardner, J. S., Fukaya, A., Gat-Malureanu, I. M., Russo, P. L., Savici, A. T., Uemura, Y. J., "Frustration-Driven Spin Freezing in the S=1/2 fcc Perovskite Sr_2MgReO_6," Phys. Rev. B **68**, 134410 (2003).

Wietfeldt, F. E., Dewey, M. S., Gilliam, D. M., Nico, J. S., Fei, X., Snow, W. M., Greene, G. L., Pauwels, J., Eykens, Lamberty, A., Van Gestel, J., "Measurement of the Neutron Lifetime by Counting Trapped Protons," in "*Quark-Mixing, CKM Unitarity*" edited by Abele, H., Mund, D., (Mattes Verlag, Heidelberg, 2003) p. 85.

Wiyatno, W., Fuller, G. G., Pople, J. A., Gast, A. P., Chen, Z.-R., Waymouth, R. M., Myers, C. L., "Component Stress-Strain Behavior and Small-Angle Neutron Scattering Investigation of Stereoblock Elastomeric Polypropylene," Macromol. **36**, 1178 (2003).

Won, Y.-Y., Davis, H. D., Bates, F. S., "Molecular Exchange in PEO-PB Micelles in Water," Macromol. **36** (3), 953 (2003).

Woodward, F. M., Lynn, J. W., Stone, M. B., Mahendiran, R., Schiffer, P., Mitchell, J. F., Argyriou, D. N., Chapon, L. C., "Field Induced Avalanche to the Ferromagnetic State in the Phase-Separated Ground State of Magnanites," Phys. Rev. B, in press.

Woodward, P. M., Karen, P., "Mixed Valence in $YBaFe_2O_5$," Inorg. Chem. **42** (4), 1121 (2003).

Wu, W.-L., Lin, E. K., Soles, C. L., "Structure Characterization of Porous Interlevel Dielectric Films," FUTURE FAB International **17**, 133 (2004).

Xu, G., Gehring, P. M., Ghosh, V. J., Shirane, G., "High *q*-resolution Neutron Scattering Technique Using Triple-Axis Spectrometers," Acta. Crystallogr. A, in press.

Xu, G., Shirane, G., Copley, J. R. D., Gehring, P. M., "A Neutron Elastic Diffuse Scattering Study of $Pb(Mg_{1/3}Nb_{2/3})O_3$," Phys. Rev. B **69**, 064112 (2004).

Xu, G., Viehland, D., Li, J. F., Gehring, P. M., Shirane, G., "Evidence of Decoupled Lattice Distortion and Ferroelectric Polarization in the Relaxor System PMN-*x*PT," Phys. Rev. B **68**, 212410 (2003).

Xu, T., Zhu, Y., Gido, S. P., Russell, T. P., "Electric Field Alignment of Symmetric Diblock Copolymer Thin Films," Macromol. **37** (7), 2625 (2004).

Yamaura, K., Huang, Q., Young, D. P., Takayama-Murmachi, E., "Crystal Structure and Magnetic Properties of the Trilayered Pervoskite $Sr_4Rh_3O_{10}$: A New Member of the Strontium Rhodate Family," Chem. Mater., in press.

Yang, C. C., Tsao, F. C., Wu, S. Y., Li, W.–H., Lee, K. C., Lynn, J. W., Liu, R. S., "Short Range Magnetic Corrections in Spinel $Li(Mn_{0.976}Co_{0.024})_2O_4$," J. Magn. Magn. Mater. **272-276** Part 2, 833 (2004).

Yang, L., Dzhosyuk, S. N., Gabrielse, J. M., Huffman, P. R., Mattoni, C. E. H., Maxwell, S. E., McKinsey, D. N., Doyle, J. M., "Performance of a Large-Area Avalanche Photodiode at Low Temperature for Scintillation Detection," Nucl. Instrum. Methods A **508** (3), 388 (2003).

Yildirim, T., Gulseren, O., Ciraci, S., "Intimate Relationship Between Structural Deformation and Properties of SWNT and its Hydrogenated Derivatives," in *Nanoengineered Nanofibrous Materials,* NATO-ASI Science Series II **169**, 181 (2004).

Yim, H., Kent, M. S., Mendez, S., Balamurugan, S. S., Balamurgan, S., Lopez, G. P., Satija, S., "Temperature-Dependent Conformational Change of PNIPAM Grafted Chains at High Surface Density in Water," Macromol. **37** (5), 1994 (2004).

Yun, S. I., Briber, R. M., Kee, R. A., Gauthier, M., "Small-Angle Neutron Scattering of Arborescent Polystyrene-*graft*-poly(2-vinylpyridine) Copolymers," Polymer **44** (21), 6579 (2003).

Yurekli, K., Karim, A., Amis, E. J., Krishnamoorti, R., "Influence of Layered Silicates on the Phase Separated Morphology of PS-PVME Blends," Macromol. **36** (19), 7256 (2003).

Yurekli, K., Karim, A., Amis, E. J., Krishnamoorti, R., "Phase Behavior of PS-PVME Nanocomposites," Macromol. **37**, 507 (2004).

Zaliznyak, I. A., Lee, S.-H., "Magnetic Neutron Scattering: Recent Developments in Triple Axis Spectroscopy," in *Modern Techniques for Characterizing Magnetic Materials*, edited by Yimei, Z., (Kluwer Academic Publishing Co.), in press.

Zaliznyak, I. A., Lee, S.-H., Petrov, S. V., "Continuum in the Spin-Excitation Spectrum of a Haldane Chain Observed by Neutron Scattering $CsNiCl_3$ (Vol. 87, art no. 017202, 2001)," Phys. Rev. Lett. **91** (3), 039902 (2003).

Zaliznyak, I. A., Tranquada, J. M., Gu, G., Erwin, R. W., Moritomo, Y., "Universal Features of Charge and Spin Order in a Half-Doped Layered Perovskite," J. Appl. Phys. **95** (11), 7369 (2004).

Zawisza, I., Burgess, I., Szymanski, G., Lipkowski, J., Majewski, J., Satija, S., "Electrochemical, Neutron Reflectivity and in Situ PM-FT-IRRAS Studies of a Monolayer of n-octadecanol at a Au (111) Electrode Surface," Electrochimica Acta, in press.

Zeisler, R., "New NIST Sediment SRMs for Inorganic Analysis," Anal. & Bioanal. Chem. **378**, 1277 (2004).

Zhao, W., Lukic-Zrnic, R., Gorman, B. P., Cottier, R. L., Golding, T. D., Littler, C. L., Dinan, J. H., Almeida, L. A., Dura, J. A., Lindstrom, R. M., Schaake, H. F., Liao, P., "Magnetoconductivity Tensor Analysis of Anomalous Transport Effects in Neutron Irradiated HgCdTe Epilayers," Physica E **20**, 246 (2004).

Zheludev, A., Honda, Z., Broholm, C. L., Katsumata, K., Shapiro, S. M., Kolezhuk, A., Park., S., Qiu, Y., "Massive Triplet Excitations in a Magnetized Anisotropic Haldane Spin Chain," Phys. Rev. B **68** (13), 134438 (2003).

Zheludev, A., Masuda, T., Sales, B., Mandrus, D., Papenbrock, T., Barnes, T., Park, S., "Distribution of Exchange Energy in Bond-Alternating *S*=1 Quantum Spin Chain," Phys. Rev. B **69** (14), 144417 (2004).

Zheludev, A., Sato, T., Masuda, T., Uchinokura, K., Shirane, G., Roessli, B.,"Spin Waves and the Origin of Commensurate Magnetism in $Ba_2CoGe_2O_7$," Phys. Rev. B 68 (2), 024428 (2003).

Zhou, W., Islam, M. F., Wang, H., Ho, D. L., Yodh, A. G., Winey, K. I., Fischer, J. E., "Small Angle Neutron Scattering from Single-Wall Carbon Nanotube Suspensions: Evidence for Isolated Rigid Rods and Rod Networks," Chem. Phys. Lett. **384** (1-3), 185 (2004).

Instruments and Contacts

High resolution powder diffractometer (BT-1):
J.K. Stalick, (301) 975-6223, judith.stalick@nist.gov
B.H. Toby, (301) 975-4297, brian.toby@nist.gov

DARTS, Residual stress and texture diffractometer (BT-8):
T. Gnaeupel-Herold, (301) 975-5380, tg-h@nist.gov
H.J. Prask, (301) 975-6226, hank@nist.gov
V. Luzin, (301) 975-5303, luzin@nist.gov

30-m SANS instrument (NG-7):
P. Butler, (301) 975-2028, butler@nist.gov
J.G. Barker, (301) 975-6732, john.barker@nist.gov
L. Porcar, (301) 975-5049, lionel.porcar@nist.gov

30-m SANS instrument (NG-3) (CHRNS):
B. Hammouda, (301) 975-3961, hammouda@nist.gov
S.R. Kline, (301) 975-6243, steven.kline@nist.gov
D. Ho, (301) 975-6422, derek.ho@nist.gov

8-m SANS instrument (NG-1):
D. Ho, (301) 975-6422, derek.ho@nist.gov
P. Butler, (301) 975-2028, butler@nist.gov
J.G. Barker, (301) 975-6732, john.barker@nist.gov

USANS, Perfect Crystal SANS (BT-5) (CHRNS):
J.G. Barker, (301) 975-6732, john.barker@nist.gov
M-H. Kim, (301) 975-6469, man-ho.kim@nist.gov
P. Butler, (301) 975-2028, butler@nist.gov

Cold neutron reflectometer-vertical sample-polarized beam option (NG-1):
C.F. Majkrzak, (301) 975-5251, cmajkrzak@nist.gov
J.A. Dura, (301) 975-6251, jdura@nist.gov

Advanced neutron diffractometer/reflectometer (NG-1):
Ursula Perez-Salas, (301) 975-8395, ula@nist.gov
Kevin O'Donovan, (301) 975-8380, kevin.odonovan@nist.gov

Cold neutron reflectometer-horizontal sample (NG-7):
S.K. Satija, (301) 975-5250, satija@nist.gov
Y-S. Seo, (301) 975-5660, ysseo@nist.gov

Triple-axis polarized-beam spectrometer (BT-2):
J.W. Lynn, (301) 975-6246, jeff.lynn@nist.gov
R.W. Erwin, (301) 975-6245, rerwin@nist.gov

Double-focusing triple-axis spectrometer (BT-7):
J.W. Lynn, (301) 975-6246, jeff.lynn@nist.gov
Y. Chen, (301) 975-6442, ying.chen@nist.gov

Triple-axis spectrometer (BT-9):
R.W. Erwin, (301) 975-6245, rerwin@nist.gov
Y. Chen, (301) 975-6442, ying.chen@nist.gov

SPINS, Spin-polarized triple-axis spectrometer (NG-5) (CHRNS):
S-H. Lee, (301) 975-4257, seung-hun.lee@nist.gov
J-H. Chung, (301) 975-8369, jae-ho.chung@nist.gov

FANS, Filter-analyzer neutron spectrometer (BT-4):
T.J. Udovic, (301) 975-6241, udovic@nist.gov
C.M. Brown, (301) 975-5134, craig.brown@nist.gov

FCS, Fermi-chopper time-of-flight spectrometer (NG-6):
C.M. Brown, (301) 975-5134, craig.brown@nist.gov
T.J. Udovic, (301) 975-6241, udovic@nist.gov

DCS, Disk-chopper time-of-flight spectrometer (NG-4) (CHRNS):
J.R.D. Copley, (301) 975-5133, jcopley@nist.gov
I. Peral, (301) 975-6235, inma@nist.gov
Y. Qiu., (301) 975-3274, yiming.qiu@nist.gov

HFBS, High-flux backscattering spectrometer (NG-2) (CHRNS):
Z. Chowdhuri, (301) 975-4404, zema.chowdhuri@nist.gov
E. Mamontov, (301) 975-6232, mamontov@nist.gov

NSE, Neutron spin echo spectrometer (NG-5) (CHRNS):
D.A. Neumann, (301) 975-5252, dan@nist.gov

Prompt-gamma neutron activation analysis (NG-7):
R.M. Lindstrom, (301) 975-6281, dick.lindstrom@nist.gov
R.L. Paul, (301) 975-6287, rpaul@nist.gov

Thermal neutron prompt-gamma activation analysis (VT-5):
E.A. Mackey, (301) 975-5149, liz.mackey@nist.gov

Other activation analysis facilities:
R.R. Greenberg, (301) 975-6285, rgreenberg@nist.gov

Cold neutron depth profiling (NG-0):
G. Lamaze, (301) 975-6202, lamaze@nist.gov

Instrument development station (NG-0):
D.F.R. Mildner, (301) 975-6366, mildner@nist.gov

Neutron interferometer (NG-7):
M. Arif, (301) 975-6303, muhammad.arif@nist.gov
D. Jacobson, (301) 975-6207, jacobson@nist.gov

Neutron Imaging Facility (BT-6):
M. Arif, (301) 975-6303, muhammad.arif@nist.gov
D. Jacobson, (301) 975-6207, jacobson@nist.gov

Fundamental neutron physics station (NG-6):
NG-6M: M.S. Dewey, (301) 975-4843, mdewey@nist.gov
NG-6U: H. P. Mumm, (301) 975-8355, pieter.mumm@nist.gov
NG-6: J. Nico, (301) 975-4663, nico@nist.gov

Theory and modeling:
N.F. Berk, (301) 975-6224, nfb@nist.gov
T. Yildirim, (301) 975-6228, taner@nist.gov

Sample environment:
D.C. Dender, (301) 975-6225, dender@nist.gov

NIST Center for Neutron Research

For copies of or information on this report, contact:

Ronald L. Cappelletti
301-975-6221
ron.cappelletti@nist.gov

For additional information on the facility, contact:

Patrick D. Gallagher
301-975-6210
patrick.gallagher@nist.gov

John J. Rush
301-975-6231
john.rush@nist.gov

To obtain guidelines for preparing proposals to conduct research at the facility, contact:

William A. Kamitakahara
301-975-6878
william.kamitakahara@nist.gov

Location of all contacts:

NIST Center for Neutron Research
National Institute of Standards and Technology
100 Bureau Drive, Mail Stop 8562
Gaithersburg, MD 20899

Copies of this report and other information are available electronically. Please visit our website.

www.ncnr.nist.gov